CONTRACTOR REPORT

SAND92–7293
Unlimited Release
UC–235

Wind Effects on Convective Heat Loss From a Cavity Receiver for a Parabolic Concentrating Solar Collector

Robert Y. Ma
Department of Mechanical Engineering
California State Polytechnic University
Pomoma, CA 91768

Prepared by Sandia National Laboratories Albuquerque, New Mexico 87185 and Livermore, California 94550 for the United States Department of Energy under Contract DE-AC04-76DP00789

Printed September 1993

Issued by Sandia National Laboratories, operated for the United States Department of Energy by Sandia Corporation.

Available to DOE and DOE contractors from
Office of Scientific and Technical Information
PO Box 62
Oak Ridge, TN 37831

Prices available from (615) 576-8401, FTS 626-8401

Available to the public from
National Technical Information Service
US Department of Commerce
5285 Port Royal Rd
Springfield, VA 22161

NTIS price codes
Printed copy: A04
Microfiche copy: A01

SAND92-7293
Unlimited Release
Printed September 1993

Distribution
Category UC-235

WIND EFFECTS ON CONVECTIVE HEAT LOSS FROM A CAVITY RECEIVER FOR A PARABOLIC CONCENTRATING SOLAR COLLECTOR

Robert Y. Ma
Department of Mechanical Engineering
California State Polytechnic University
Pomoma, California 91768

Tests were performed to determine the convective heat loss characteristics of a cavity receiver for a parabolid dish concentrating solar collector for various tilt angles and wind speeds of 0-24 mph. Natural (no wind) convective heat loss from the receiver is the highest for a horizontal receiver orientation and negligible with the reveler facing straight down. Convection from the receiver is substantially increased by the presence of side-on wind for all receiver tilt angles. For head-on wind, convective heat loss with the receiver facing straight down is approximately the same as that for side-on wind. Overall it was found that for wind speeds of 20-24 mph, convective heat loss from the receiver can be as much as three times that occurring without wind.

Table of Contents

List of Figures

List of Tables

1.0 Introduction

One of the parameters which affects the overall system efficiency of parabolic-dish concentrating solar energy systems is the efficiency of the receiver used. An understanding of the various modes of heat transfer from the receiver is required in order to adequately predict receiver efficiency. Radiation and conduction heat losses from the receiver can be predicted reasonably well by analytical techniques; however, convection from the cavity is much more complicated and, at present time, is not amenable to analytical predictions. Wind effects and varying receiver orientation make it an even more difficult phenomenon to predict analytically. Because of these reasons, convective heat loss from a cavity receiver is usually determined experimentally.

In the past few years, several test series have been conducted by the Mechanical Engineering Department at California State Polytechnic University, Pomona, to determine the convective heat loss characteristics of a cavity receiver for a parabolic-dish concentrating solar collector. The goal early in these test series was to determine natural convective heat losses from the receiver for various receiver tilt angles, temperatures, and apertures sizes. Recently, however, test efforts have concentrated on the effects of wind on convective heat loss from the cavity receiver. Wind speeds up to 24 mph (10.7 m/s) from two directions have been tested in conjunction with various receiver tilt angles, from aperture facing horizontally to aperture facing down.

This thesis presents and interprets the results from these latest tests, which are focused on wind effects. Data from these tests are reduced to obtain convective heat loss correlations for the different wind conditions, and an uncertainty analysis is performed in order to determine data reliability. An attempt is made to explain some of the physical phenomena underlying the convective transport for the various test conditions. Where possible, test results are compared with results from past studies. The convective heat loss correlations developed should aid in the design process and serve as background for future studies.

2.0 Experimental Setup

The cavity receiver tested is from a parabolic-dish concentrating solar collector from the Shanandoah Project, located in Shanandoah, Georgia. The receiver, shown in Figure 1, is a tube-wound type and is cylindrical in shape. One end of the receiver is a closed conical frustum, and the other end consists of a cylindrical section with an 18-inch (46-cm) diameter aperture. The maximum receiver internal diameter is 26 inches (66 cm) and the internal length is 27 inches (69 cm). The receiver tubing is 0.5 inch (12.7 mm) outer diameter and is made of stainless steel. The region outside the tubing is packed with Kaowool™ (Babcock and Wilcox) insulation and the entire assembly is covered with a chrome-plated-steel shell. The receiver is mounted in a stand which permits 180 degrees of rotation in 15° increments, from aperture-down (+90°) to aperture-up (-90°), with 0° defined as the aperture facing horizontally. (In these tests, only receiver tilt angles of 0° to +90° were examined).

The tests were performed in a laboratory environment without solar insolation. The basic methodology for determining receiver heat loss was to flow hot heat transfer fluid (Syltherm® 800, Dow Corning) through the receiver and calculate overall receiver heat loss based on the measured temperature drop of the heat transfer fluid. The heat transfer fluid was supplied from a flow loop containing pumps, electric heaters, and appropriate controls and expansion volume. When wind was required, it was generated by a 4'x4'x14' wind machine driven by a 4-ft diameter fan. The airstream was run through several honeycombed screens to ensure that the air velocity was uniform at the receiver.

The primary test measurements were recorded on a digital data acquisition system. At the receiver inlet and outlet, the heat transfer fluid temperature was measured with two type-K immersion thermocouple probes, located at piping bends to provide good flow mixing. One probe at each location was connected directly to the cold-junction compensation of the data acquisition system, providing a measurement of absolute fluid temperature. The other two probes were connected together to obtain a direct measurement of temperature difference between the receiver inlet and outlet. Volumetric flow of heat transfer fluid to the receiver was measured by a turbine-type flow meter.

Figure 1. Illustration of cavity receiver tested.

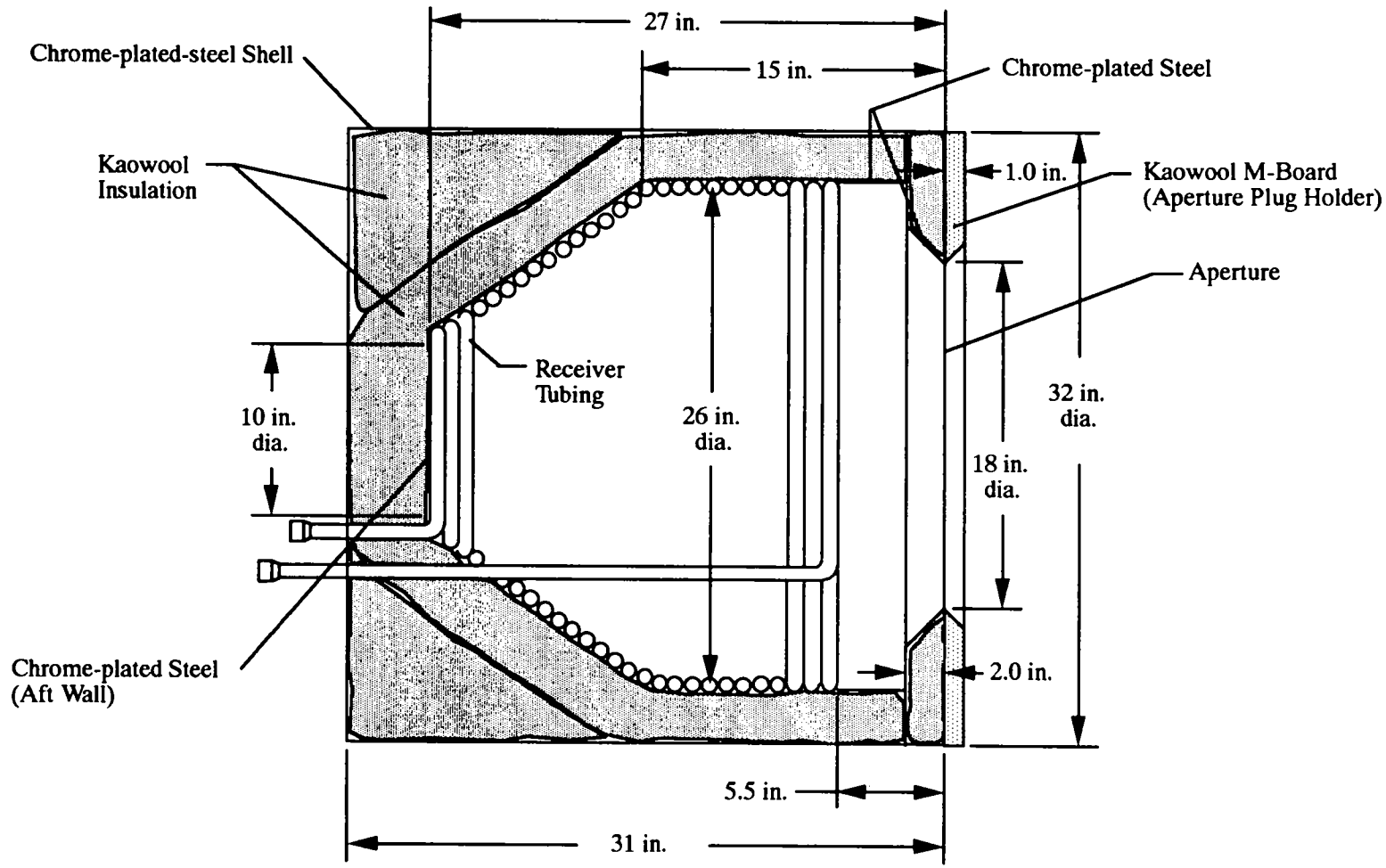

A more detailed description of the experimental apparatus is documented in Haddad (1991). Earlier tests dealing with natural convective heat loss, for various receiver temperatures, orientations, and aperture sizes, are described in McDonald (1992).

3.0 Test Matrix

The test results presented are from the two most recent receiver test series. The majority of this thesis focuses on the first of the two series, which was conducted in order to determine receiver convective heat loss for different wind conditions and receiver tilt angles. Head-on and side-on winds of 6, 8, and 20 mph (2.7, 3.6, and 8.9 m/s) were tested in conjunction with receiver tilt angles of 0°, 30°, 60°, and 90°. Figure 2 illustrates the wind-direction convention relative to the receiver. For this first test series, the no-wind condition was tested every time a new wind speed and direction were tested, so that a total of six no-wind test sets were conducted. In this way, the level of convective heat loss without wind was fully established.

As the data from the first test series were being examined, it became clear that some interesting and counter-intuitive convective heat loss results were occurring for the head-on wind tests. Therefore, to confirm some of these results and to obtain a better understanding, a second small test series was conducted for head-on winds only. The test conditions for this second test series were chosen specifically to clear up the areas of uncertainty from the first test series. Wind speeds of 15 and 24 mph (6.7 and 10.7 m/s) were tested to better define the dependence of head-on wind convective heat loss upon wind speed. For the 24-mph wind speed, data were collected for receiver tilt angles at 15° increments, to better define the dependence of convective heat loss upon receiver tilt angle. In addition, a smaller receiver aperture of 6 inches was also examined for a 24-mph wind, in order to check if the same trends occur for a different aperture size. For this second test series, convective heat loss tests for the no-wind condition were not performed.

4.0 Test Procedure

During testing at each wind condition, data were first collected with the aperture facing down and plugged, both with and without wind. Then the various receiver tilt angles were tested with the aperture open, again with and without wind. During each test,

Figure 2. Receiver-orientation and wind-direction conventions.

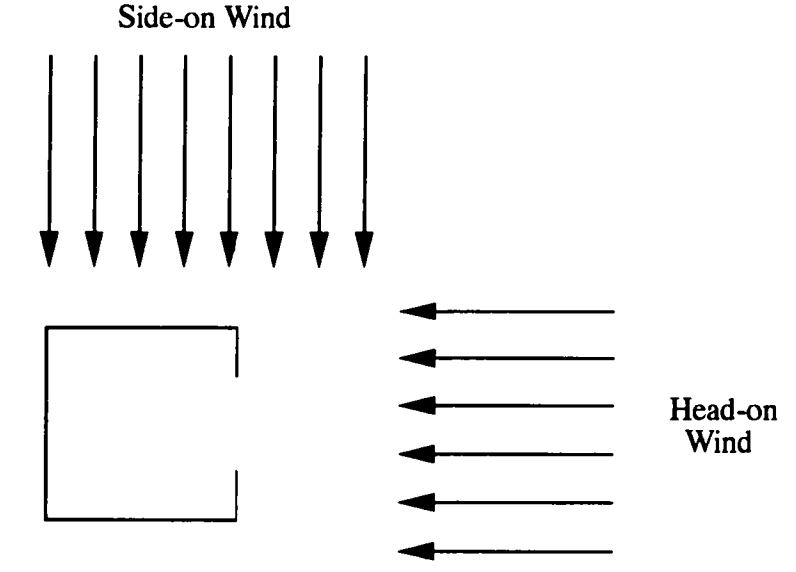

Top View - Looking Down

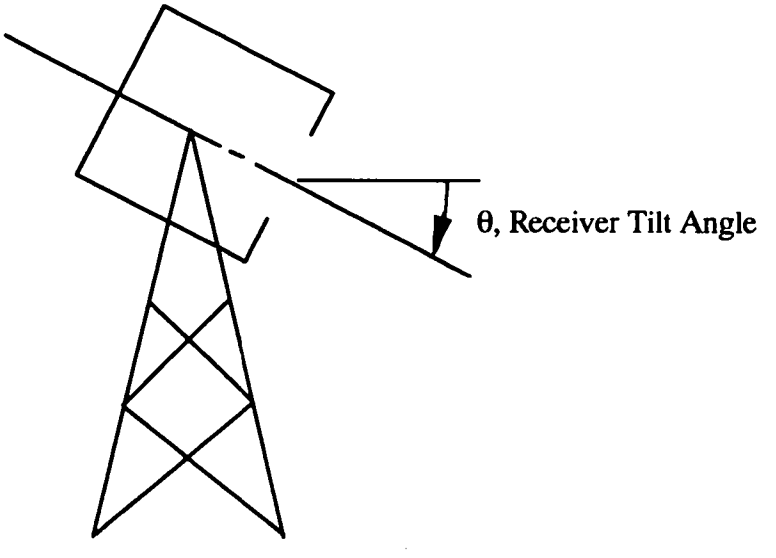

Elevation View

heat transfer fluid was passed through the receiver until the measured temperatures stabilized. Then pertinent data, such as heat-transfer-fluid inlet and outlet temperatures, inlet-to-outlet temperature difference, ambient temperature, and heat-transfer-fluid flow rate, were recorded. The total receiver heat loss for each test was subsequently calculated using the following equation:

$$q_{meas} = \dot{m}\, c_p\, (T_{in} - T_{out}) \tag{1}$$

where q_{meas} = total receiver heat loss rate calculated from measurements

$\dot{m}$ = measured heat-transfer-fluid mass flow rate

c_p = heat-transfer-fluid specific heat

T_{in} = measured heat-transfer-fluid temperature at inlet

T_{out} = measured heat-transfer-fluid temperature at outlet

The thermal properties of Syltherm® 800 heat transfer fluid which are required for the evaluation of Eq. (1) are given in Appendix A.

To allow for the comparison of heat losses from one test to another, all of the measured heat losses were normalized linearly to a receiver temperature of 530°F and an ambient temperature of 70°F, according to

$$q_{total} = \frac{q_{meas}\,(T_{rec,\,norm} - T_{amb,\,norm})}{T_{rec,\,meas} - T_{amb,\,meas}} \tag{2}$$

where q_{total} = normalized total heat loss rate

q_{meas} = total measured heat loss rate defined in Eq. (1)

$T_{rec,\,meas}$ = measured receiver temperature
(average temperature of the heat transfer fluid)

$T_{amb,\,meas}$ = measured ambient temperature

$T_{rec,\,norm}$ = nominal or normal receiver temperature (530°F)

$T_{amb,\,norm}$ = nominal or normal ambient temperature (70°F)

A nominal receiver temperature of 530°F was chosen because it represents the average receiver temperature among the different tests and would therefore require the least amount of normalization. This normalization procedure is justified since the deviation of the measured temperatures from the nominal temperatures is small.

Conduction heat loss from the receiver was calculated as the total receiver heat loss measured with the aperture plugged, minus the calculated amount of conduction through the aperture plug. Radiation heat loss was calculated as the total receiver heat loss with the aperture open, at a receiver orientation of 90° and without wind, minus the conduction heat loss without wind. According to Stine and McDonald (1988 and 1989), Koenig and Marvin (1981), and Kugath et al. (1979), natural convection from a cavity receiver at 90° tilt angle is essentially zero; therefore, the calculation of radiation heat loss in this manner is justified. Finally, convective heat loss from the receiver was calculated by subtracting radiation and conduction heat losses from the total receiver heat loss:

$$q_{conv} = q_{total} - q_{rad} - q_{cond} \tag{3}$$

5.0 Background

5.1 Natural Convection Correlations

Because of the complex natural convection phenomena occurring in cavity receivers, it is very difficult to analytically predict receiver natural convective heat loss. Design correlations for estimating natural convective heat loss from cavity receivers are usually derived experimentally.

Koenig and Marvin (1981) performed one such experiment and developed the following correlation for natural convection from cavity receivers:

$$\overline{Nu}_L = \frac{\bar{h} L}{k} = 0.52\, P(\theta)\, l_c^{1.75}\, (Gr_L\, Pr)^{0.25} \tag{4}$$

$$q_{conv} = \bar{h}\, A_T (T_{cavity} - T_o) \tag{5}$$

where

$P(\theta) = \cos^{3.2}\theta$ when $0° \le \theta \le 45°$

$P(\theta) = 0.707 \cos^{2.2}\theta$ when $45° \le \theta \le 90°$

θ = receiver tilt angle

$l_c = R_{aperture}/R_{cavity}$

$L = \sqrt{2}\, R_{cavity}$

$$Gr_L = \frac{g \beta (T_{cavity} - T_o) L^3}{\nu^2}$$

A_T = exposed surface area of receiver heat transfer tubing

T_{cavity} = average temperature of heat transfer tubing

T_o = ambient temperature

β = coefficient of thermal expansion of air = 1/T

ν = kinematic viscosity of air

where all fluid properties are evaluated at

$T_{prop} = 11/16\, T_{cavity} + 3/16\, T_o$

Note that the area used in Eq. (5) is the exposed area of the heat transfer tubing inside the receiver.

Stine and McDonald (1988) found that for the cavity receiver described in this thesis, natural convective heat loss is better predicted if the constant in Eq. (4) is 0.78, instead of 0.52, and if the full interior geometric surface area of the cavity is used (i.e., the interior area covered with heat transfer tubing should be considered planar). The resultant equation is referred to in this report as the modified Koenig and Marvin correlation:

$$\overline{Nu}_L = 0.78\, P(\theta)\, l_c^{1.75} (Gr_L\, Pr)^{0.25} \qquad (6)$$

Siebers and Kraabel (1984) reported the following correlation for predicting turbulent natural convection from central receiver cubical cavities, over the range of $10^5 \le Gr_L \le 10^{12}$:

$$\overline{Nu}_L = 0.088\, Gr_L^{1/3} \left(\frac{T_w'}{T_o}\right)^{0.18} \qquad (7)$$

where L = height of the interior of the cavity
T_o = ambient temperature, K or °R
T_w = average internal wall temperature, K or °R

This correlation was derived based on the results of a large 2.2-m cubical cavity experiment performed by Kraabel (1983), and experiments of 0.2-m and 0.6-m cubical cavities performed by LeQuere, Penot, and Mirenayat (1981). To account for the effects of receiver tilt angle and the addition of "lips" at both the top and the bottom of the receiver aperture, a method using receiver area ratios is also described by Siebers and Kraabel (1984). In Eq. (7), all fluid properties are evaluated at ambient temperature, and the area to be used for heat transfer calculations is the full interior geometric surface area of the receiver.

Stine and McDonald (1989) performed natural convective heat loss experiments on the cavity receiver described in this report. Their experiments included the effects of different receiver temperatures, tilt angles, and aperture sizes. Using the Siebers and Kraabel correlation [Eq. (7)] as a basis, the effects of different receiver temperatures, orientations, and aperture sizes were included to obtain the following equation:

$$\overline{Nu}_L = 0.088\, Gr_L^{1/3} \left(\frac{T_w}{T_o}\right)^{0.18} (\cos\theta)^{2.47} \left(\frac{d}{L}\right)^s \qquad (8)$$

where $s = 1.12 - 0.982\,(d/L)$
d = aperture diameter
L = receiver internal diameter at cylindrical region
θ = receiver tilt angle

In this report, this correlation is referred to as the Stine-McDonald correlation. The heat transfer area to be used with Eq. (8) depends on whether solar insolation is present. For off-sun testing, only the portion of the receiver interior geometric surface area covered with heat transfer tubing should be used. For on-sun situations, the entire receiver interior geometric surface area should be used.

It is worth noting that in all of the equations above which account for varying receiver tilt angle, natural convective heat loss from the receiver is predicted to be maximum with the aperture facing horizontally (0° tilt angle) and zero with the aperture facing down (90° tilt angle).

5.2 Forced Convection Correlations

No correlations are available for predicting forced or mixed convection from cavity receivers. Few experimental investigations have been performed in this area, with the results being somewhat contradictory.

Clausing (1981) performed simplified numerical experiments which calculated convective heat losses in a large central cavity receiver based on an energy balance of: (1) the energy transferred from the hot receiver interior walls to the air inside the cavity and (2) the energy transfer across the aperture by the combined influences of flow over the aperture due to wind and the buoyancy-induced flow due to the cold external air. The results of this numerical work show that the influence of wind at 18 mph or less is minimal. This finding is in agreement with the experimental results of McMordie (1984) who examined wind effects on convection from central cavity receivers. McMordie found that for winds of 3 to 15 mph, wind-speed and wind-direction effects were indistinguishable.

On the other hand, Kugath et al. (1979) measured the effects of a 10-mph wind on convective heat loss from a cavity receiver from the Shanandoah project (similar to the receiver described in this report) and found convective heat loss to be highly dependent upon receiver orientation. The highest convective heat loss was observed with the wind blowing directly into the cavity, being as much as four times the level of natural convection. They also found that for wind blowing from directly behind the receiver, total convective heat loss was not much higher than pure natural convection.

An experimental investigation conducted by Faust et al. (1981) showed that a noticeable increase in receiver convection occurred with a wind speed of only 2 mph. In Faust's experiment, it was observed that winds parallel to the aperture plane result in the highest convective heat loss. It was explained that with wind blowing in this direction, the aperture lies in the separation region and is subjected to the suction pressure of the air flow.

On the other hand, winds perpendicular to the aperture plane were found to reduce convective heat loss because flow stagnation supposedly decreases the pressure gradient responsible for natural convection.

From the studies referred to above, it is apparent that no conclusions can be made regarding forced or mixed convection from cavity receivers. Wind seems to have noticeable effects in small cavity receivers for parabolic-dish solar collectors, but little effect in larger cavity receivers for central receiver systems.

In the absence of a reliable correlation to predict forced convection from cavity receivers, Siebers and Kraabel (1984) suggest that as a first approximation, forced convection from a flat plate the size of the aperture and at the receiver average temperature be used. They also recommend that pure forced and natural convection from a cavity receiver be simply added together to obtain the total convective heat loss. However, this recommendation is based on engineering judgement since there is no directly applicable information on the subject of mixed convection from cavities.

6.0 Analysis of Direct Measurements of Convection

This section discusses the experimental results from both the first and second test series; however, because the majority of the results presented here were obtained from the first test series, the discussions will focus on those results. In the remainder of this thesis, all discussions refer to the first test series unless otherwise noted.

The detailed experimental results and data reduction for all of the tests from both test series are given in spreadsheets in Appendix B. Raw experimental data, intermediate calculated values, and final heat loss results are included in these spreadsheets. A more concise summary of receiver heat losses, due to convection, conduction and radiation, is given in Appendix C.

6.1 Convective Heat Loss Without Wind

Figure 3 presents receiver heat loss as a function of tilt angle for all six of the no-wind test sets. The results are given for a nominal receiver temperature of 530°F. Natural

Figure 3. Natural convective heat loss from receiver at 530°F.

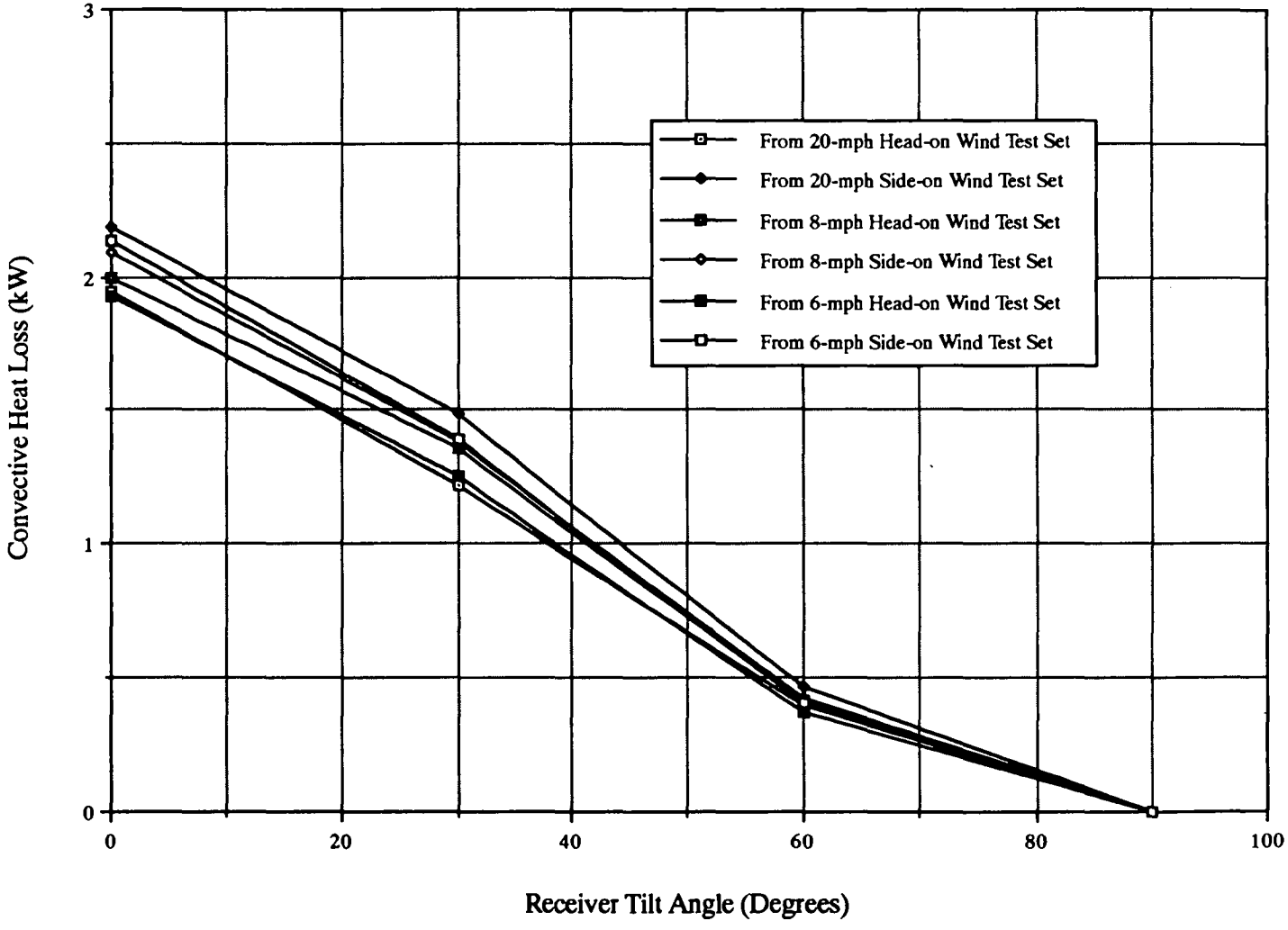

convective heat loss from the receiver is the highest with the receiver facing horizontally (0° receiver tilt angle) and the lowest with the receiver facing straight down (90° receiver tilt angle). With the receiver facing horizontally, natural convective heat loss is approximately 2 kW. With the receiver facing straight down, natural convective heat loss is presumed to be zero. From examining Figure 3, it can be seen that the scatter of convective heat loss data at each receiver tilt angle is reasonably small (about 5-10 percent standard deviation), which suggests that these experimental results are quite repeatable.

These natural convective heat loss results are qualitatively in agreement with the experimental findings of Stine and McDonald (1988 and 1989), Kugath (1979), Koenig and Marvin (1981), and Siebers and Kraabel (1984). The decreased natural convective heat loss as the receiver is tilted downward is due to a larger portion of the receiver volume being in the so-called stagnant zone, where convective currents are virtually non-existent and air temperature is high, and a smaller portion being in the so-called convective zone, where significant air currents exist. This convective behavior is illustrated in Figure 4. It has been observed by Siebers and Kraabel (1984) and Clausing (1981) that the interior volume above the horizontal plane passing through the uppermost portion of the aperture is relatively stagnant and high-temperature air.

The presumption that natural convective heat loss is zero with the receiver facing straight down was necessary in order to separate heat loss components in data reduction and is supported by observations made in the past by Stine and McDonald (1988 and 1989) and Kugath (1979). Recent flow visualization experiments at this facility, using smoke, have also confirmed the lack of convective flow entering or leaving the cavity when it is tilted facing down. The lack of natural convection with the receiver aperture facing down is reasonable considering that the entire receiver internal volume is in the so-called stagnant zone.

Figure 5 compares the experimental results from the six no-wind test sets to predictions obtained using the Stine-McDonald correlation [Eq. (8)] and the modified Koenig-Marvin correlation [Eq. (6)]. The Stine-McDonald correlation matches the experimental data very well, but the modified Koenig-Marvin correlation is as much as 20 percent low. It is emphasized that great care should be taken to ensure that the correct area is used with these heat transfer correlations. The correct area for Eq. (6) is the full interior

Figure 4. Illustration of stagnant and convective zones in a cavity receiver.

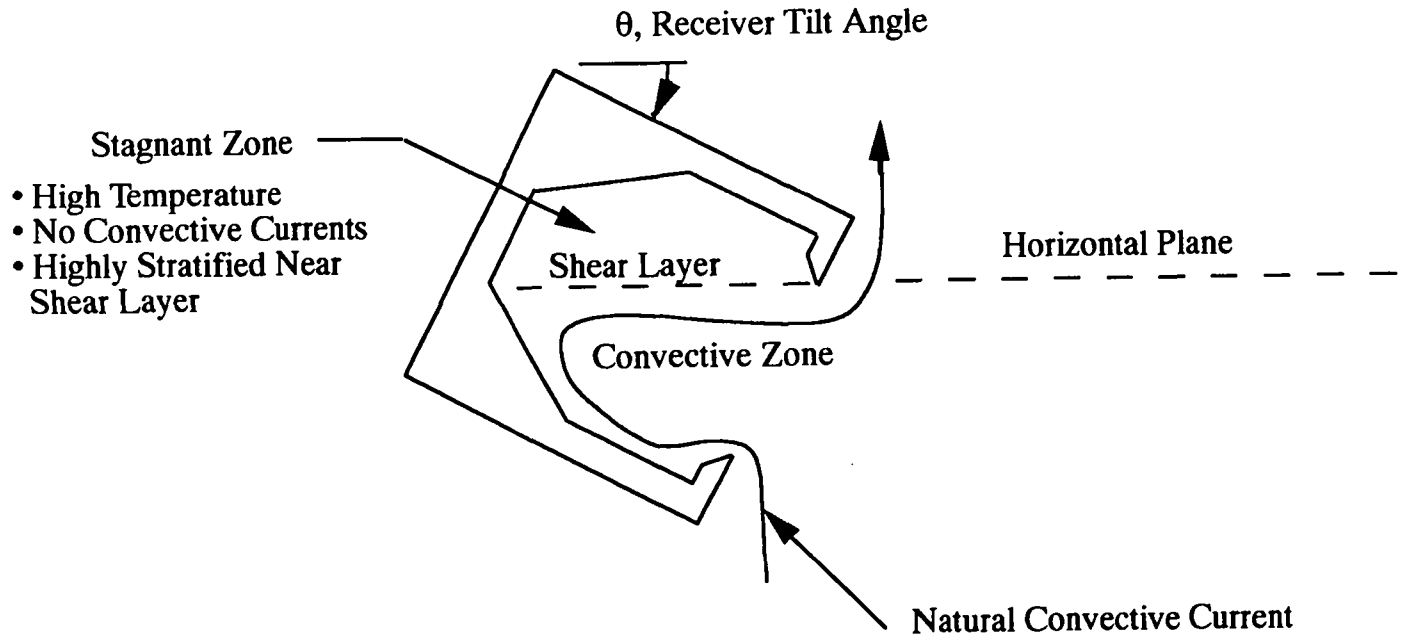

Figure 5. Predicted and experimental natural convective heat loss from the receiver at 530°F.

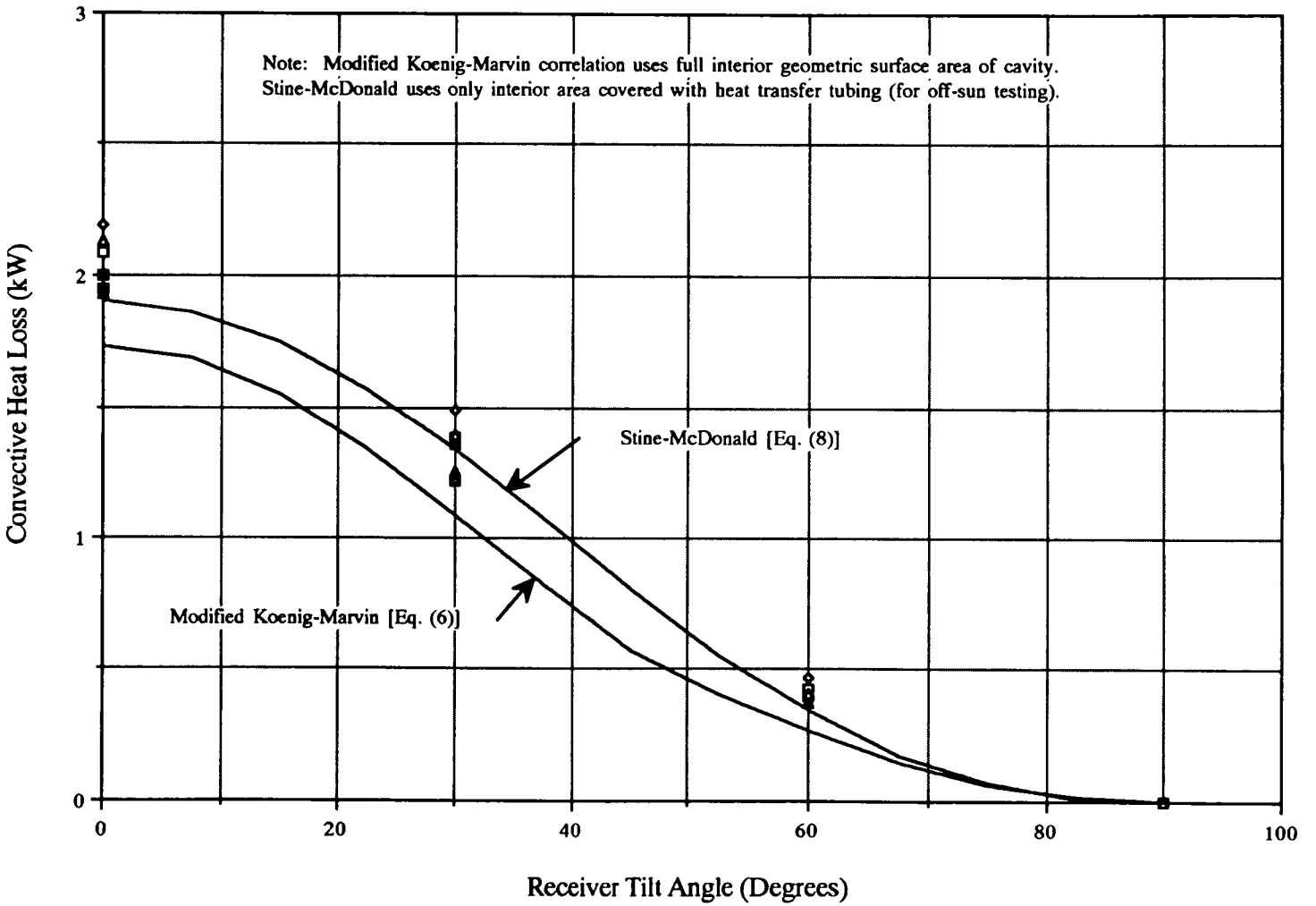

geometric surface area of the receiver, whereas that for Eq. (8) is only the interior area covered with heat transfer tubing (for off-sun testing).

Figure 6 shows the average conduction, radiation, and convection heat losses for the six no-wind test sets. While convective heat loss varies as a function of receiver tilt angle, conduction and radiation heat losses are assumed to be independent of tilt angle and are 0.60 kW and 0.62 kW, respectively. Figure 7 shows the percentage of the total receiver heat loss attributed to the different heat loss modes. At 0° receiver tilt angle, natural convection represents about 63 percent of the total receiver heat loss. However, at 90° tilt angle, natural convection is negligible, and conduction and radiation heat loss percentages are about 50 percent each.

6.2 Convective Heat Loss With Wind

Convective heat loss results from the first test series for side-on and head-on winds of 6, 8 and 20 mph (2.7, 3.6, and 8.9 m/s) are shown in Figures 8 and 9, respectively. The average of the six no-wind test sets is also shown in each of these figures for reference. For 6- and 8-mph wind speeds, increases in convective heat loss due to wind are only moderate. The maximum convective heat loss for an 8-mph side-on wind is about 35 percent higher than the maximum natural convective heat loss from the receiver. The corresponding increase for an 8-mph head-on wind is less than 10 percent. However, wind effects at 20 mph are significant, with convective heat loss being as high as 2-3 times the maximum level of natural convection from the receiver.

These experimental results are in sharp contrast to the findings of McMordie (1984) that wind effects on convective heat loss from a cavity receiver are minimal compared to natural convection. A plausible explanation for this discrepancy is that the maximum Re^2/Gr ratio is about 14 for the tests described here, compared to $Re^2/Gr \approx 1$ for McMordie's experiments. It is reasonable that forced convection effects are large in these tests because Re^2/Gr is so large. Nevertheless, $Re^2/Gr \approx 1$ for McMordie's experiments is large enough that forced convection should be comparable to natural convection.

By examining Figures 8 and 9, it is evident that the convective behavior of the receiver is quite different for the different wind directions tested. For side-on winds,

Figure 6. Average conduction, radiation, and convection heat loss for the six no-wind test sets (530°F receiver temperature).

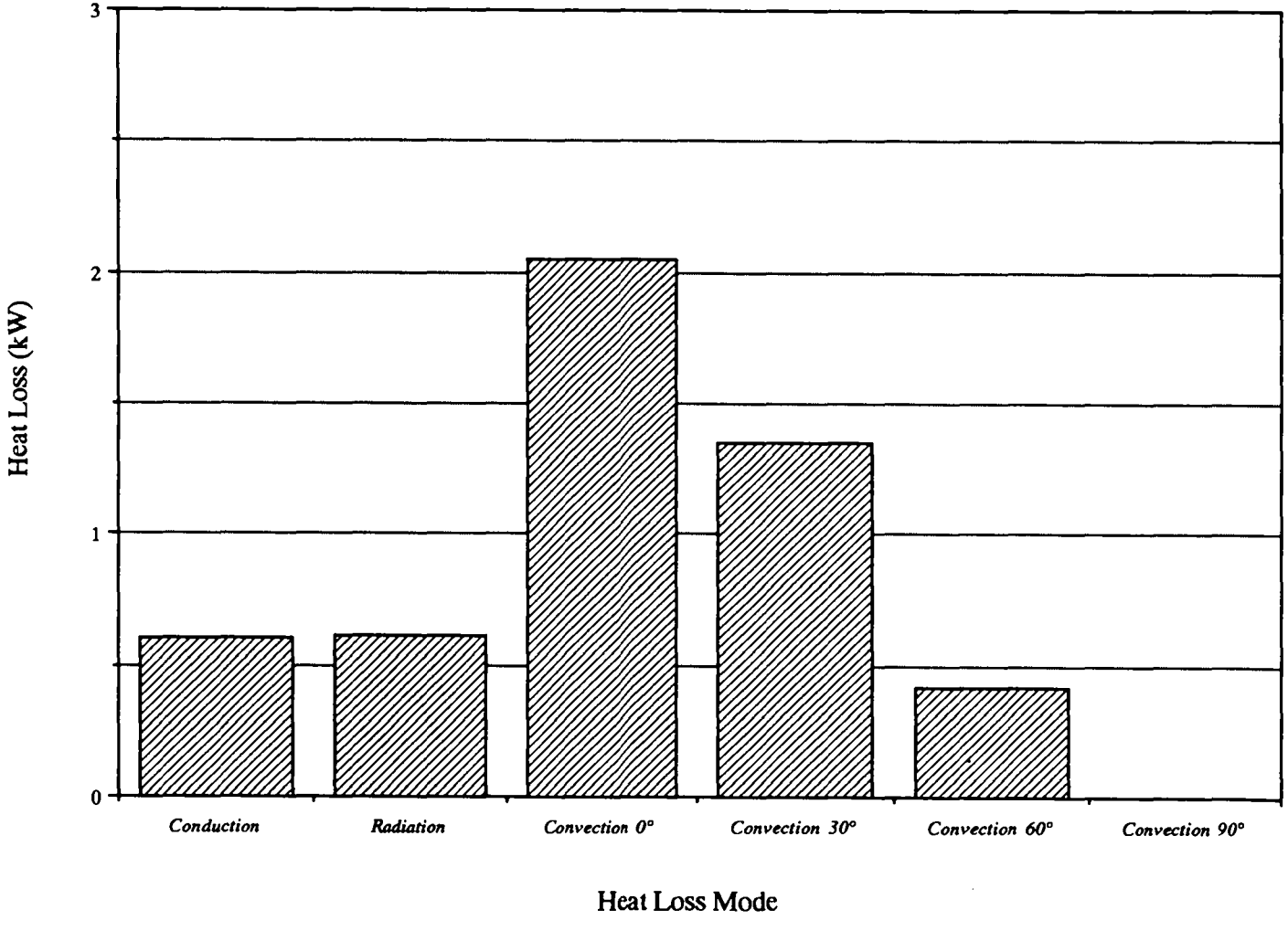

Figure 7. Heat loss components from receiver at 530°F without wind (average of 6 no-wind sets).

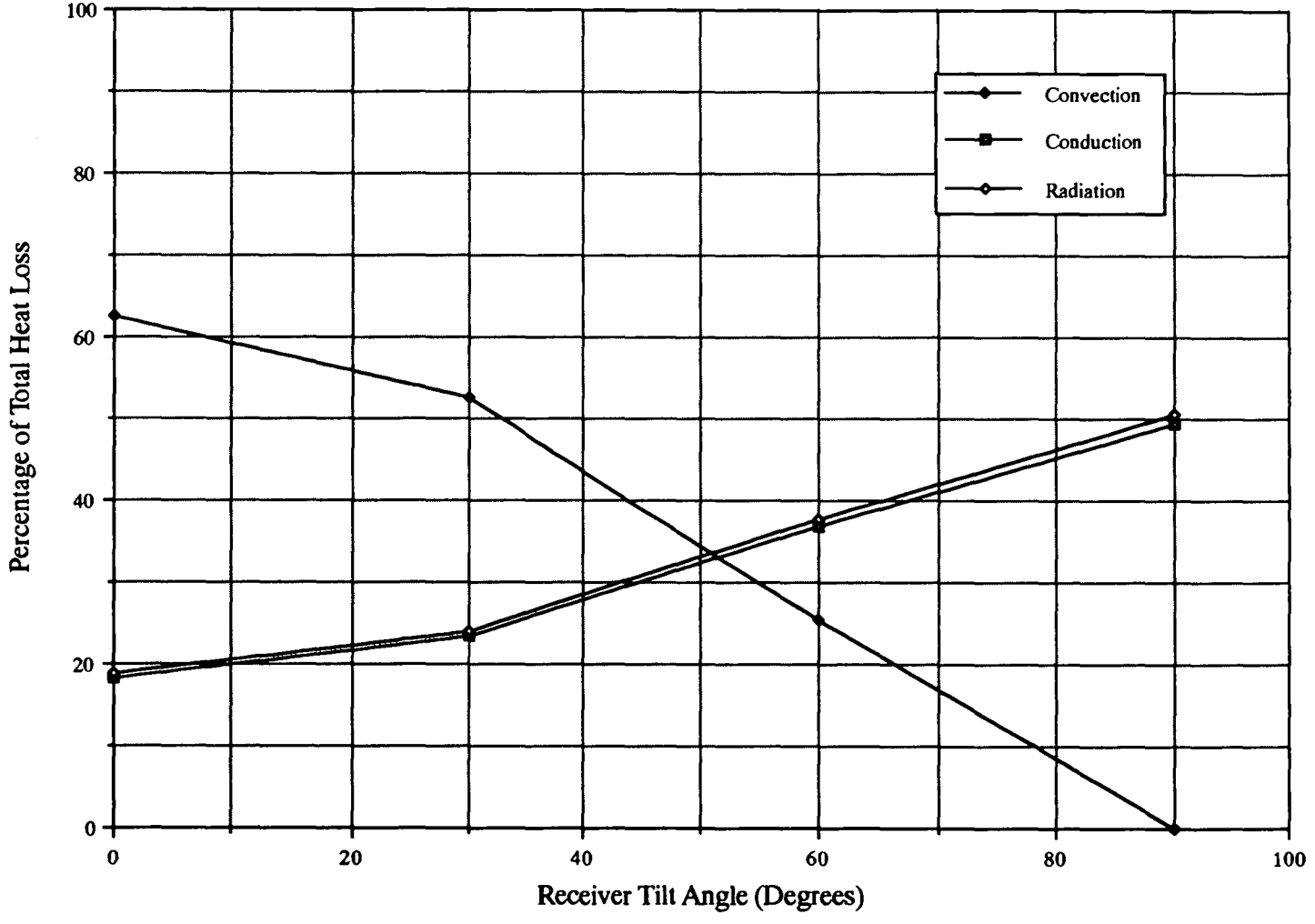

Figure 8. Convective heat loss from receiver at 530°F for side-on winds of various speeds.

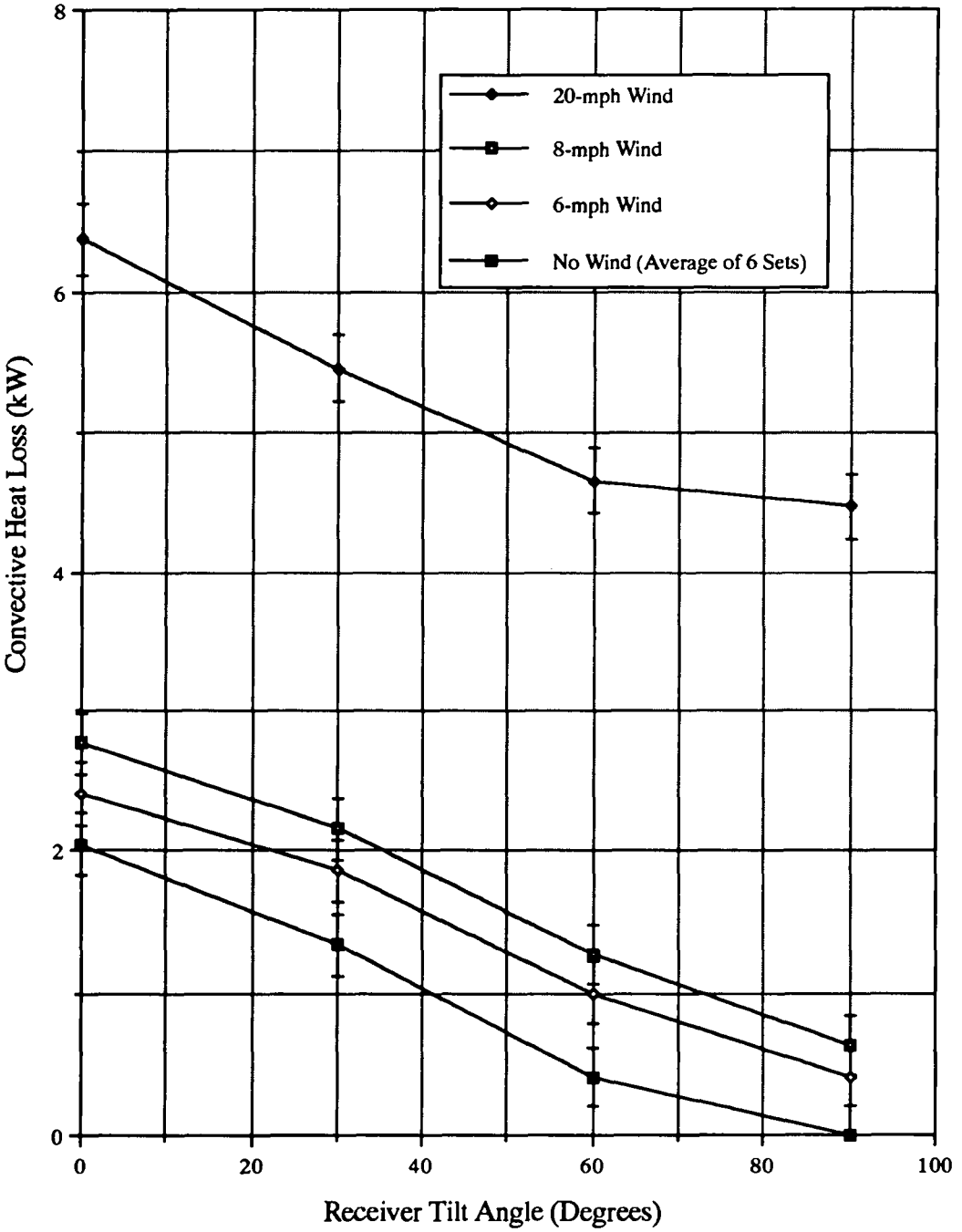

Figure 9. Convective heat loss from receiver at 530°F for head-on winds of various speeds.

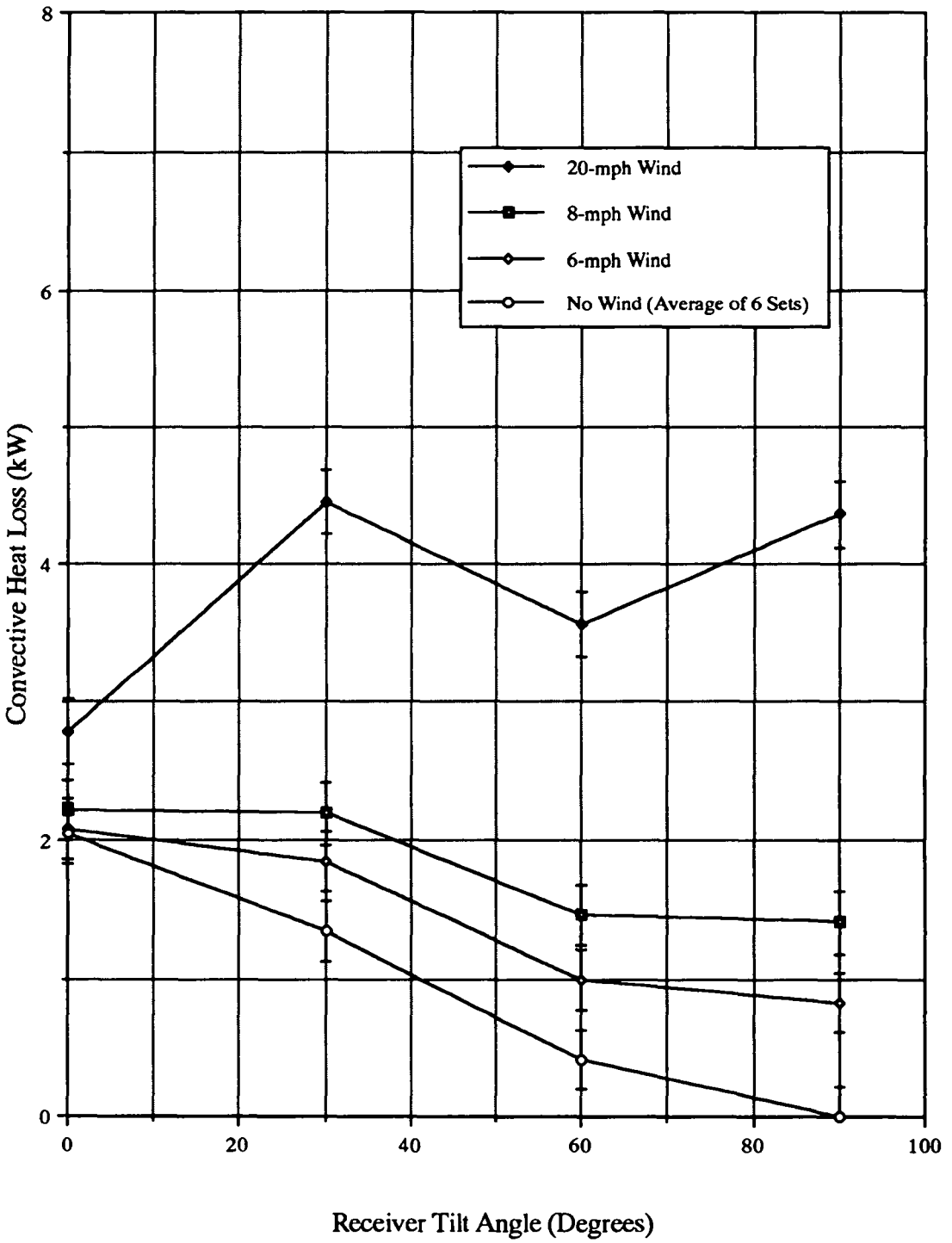

higher wind speeds result in increases in convective heat loss, above natural convection, which are invariant with tilt angle. In addition, for all of the wind speeds examined, the highest convective heat loss for side-on wind occurs with the receiver facing horizontally, and the lowest occurs with the receiver facing down. For head-on winds, however, the amount of increase in convective heat loss varies as a function of receiver tilt angle. Increases in convective heat loss due to wind are minimal with the receiver facing horizontally; however, with the receiver facing down, convective heat loss increases are large.

Figures 10 and 11 present the convective heat loss results as a function wind speed, for side-on and head-on winds, respectively. Convective heat loss versus wind speed appears to be well behaved for side-on winds, but is more erratic for head-on winds. In an attempt to obtain a better understanding of the effects of wind, natural convective heat loss was subtracted from the total convective heat loss at each condition (see Figures 12 and 15). The resultant curves, discussed in detail below, represent the increase in convective heat loss due to the presence of wind. It is believed that with the data presented in this fashion, insight into the forced convection problem may be more easily obtained.

6.2.1 Analysis of Forced Convection Due to Side-On Wind

Generally speaking, natural convective currents flow inside the receiver from bottom to top, in a vertical plane. For side-on winds, forced convective currents are generally in a direction normal to the plane of natural convective currents. Because of this orthogonal relationship between natural and forced convective currents, it is reasonable to hypothesize that forced convection from the receiver is independent of natural convection. In addition, pure forced convection should not change at all as the receiver tilt angle changes. Indeed, in the absence of gravity, side-on wind convective heat loss would be the same for any receiver tilt angle. The result of this hypothesis is that natural and forced convection should be additive for side-on wind:

$$q_{conv\ overall} = q_{natural} + q_{forced} \tag{9}$$

or

Figure 10. Convective heat loss from receiver as a function of wind speed for side-on winds (530°F receiver temperature).

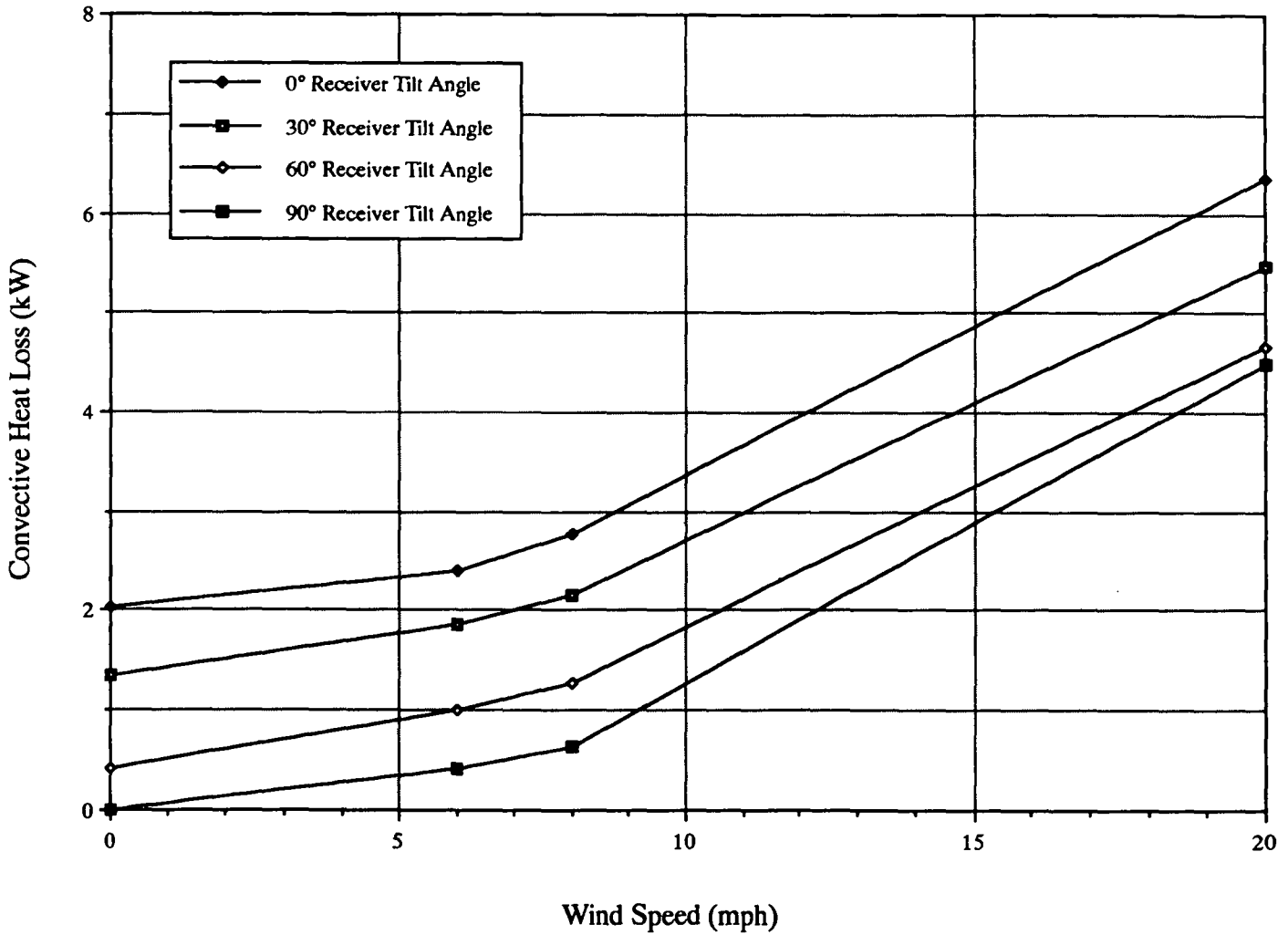

Figure 11. Convective heat loss from receiver as a function of wind speed for head-on winds (530°F receiver temperature).

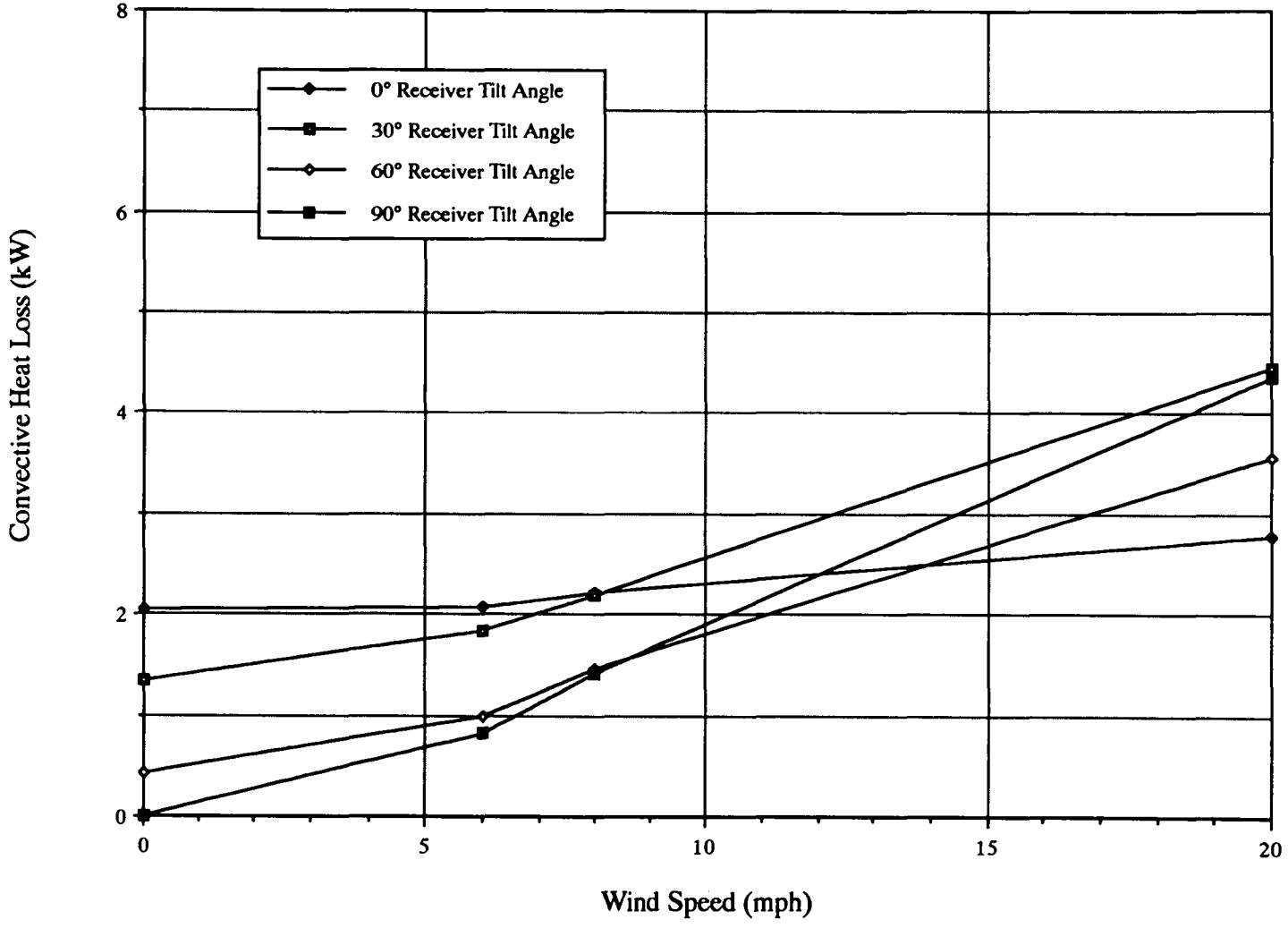

$$\bar{h}_{overall} = \bar{h}_{natural} + \bar{h}_{forced} \tag{10}$$

In addition, the forced convection component should be a function of wind speed only. Equations (9) and (10) are in agreement with the recommendation given by Siebers and Kraabel (1984) for predicting mixed convection from cavity receivers.

Figure 12 shows the increase in measured convective heat loss from the receiver due to side-on wind. These experimental results confirm that the increase in convective heat loss due to side-on wind follows the same trend regardless of receiver tilt angle. For a 20-mph side-on wind, the convective heat loss increases for the different receiver tilt angles vary by only about 3-percent standard deviation. Indeed, it appears that the increase in convective heat loss due to side-on wind is a function of wind speed only, and that natural and forced convection are additive according to Equations (9) and (10) above.

A curve fit of the data shown in Figure 12 gives the pure forced convection heat transfer coefficient as a function of wind speed for side-on wind:

$$\bar{h}_{forced} = 0.1967\ V^{1.849} \tag{11}$$

where $\bar{h}_{forced}$ = forced convection heat transfer coefficient, $W/(m^2 \cdot K)$
V = side-on wind velocity, m/s

This equation is based on the full interior geometric surface area of the receiver, which is 1.472 m^2. Comparison of this curve-fit to the experimental data from all of the side-on wind tests is shown in Figure 13. It can be seen that the experimental data are represented very well by this single curve-fit.

It is interesting to note that the exponent of 1.849 in the velocity term of Eq. (11) is much larger than that usually associated with convective heat transfer. For example, for turbulent heat transfer from a flat plate, the Nusselt number relationship is

$$\overline{Nu}_L = \frac{\bar{h}L}{k} = 0.037\ Re_L^{0.8}\ Pr^{1/3} \tag{12}$$

Figure 12. Increased convective heat loss from receiver due to side-on wind, i.e., total convective heat loss minus natural convective heat loss (530°F receiver temperature).

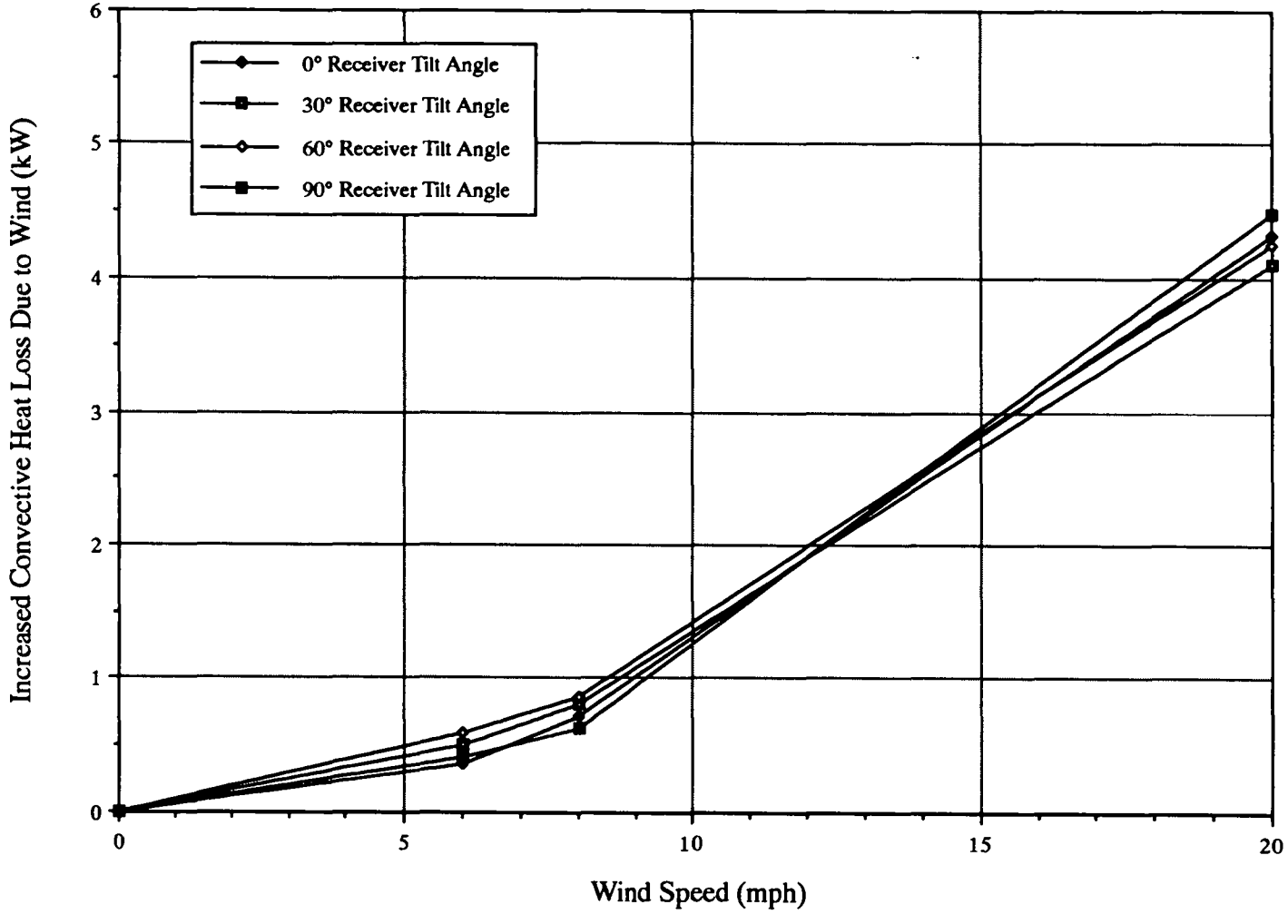

Figure 13. Increased convective heat loss due to side-on wind: experimental vs. predictions (530°F receiver temperature).

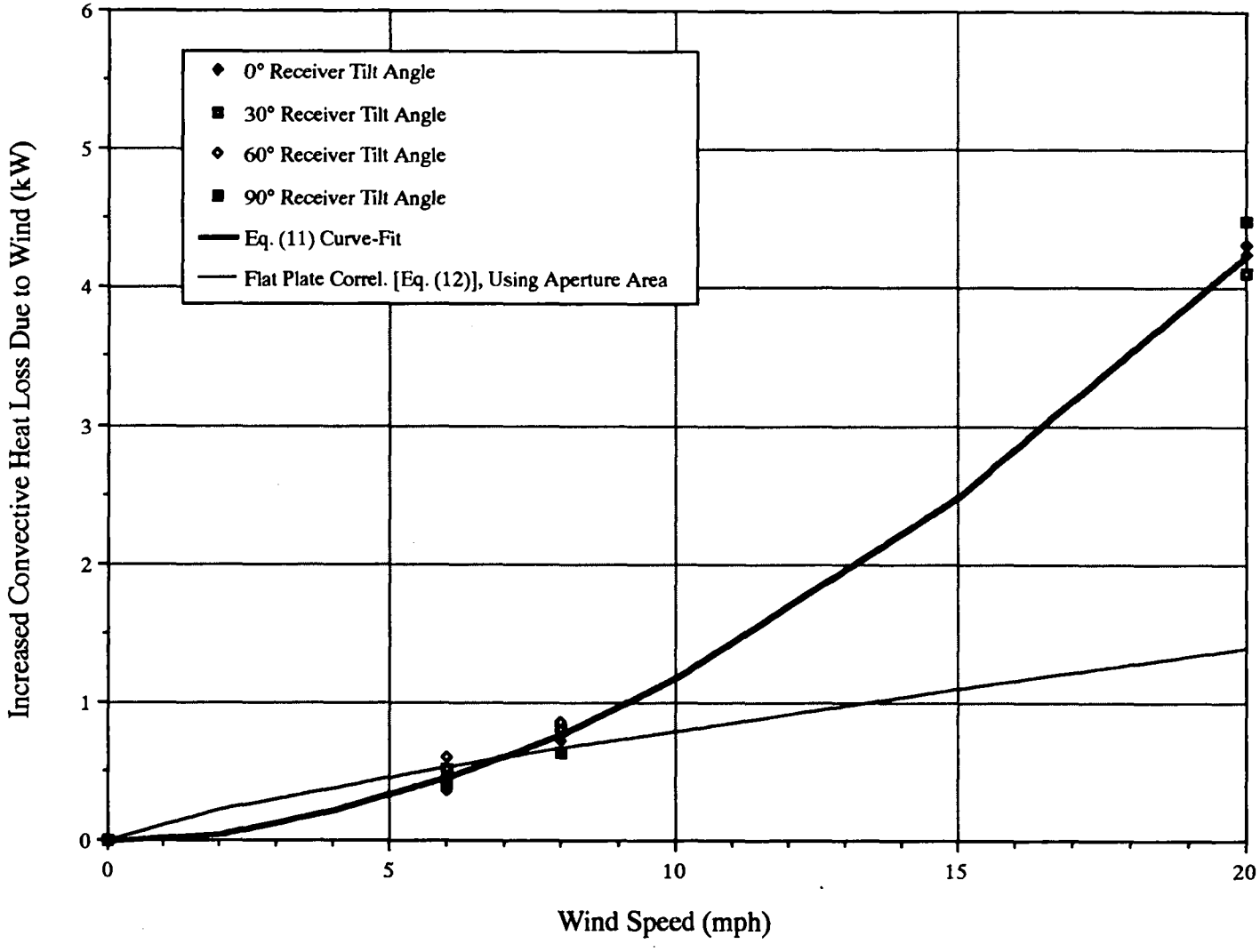

with the heat transfer coefficient being proportional to velocity raised to the 0.8 power. The exponent of 1.849 in Eq. (11) is closer to that normally associated with shear stress. For example, for turbulent flow over a flat plate, shear force is proportional to velocity raised to the 1.8 power. The fact that the heat transfer coefficient in Eq. (11) varies about the same as for shear force suggests that the determining factor for heat transfer from the cavity may be the ability of wind to transfer mass and energy across the aperture via fluid shear, not the ability of the receiver walls to transfer energy to the air inside the cavity. This argument is consistent with that given by Clausing (1981).

As previously mentioned, Siebers and Kraabel (1984) recommended that in the absence of a reliable correlation for predicting forced convective heat loss from a cavity receiver, the heat loss from a flat plate the size of the receiver aperture and at the receiver average temperature be used. Following this recommendation, Eq. (12) was used to predict receiver force convection. The resultant heat loss curve is shown in Figure 13. Note that Eq. (12) matches the experimental data adequately for low wind speeds, but grossly underpredicts convective heat loss at wind speeds above 10 mph. It is obvious that the curve of Eq. (12) is not representative of the experimental data, and that the curve-fit of Eq. (11) is a better match.

As a side-note on convective heat loss due to side-on wind, let us examine the percentage of total receiver heat loss attributed to convection, conduction, and radiation, for a 20-mph side-on wind. These data are shown in Figure 14. It can be seen that for a 20-mph side-on wind, convective heat loss is over 75 percent of the total receiver heat loss for all receiver tilt angles. This is in sharp contrast to the no-wind condition (Figure 7) where natural convection accounts for 63 percent of the total receiver heat loss at 0° tilt angle and is negligible at 90° tilt angle.

6.2.2 Analysis of Forced Convection Due to Head-On Wind

Comparison of Figures 8 and 9 shows that receiver convective heat loss characteristics are very different for head-on and side-on winds. For side-on winds, the heat loss curves as a function receiver tilt angle are shaped the same regardless of wind speed. However, for head-on winds, the heat loss curves versus receiver tilt angle do not all follow the same trend.

Figure 14. Receiver heat loss components at 530°F for 20-mph side-on wind.

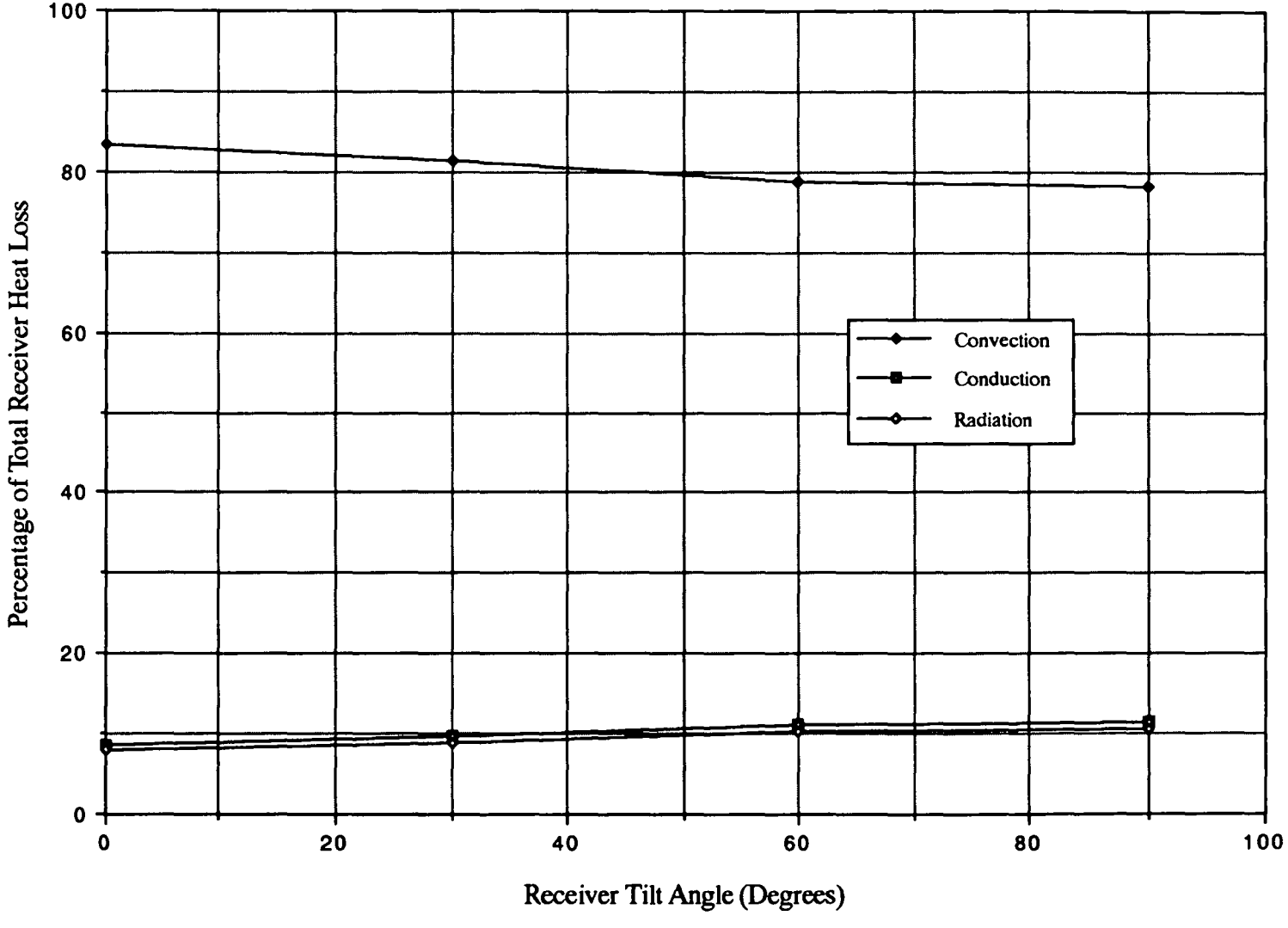

Figure 15 shows the increase in convective heat loss due to head-on wind. Different receiver tilt angles result in different curves as a function of wind speed. With the aperture facing down (90° tilt angle), the increased convective heat loss due to wind increases rapidly with wind speed. At receiver tilt angles of 30° and 60°, increased convective heat loss due to wind are similar to each other. At a receiver tilt angle of 0°, increased convective heat loss due to wind is very small, even for high-speed wind. These results show that, in general, wind effects diminish as the receiver is tilted upward from 90° tilt angle to 0° tilt angle.

Because the convective heat loss results from these head-on wind tests behave much differently than those for side-on winds, a second small test series consisting of several additional head-on wind tests was conducted to confirm the results and also to provide a better understanding of the phenomena. In these additional tests, the primary objective was to validate the convective heat loss trends, both versus wind speed and receiver tilt angle. To verify the dependence of convective heat loss upon wind speed, tests were conducted at wind speeds of 15 and 24 mph, which were wind speeds not previously examined. To verify the dependence of convective heat loss upon receiver tilt angle, the 24-mph tests were conducted for receiver tilt angles from 0° to 90° at 15° increments, instead of the 30° increments previously examined. Additional tests were also conducted with a 24-mph wind using a 6-inch aperture, instead of the nominal 18-inch aperture, in order to determine if the same trends occur for a different aperture size.

The results from these three additional test sets are shown in Figure 16, along with the results from head-on wind tests from the first test series. The results from the additional tests are shown as bold lines whereas the original head-on test results are shown as plain lines. By examining this figure, it can be seen that the results from the additional tests follow the same trends as the original test data. The curvatures of all of the curves are negative at 30° receiver tilt angle and positive at 60° tilt angle. The trend is best seen in the 24-mph, 18-inch-aperture curve, where data are plotted at 15° increments. The consistency of these additional data to the original data suggests that the measured convective heat losses for head-on winds are representative of the physical phenomena and are not gross experimental error.

Figure 15. Increased convective heat loss from receiver due to head-on wind, i.e., total convective heat loss minus natural convective heat loss (530°F receiver temperature).

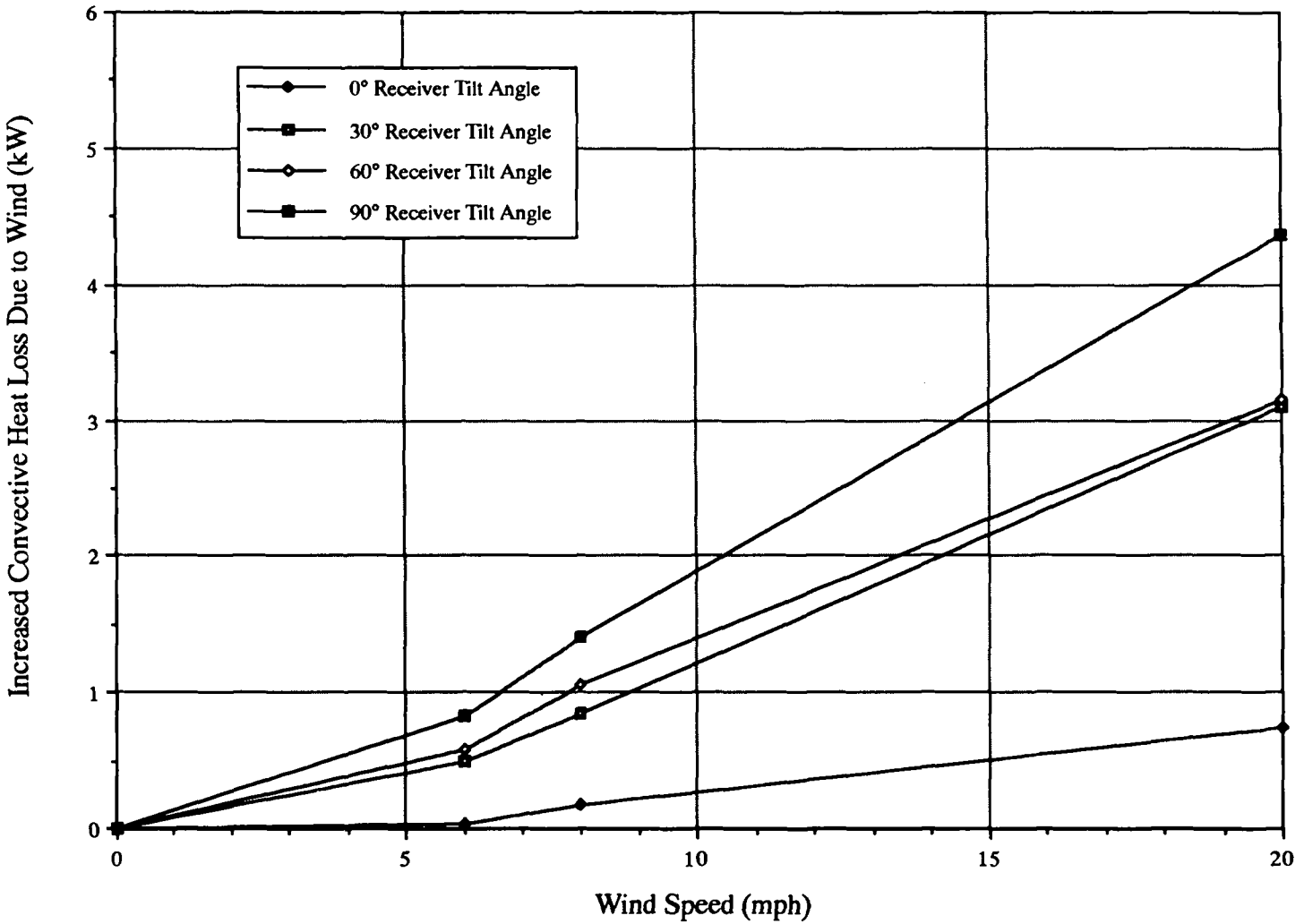

Figure 16. Convective heat loss results from all head-on wind tests (530°F receiver temperature).

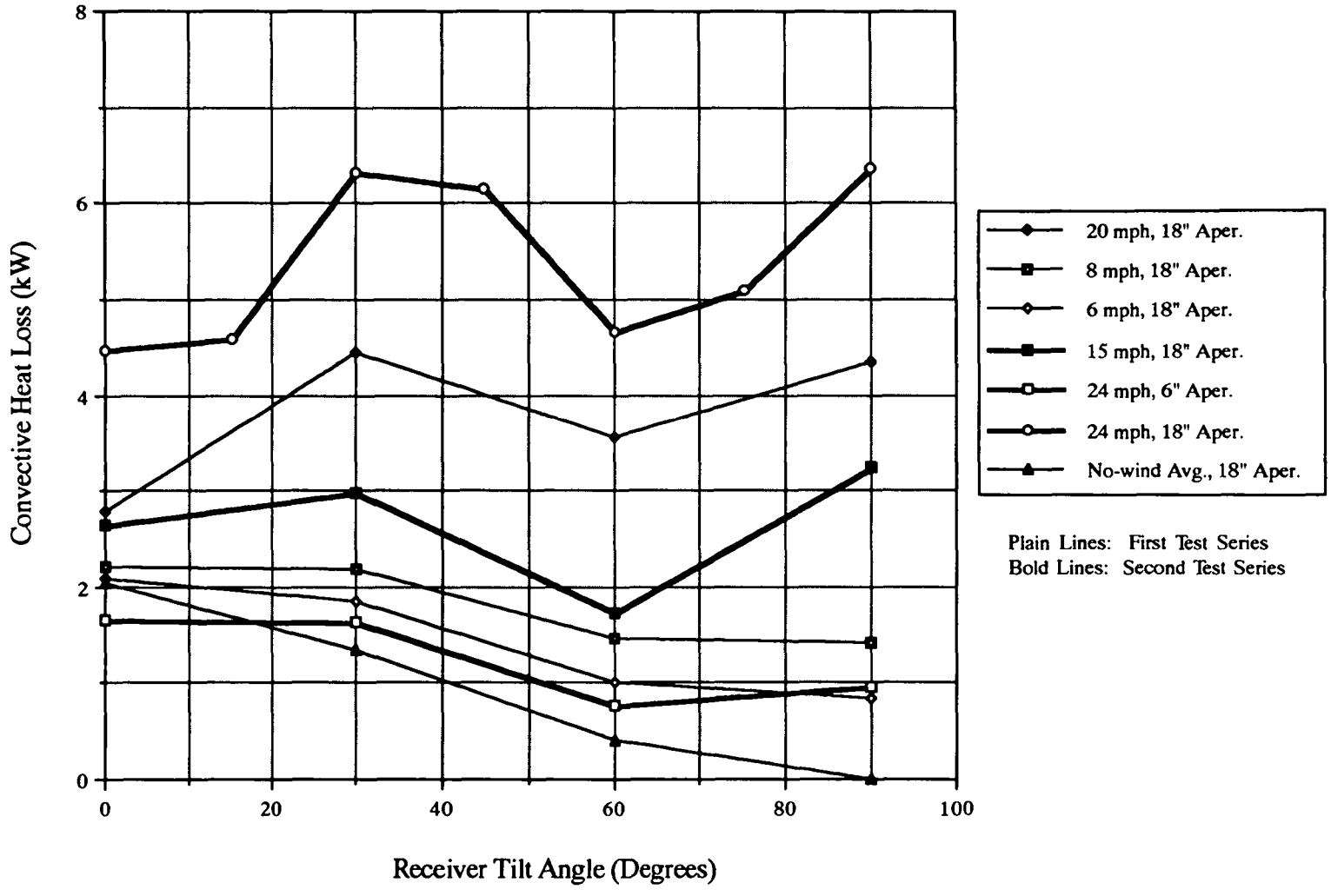

For head-on winds, it is a more difficult problem to separate natural and forced convection components. The natural and forced components are aiding since the total convective heat loss is greater than natural convection alone, but the forced and natural components are probably not additive. However, a correlation of the form

$$\bar{h}_{overall} = \bar{h}_{natural} + \bar{h}_{forced} \tag{13}$$

is a convenient form for a design correlation, especially considering the modest level of understanding that currently exists. With the assumption that natural and forced components are additive, a curve-fit of the increased convective heat loss due to head-on wind is

$$\bar{h}_{forced} = f(\theta)\, V^{1.401} \tag{14}$$

where

$$f(\theta) = 0.1634 + 0.7498 \sin \theta - 0.5026 \sin 2\theta + 0.3278 \sin 3\theta$$

$\bar{h}_{forced}$ = forced convection heat transfer coefficient, $W/(m^2 \cdot K)$
V = head-on wind velocity, m/s
θ = receiver tilt angle

Comparison of this correlation to the experimental data is given in Figures 17 and 18. The agreement between the predicted and experimental values is considered fair. This equation and Eq. (11) for side-on wind represent a relatively accurate correlation of wind effects on convective heat loss from the cavity receiver tested. They are not intended to be general equations for predicting convective heat loss from all cavity receivers since they are based on a limited number of data points. When more heat loss data become available, the correlations can be revised for broader application.

Figure 17. Comparison of increased convective heat loss due to head-on wind obtained experimentally and using the correlation of Eq. (14) (530°F receiver temperature).

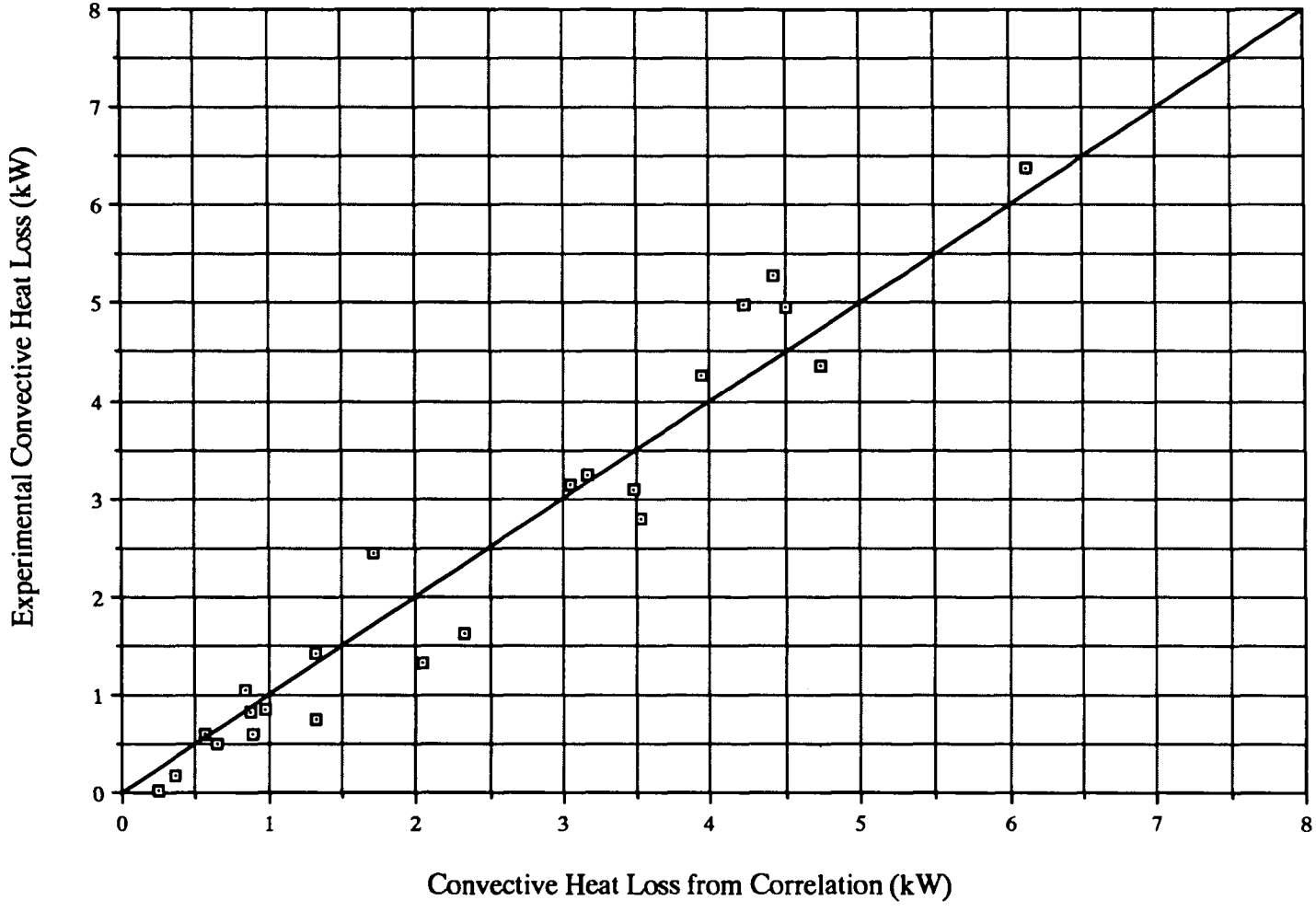

Figure 18. Increased convective heat loss due to head-on wind: experimental vs. correlation of Eq. (14) (530°F receiver temperature).

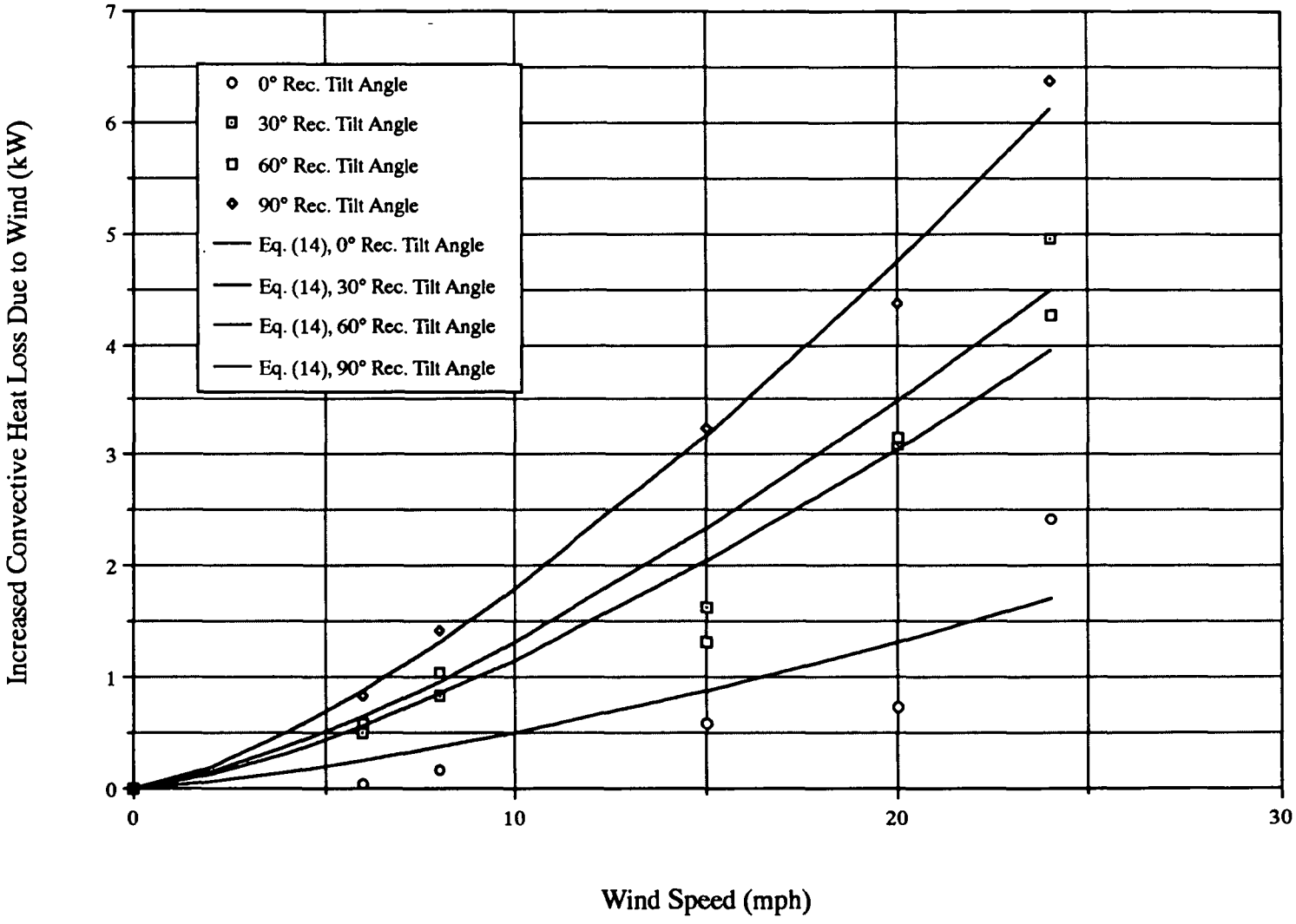

7.0 Analysis of Measured Air Temperatures and Average Internal Heat Transfer Coefficients

7.1 Measured Air Temperatures Inside Receiver

During each of the tests from the first test series, temperature measurements were made at various locations on the receiver in hope that they would provide useful information for the interpretation of convective heat loss results. The locations at which the temperature measurements were made are shown in Figure 19. A total of 26 thermocouples were used, most of which were located in representative forward and aft planes in the receiver. Twelve thermocouples were located in each plane, with three each being located at clock angles of 12, 3, 6, and 9. At each clock-angle location, three thermocouples were installed: one on the receiver outer surface, one on the heat transfer tubing facing the interior of the cavity, and one in the cavity airspace 1 in. (2.5 cm) from the heat transfer tubing. Two thermocouples were located at the receiver aft end.

Measured receiver temperatures from all of the tests are tabulated in Appendix D. Of particular interest are the air temperature measurements because they give special insight into some of the fluid and convective heat transport phenomena occurring for the different test conditions. The next several sections will discuss in detail these air temperature measurements. In all of the air temperature plots presented below, a vertical coordinate system is used as the independent variable because it was deemed most appropriate considering the fact that without wind, natural convective effects result in temperature gradients in this direction. A vertical location of zero corresponds to the horizontal plane passing through the top of the receiver aperture. This coordinate system is illustrated in Figure 20.

7.1.1 No-Wind Tests

Figures 21 through 24 show measured receiver air temperature versus vertical location within the receiver for all of the no-wind tests. The dependency of air temperature to vertical location inside the receiver, and the existence of a stagnant zone within the receiver, are clearly shown. With the receiver facing horizontally (0° tilt angle), air temperatures are only about 175°F at the bottom of the receiver, due to natural convective

Figure 19. Receiver thermocouple locations.

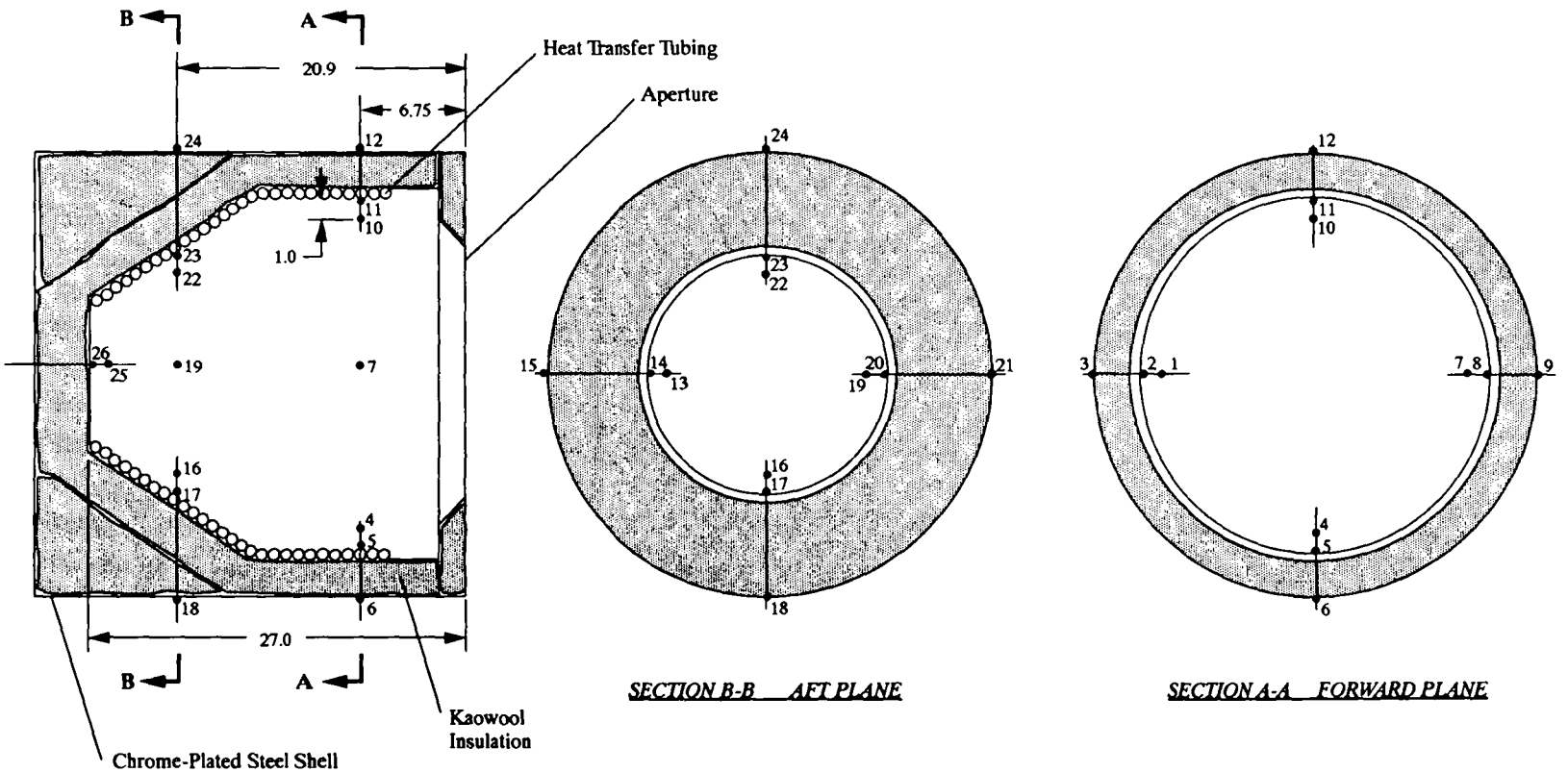

Figure 20. Vertical coordinate system used for plotting air temperatures inside receiver.

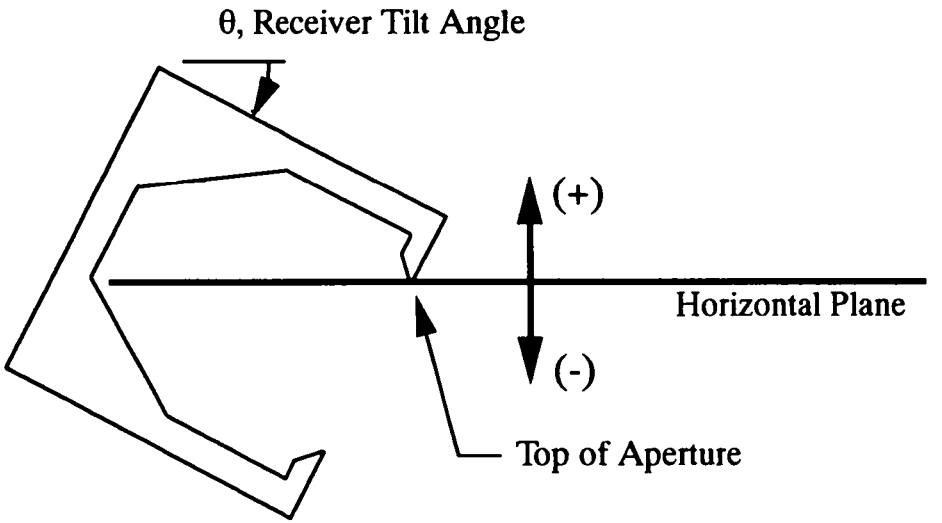

Figure 21. Air temperature as a function of vertical location in the receiver for receiver tilt angle of 0° and no wind (all six no-wind test sets).

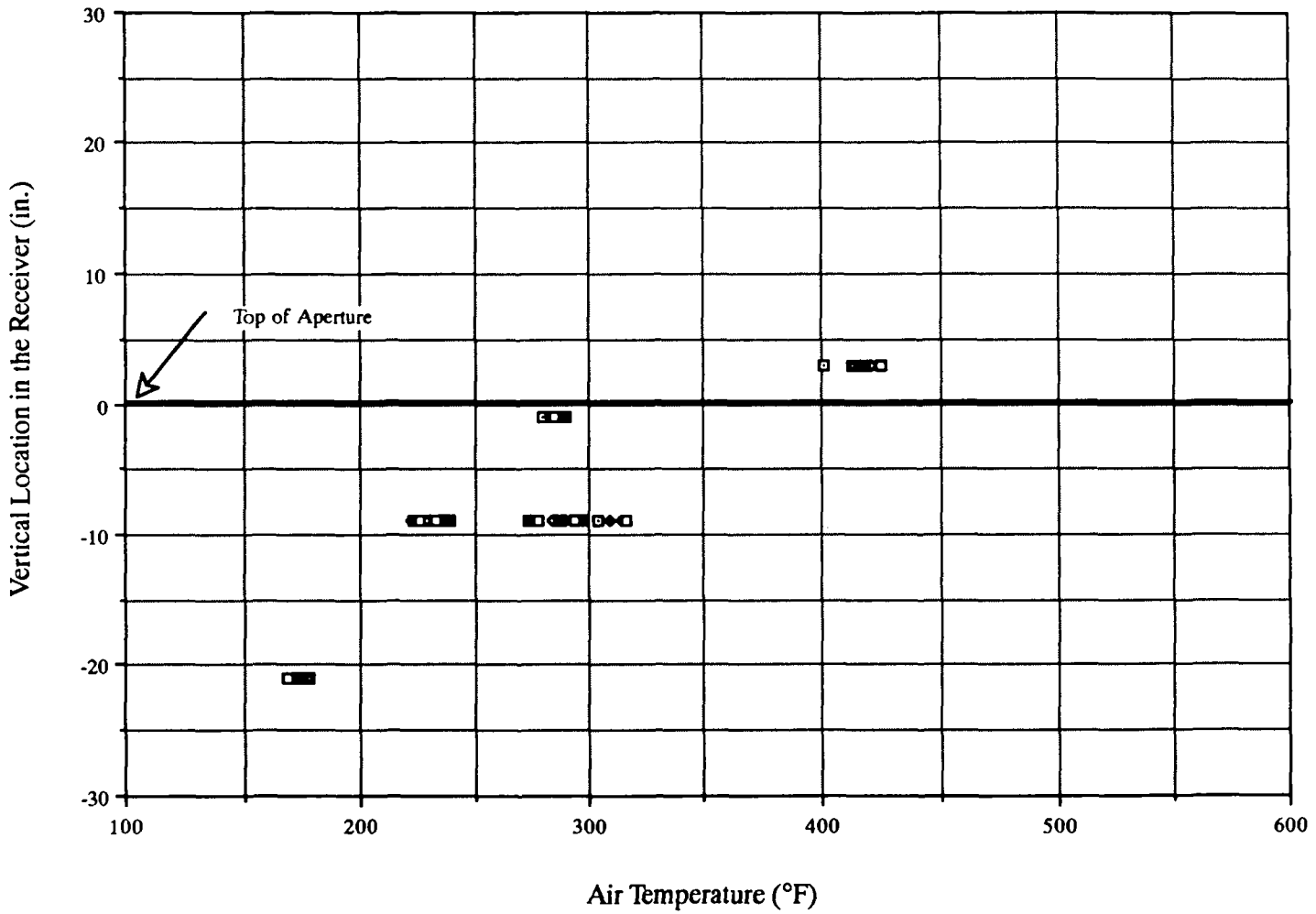

Figure 22. Air temperature as a function of vertical location in the receiver for receiver tilt angle of 30° and no wind (all six no-wind test sets).

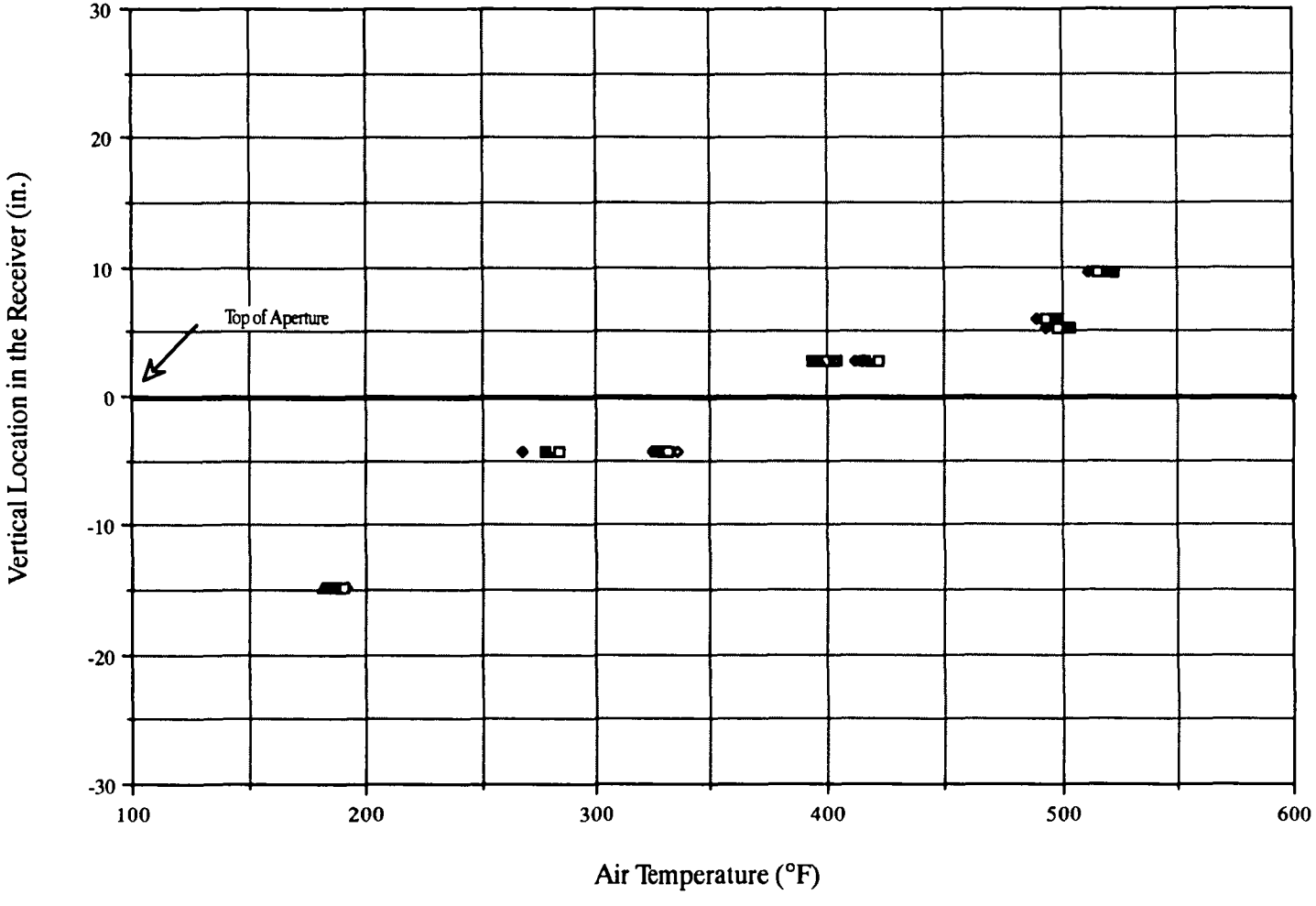

Figure 23. Air temperature as a function of vertical location in the receiver for receiver tilt angle of 60° and no wind (all six no-wind test sets).

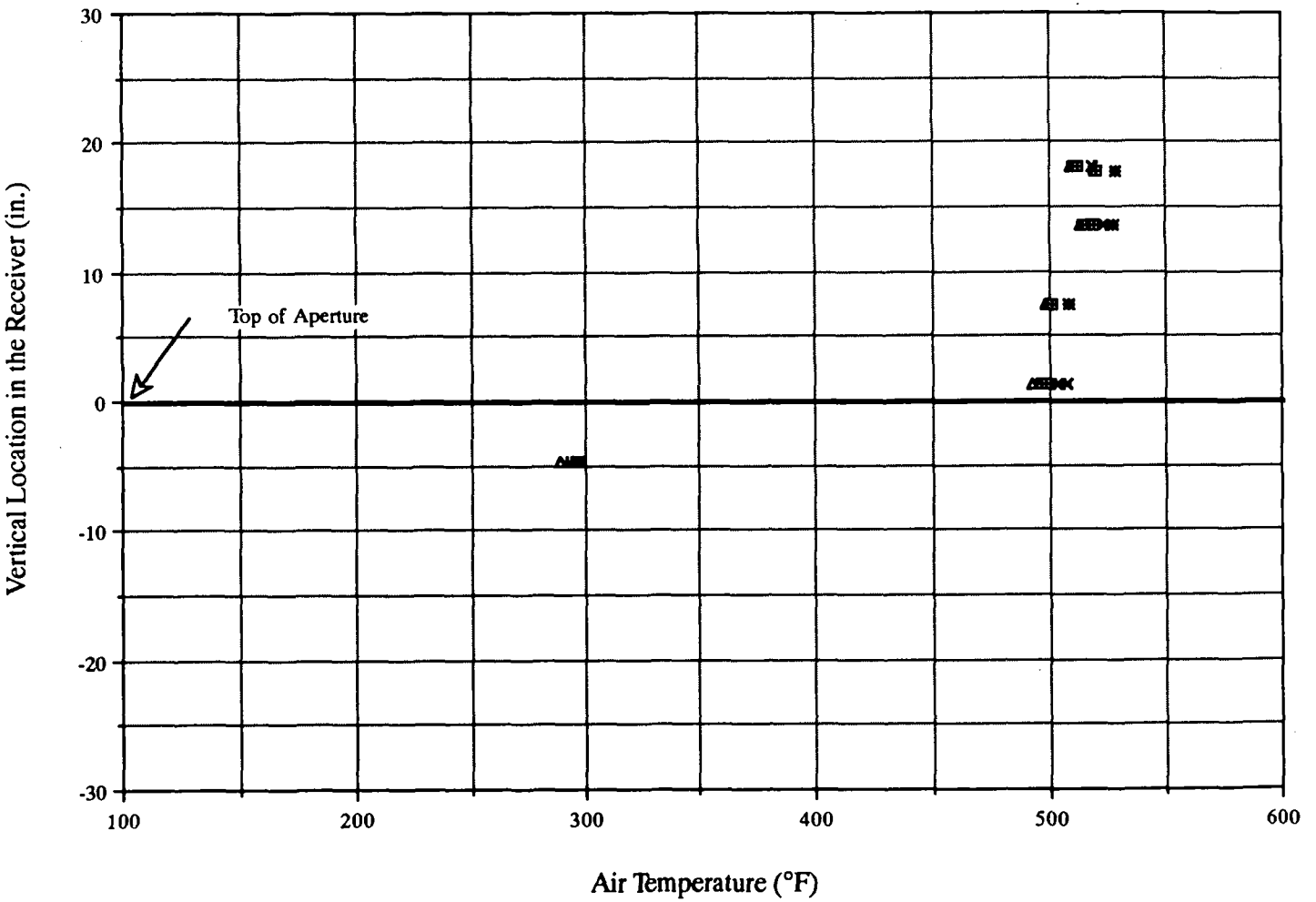

Figure 24. Air temperature as a function of vertical location in the receiver for receiver tilt angle of 90° and no wind (all six no-wind test sets).

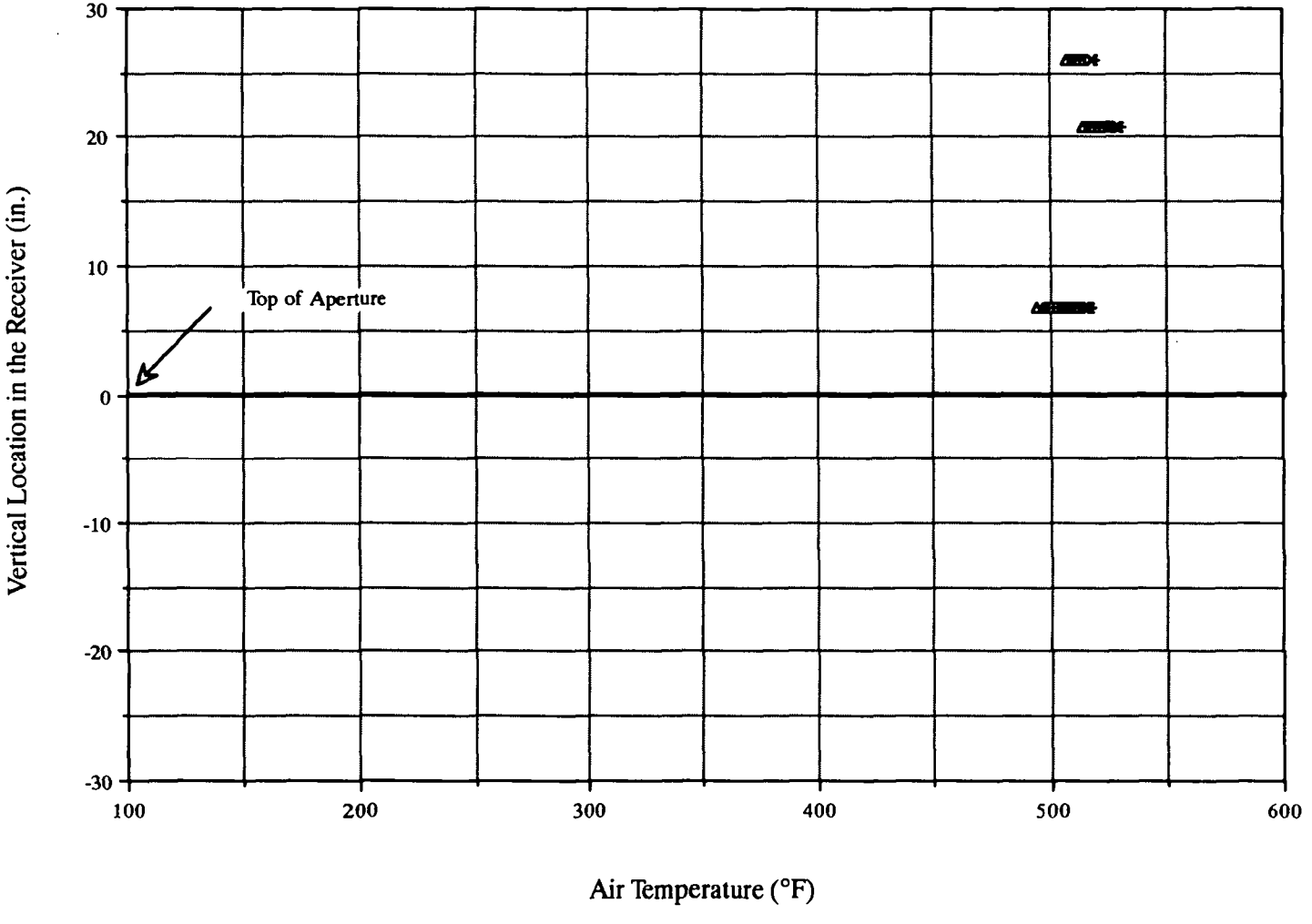

currents supplying cool outside air into the cavity. As the air is heated, it rises and becomes hotter as it absorbs more heat from the hot receiver internal surfaces. Above the top of the aperture plane (above y=0), the air is the hottest because it is stagnant since it has nowhere to escape (i.e., it is in the stagnant zone).

At 30° tilt angle, the temperature difference between the bottom and top of the receiver is larger than at 0° tilt angle because the temperatures in the stagnant zone are higher. The temperatures are less than 200°F at the bottom of the receiver, but are greater than 500°F at the top. The higher temperatures in the top portion of the receiver is most likely due to the fact that at this receiver tilt angle, the stagnant zone is larger than at 0° tilt angle. The larger stagnant zone is believed to result in less mixing between the relatively cooler air in the convective zone and the hotter air inside the stagnant zone, thus resulting in a higher-temperature stagnant zone.

At 60° tilt angle, the presence of the stagnant zone is very noticeable. Five inches below the plane passing through the top of the aperture, air temperatures are less than 300°F. However, at all of the vertical locations above the aperture plane, temperatures are generally above 500°F. This highlights the very strong vertical temperature gradients in the vicinity of the aperture plane. On the other hand, it shows that the temperatures in the bulk of the stagnant zone are essentially constant.

At 90° tilt angle, temperatures everywhere in the receiver are 500°F or above, because the entire cavity is in the so-called stagnant zone. Similar to the results at 60° tilt angle, air temperatures within the stagnant zone are essentially constant. Although no measurements were made near the aperture plane, it is reasonable to expect that very large vertical temperature gradients would exist there.

7.1.2 Side-on Wind Tests

Measured air temperatures for the side-on wind tests are shown in Figures 25 through 28. These temperatures are quite different than those for the no-wind condition. At a receiver tilt angle of 0°, the vertical temperature variation caused by natural convective effects is all but eliminated by the presence of side-on wind. The effects of wind are greatest for higher wind speeds, but are still significant at all wind speeds. For this

Figure 25. Air temperature as a function of vertical location in the receiver for receiver tilt angle of 0° and side-on winds.

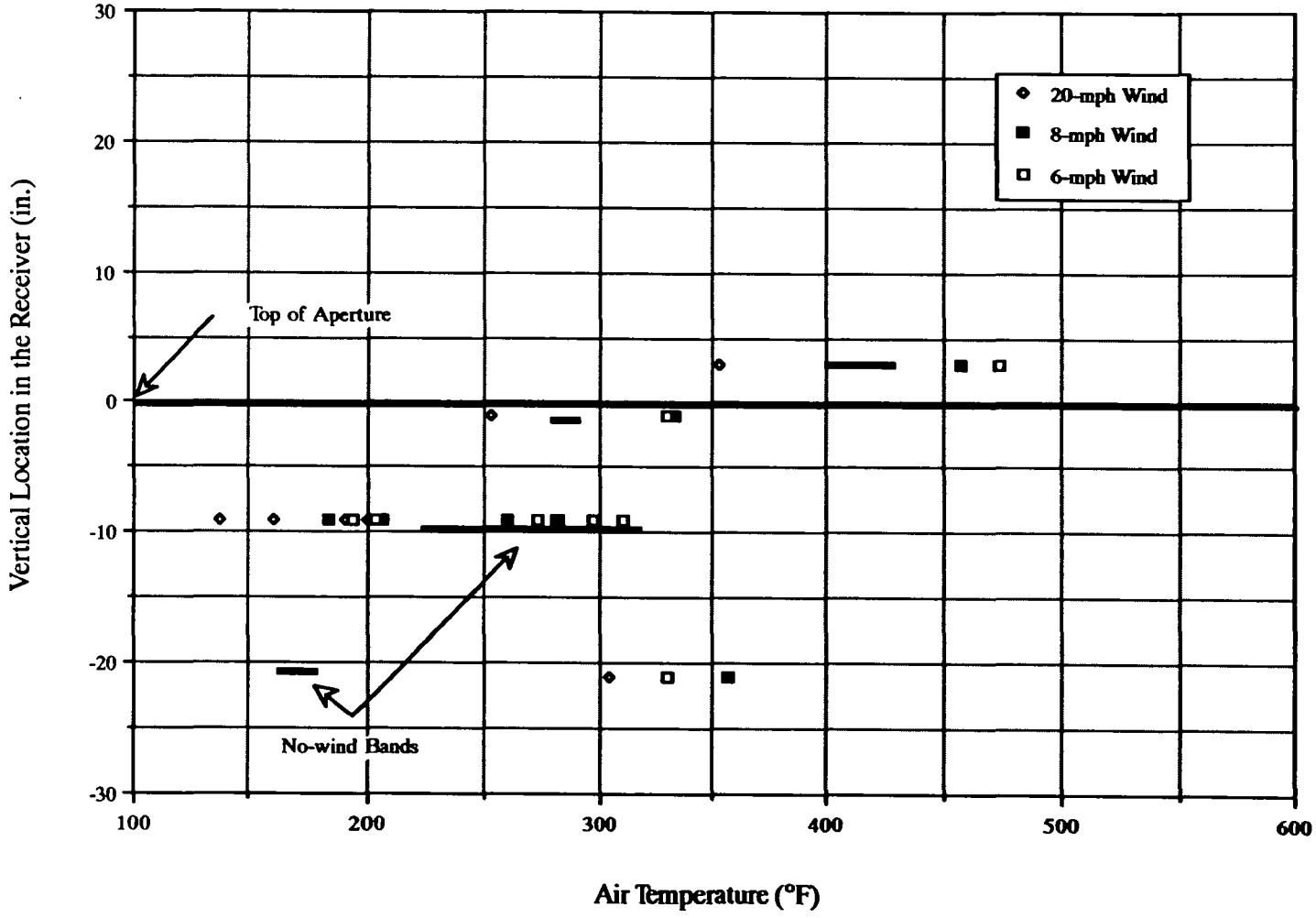

Figure 26. Air temperature as a function of vertical location in the receiver for receiver tilt angle of 30° and side-on winds.

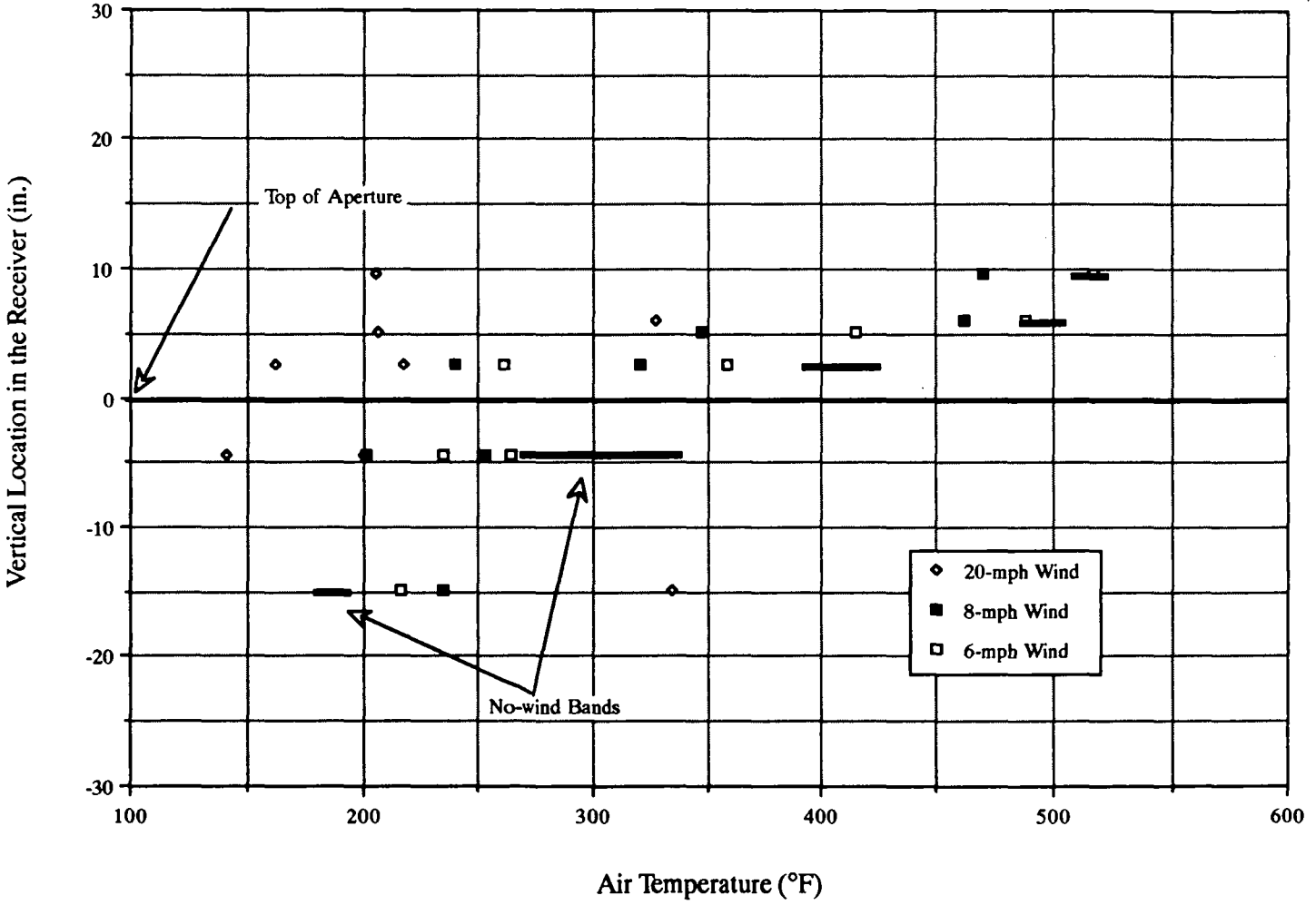

Figure 27. Air temperature as a function of vertical location in the receiver for receiver tilt angle of 60° and side-on winds.

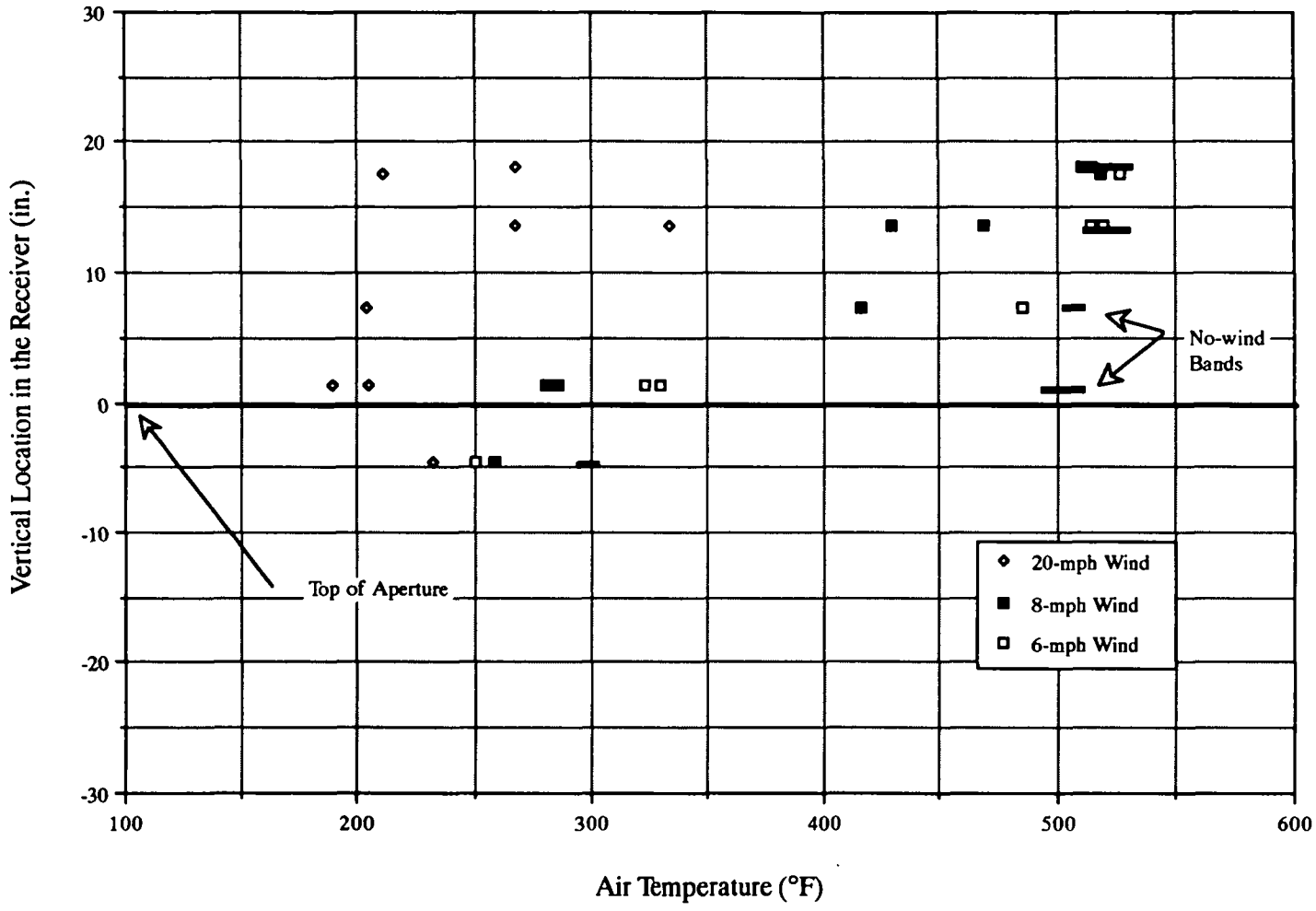

Figure 28. Air temperature as a function of vertical location in the receiver for receiver tilt angle of 90° and side-on winds.

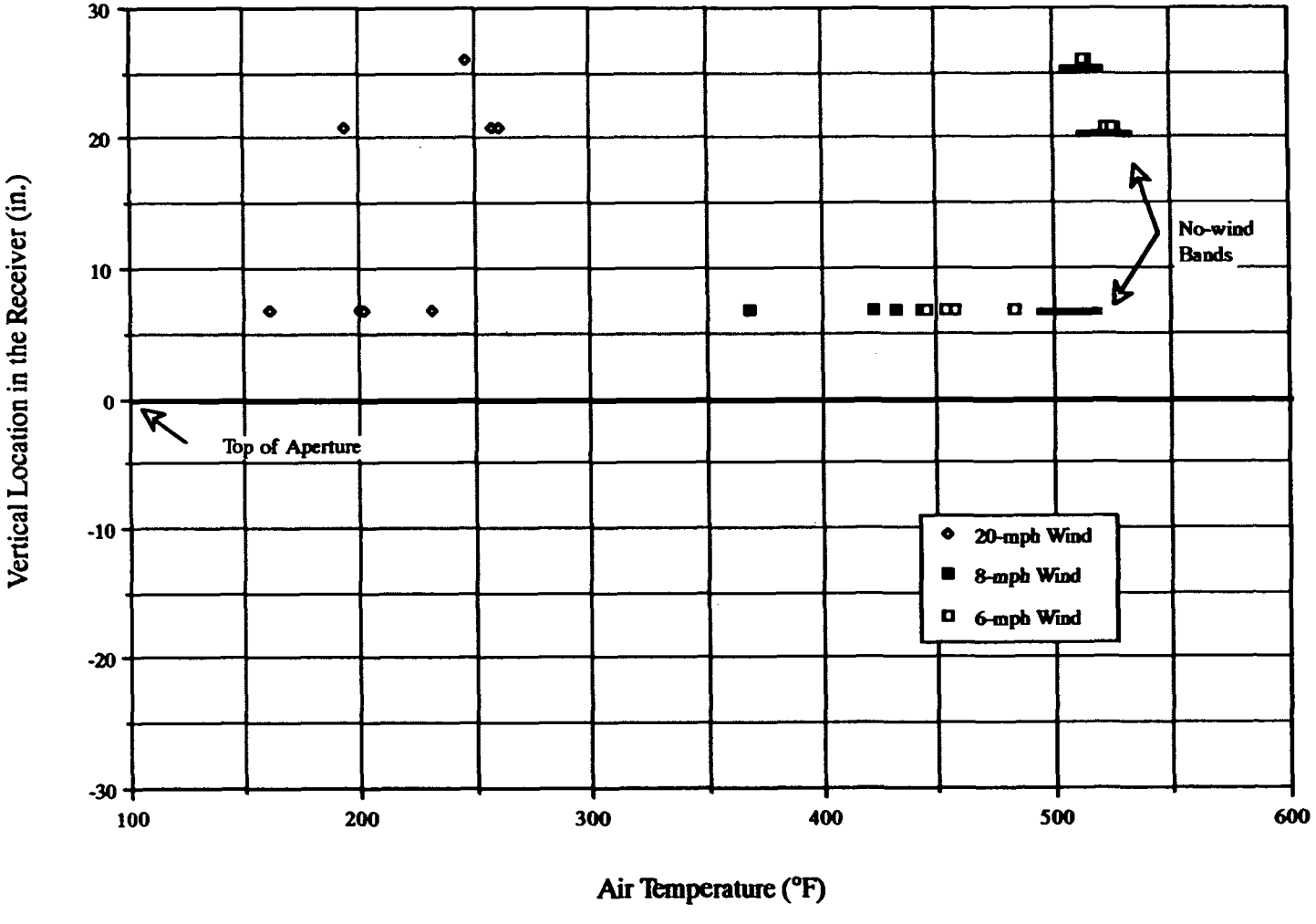

receiver tilt angle, it seems that the presence of side-on wind results in lower air temperatures at vertical locations the same as the aperture. This suggests that side-on wind causes forced convective currents in the mid-section of the receiver. It is interesting to note that although the temperatures in the receiver mid-section are lower than those occurring without wind, the temperatures in the top and bottom portions of the receiver are generally higher for side-on winds than for no wind at all. This is thought to be a result of forced convective currents within the receiver mid-section actually impeding the natural convective currents normally present in the lower and top portions of the receiver.

At 30° tilt angle, the effects of wind are noticeable, but are harder to interpret due to the more complicated receiver-orientation/wind-direction geometric relationship. Lower temperatures in the receiver vertical mid-section can be seen, but are not as distinct as those occurring for 0° tilt angle. For lower wind speeds, the air temperatures are not too far from those occurring without wind. Vertical temperature gradients can be seen and it appears that stagnant zones are being formed near the top of the receiver. However, for 20-mph wind, air temperatures virtually everywhere in the receiver are much lower than those occurring without wind.

At 60° tilt angle, the extent to which the air temperatures are lower than those without wind is dependent upon wind speed. For a 6-mph wind, temperatures in the top 10 inches of the receiver are 480-530°F, indicating that the air in that region is stagnant. At the same time, air temperatures nearer to the aperture plane are much lower, indicating that forced convective currents are present. For a 20-mph wind, forced convective currents are present everywhere in the cavity, as is evident by the low air temperatures and the lack of any distinct vertical temperature gradients.

At 90° tilt angle, the effects of wind are obvious. At wind speeds of 6 and 8 mph, wind effects are only seen near the aperture. Air temperatures slightly above the aperture plane are about 100°F less than the temperatures in the stagnant zone. However, for a 20-mph wind, air temperatures are low everywhere in the receiver, which indicates that higher-speed wind induces strong air circulation everywhere in the receiver.

7.1.3 Head-on Wind Tests

Measured air temperatures from the head-on wind tests are shown in Figures 29 through 32. For a receiver tilt angle of 90°, air temperatures are fairly similar to those for side-on winds. This is reasonable considering that head-on and side-on winds are essentially the same for this receiver tilt angle. The only significant difference in the air temperatures for the two wind directions is that it appears as though low-speed head-on wind has a larger effect in reducing air temperatures near the aperture plane. This effect may be caused by the fact that the receiver mount acts as a flow obstruction for side-on wind, but not for head-on wind.

For receiver tilt angles of 30° and 60°, the effects of wind are again dependent upon wind speed. It can be seen that the effects of low-speed winds are only moderate, with vertical temperature gradients still apparent. For a wind speed of 20 mph, however, air temperatures are much lower than those occurring without wind, and no distinct temperature gradient can be seen.

For a receiver tilt angle of 0°, the air temperatures are very similar to those occurring without wind. This is probably due to the fact that wind blowing directly into the aperture of the receiver, although creating a high pressure region near the aperture, does not create any asymmetrical flow which seems to be the most efficient for transporting air into and out of the receiver. In addition, this type of head-on flow does not appear to induce significant air currents inside the cavity. These reasons are a likely explanation for why head-on wind convective heat loss at 0° tilt angle is not much higher than that occurring without wind.

7.2 Average Air Temperatures and Internal Heat Transfer Coefficients

To gain additional insight into receiver forced convection, it is useful to examine average air temperatures within the cavity and to calculate an average internal heat transfer coefficient for each of the tests. These average internal heat transfer coefficients are based on the difference between the receiver inner wall temperature and the average air temperature inside the receiver. As such, they are only for the purpose of analyzing the convective heat loss phenomena and should not to be used for design purposes. The average air temperature is a straight numerical average of all temperature measurements in

Figure 29. Air temperature as a function of vertical location in the receiver for receiver tilt angle of 0° and head-on winds.

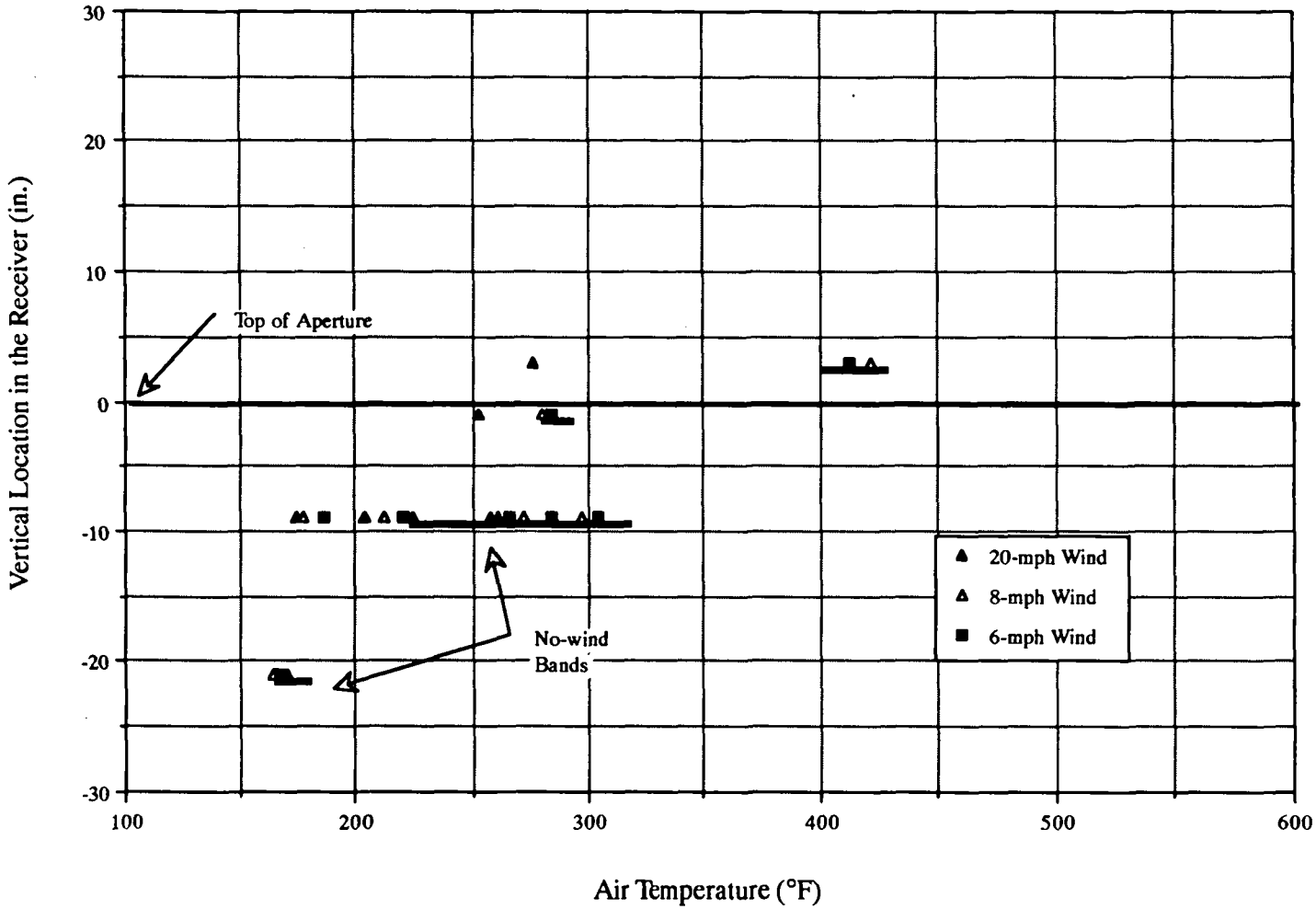

Figure 30. Air temperature as a function of vertical location in the receiver for receiver tilt angle of 30° and head-on winds.

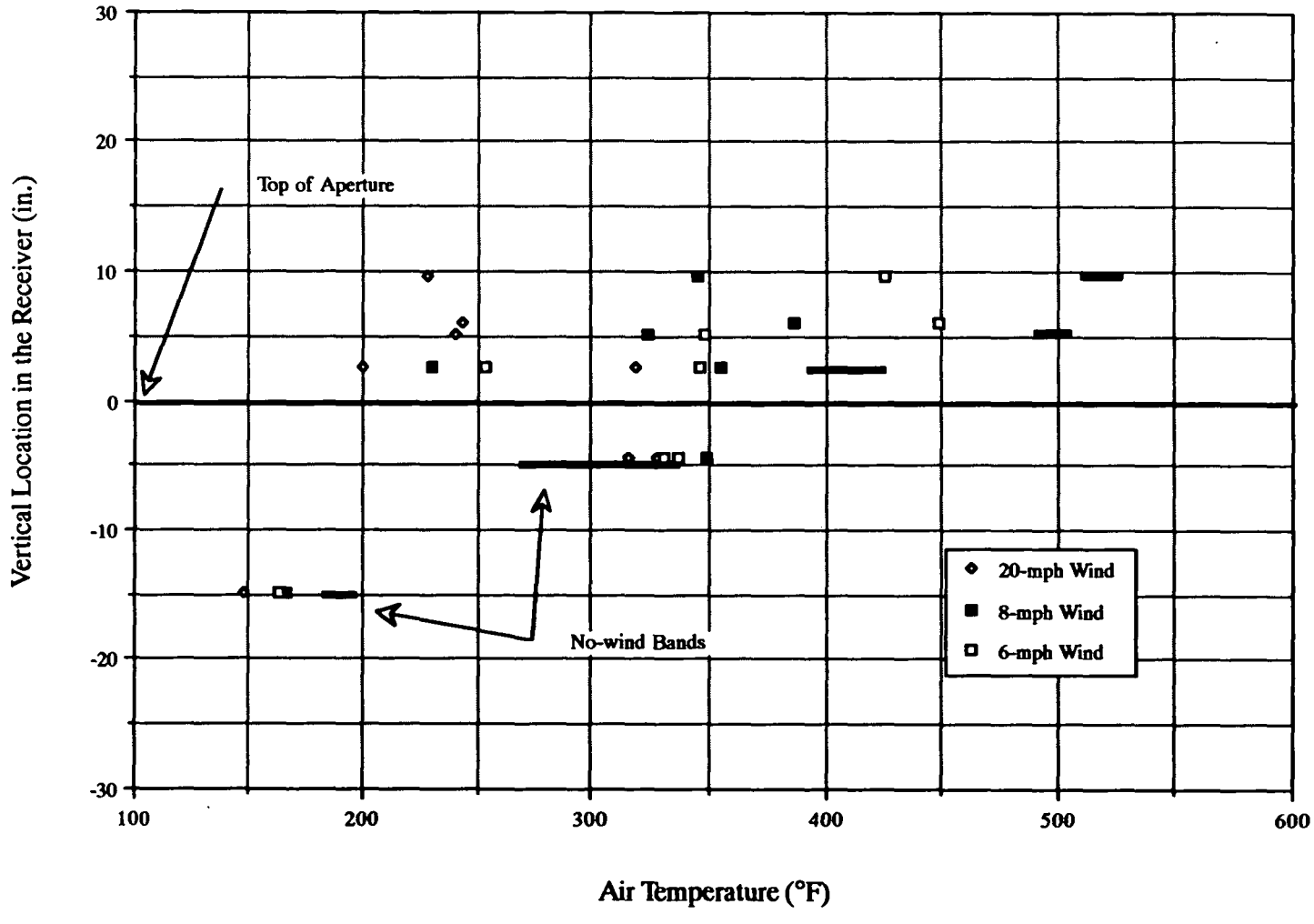

Figure 31. Air temperature as a function of vertical location in the receiver for receiver tilt angle of 60° and head-on winds.

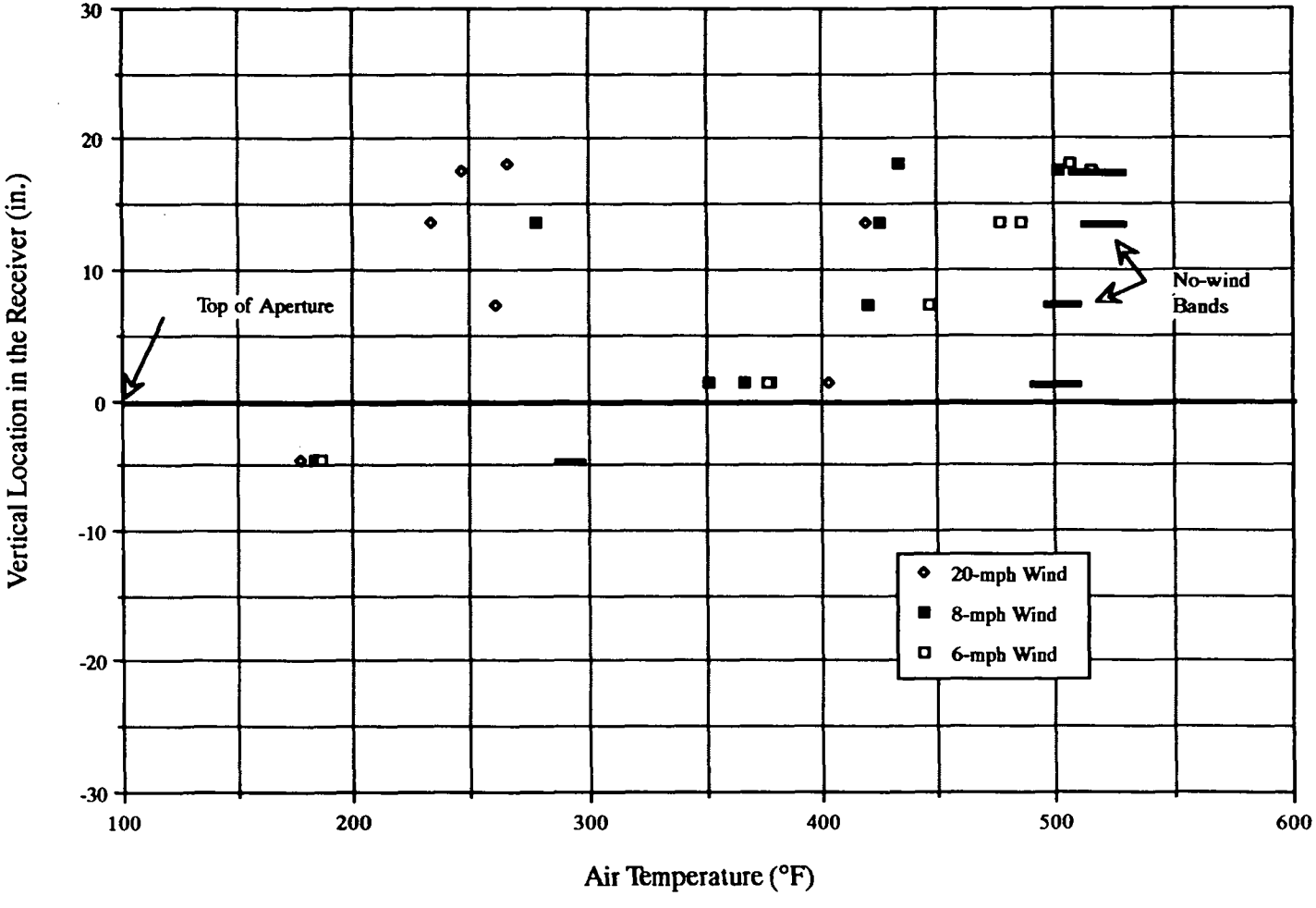

Figure 32. Air temperature as a function of vertical location in the receiver for receiver tilt angle of 90° and head-on winds.

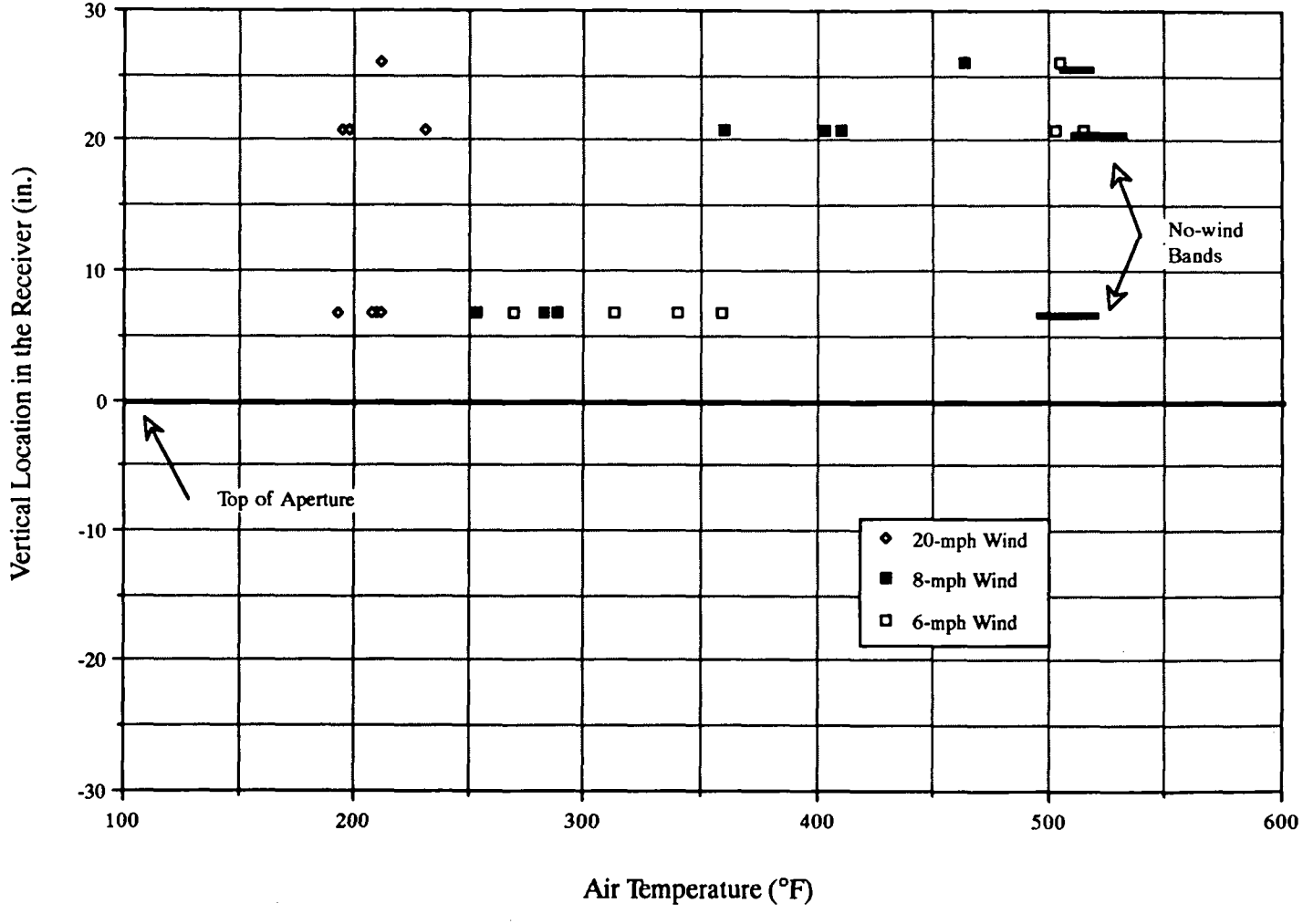

the receiver cavity airspace. It is neither an area-average nor a volume-average because the area or volume associated with a particular thermocouple measurement is undefined. However, the calculated average temperature is considered representative since the thermocouples are spaced fairly evenly.

The average internal heat transfer coefficient is based on the receiver convective heat loss and the difference between the average inner-wall temperature and average air temperature inside the cavity:

$$\bar{h}_{avg\ internal} = \frac{q_{conv}}{A(T_{avg\ i.s.} - T_{avg\ air})} \tag{15}$$

where

$\bar{h}_{avg\ internal}$ = average internal heat transfer coefficient

q_{conv} = receiver convective heat loss rate

A = full interior geometric surface area of receiver

$T_{avg\ i.s.}$ = average inner-surface temperature from measurements

$T_{avg\ air}$ = average cavity air temperature from measurements

In a broad sense, the average air temperature inside the cavity is an indication of how well fresh air is replenished inside the receiver. The average internal heat transfer coefficient is an indication of how well heat is transferred from the receiver inner surfaces to the air inside the receiver, i.e., the extent of air circulation inside the receiver.

7.2.1 No-Wind Tests

Figure 33 shows the average air temperature inside the receiver plotted against receiver tilt angle for all six of the no-wind test sets. The temperatures from the six sets agree very well with one another, indicating that the repeatability of the no-wind tests is good. As the receiver is tilted downward (as tilt angle increases), the average air temperature inside the receiver increases. This trend is consistent with the hypothesis that a stagnant zone exists inside the receiver, increasing in size as the receiver is tilted downward. The increase in receiver average air temperature corresponds to a decrease in the temperature differential between the receiver inner wall and the average air temperature, i.e., the driving potential for convective heat transfer decreases.

Figure 33. Average air temperatures inside receiver for the six no-wind test sets.

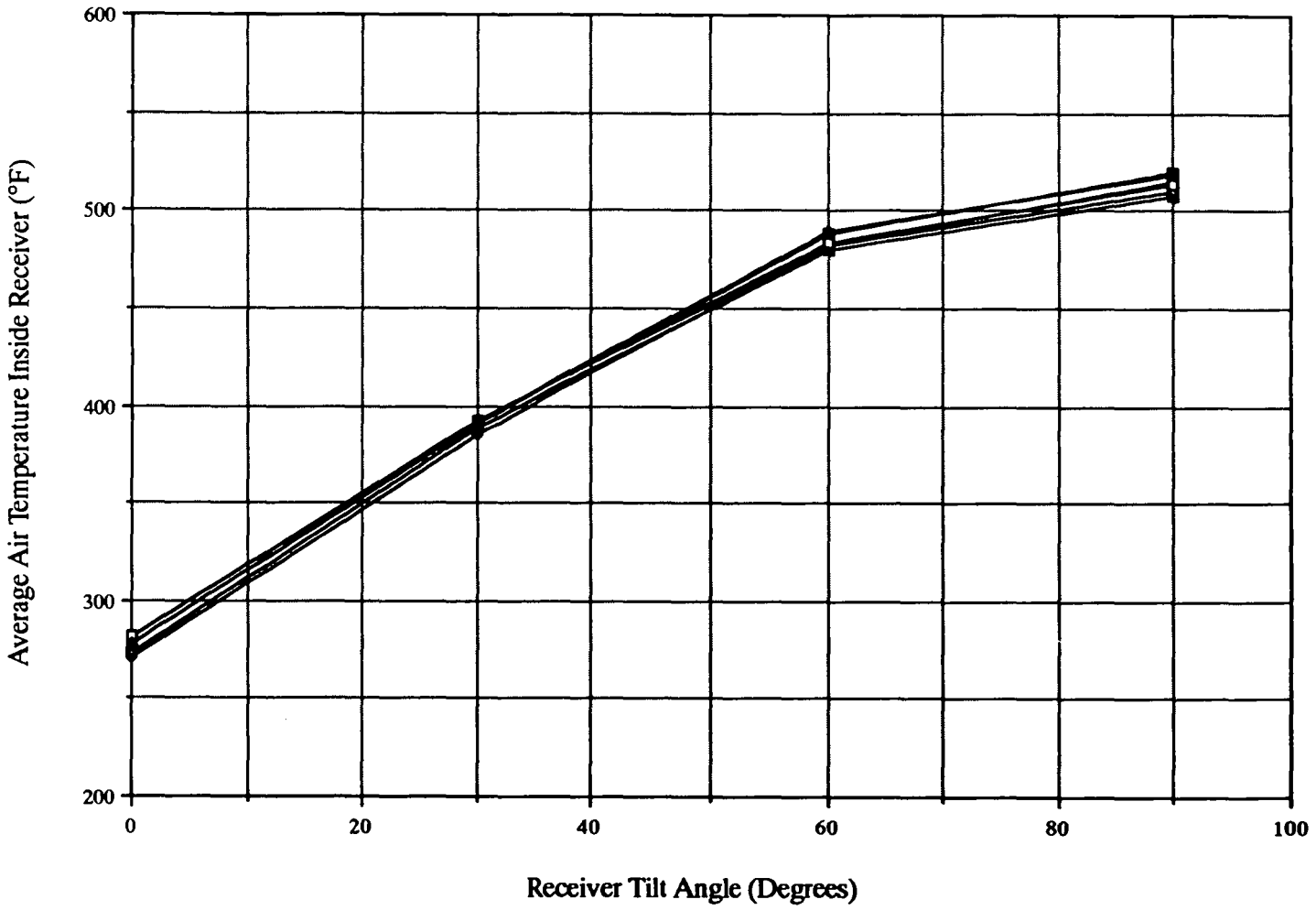

Figure 34 shows the average internal heat transfer coefficients for the no-wind tests. The heat transfer coefficients are approximately constant for all receiver tilt angles, except for a tilt angle of 90°, where natural convective heat transfer is presumably equal to zero. The high value of heat transfer coefficient at 60° tilt angle for one of the test sets appears to be anomalous, due to the fact that as convective heat loss and temperature difference become small, the quotient of these values becomes sensitive to data uncertainties.

The results shown in Figures 33 and 34 imply that between 0° and 60° tilt angle, natural convective heat loss decreases with increasing tilt angle because the stagnant zone within the receiver becomes larger and the average air temperature increases, not because of a decrease in the ability of heat to be transferred from the receiver inner wall to the air inside the receiver.

7.2.2 Side-on Wind Tests

Figure 35 shows the average air temperature inside the receiver versus receiver tilt angle for side-on winds. Increased wind speed generally results in decreased average air temperature. For wind speeds of 6 and 8 mph, the dependency of air temperature to receiver tilt angle still exists. This indicates that low-speed winds are not strong enough to overcome the existence of the stagnant zone and vertical temperature gradients. However, with a 20-mph wind, the average air temperature is independent of receiver tilt angle, which indicates that a stagnant zone no longer exists.

Note that the average air temperatures at low wind speeds and at a receiver tilt angle of 0° are actually higher than that occurring without wind. This is consistent with the observation made in the previous section that at this receiver tilt angle, side-on winds actually impede air circulation in the bottom and top portions of the receiver, thus resulting in relatively high air temperatures at those locations.

Figure 36 shows the average internal heat transfer coefficients for the side-on wind tests. The heat transfer coefficients increase as wind speed increases and as the receiver is tilted upward (from 90° to 0°). The increased heat transfer coefficient as wind speed

Figure 34. Average internal heat transfer coefficients for the six no-wind test sets.

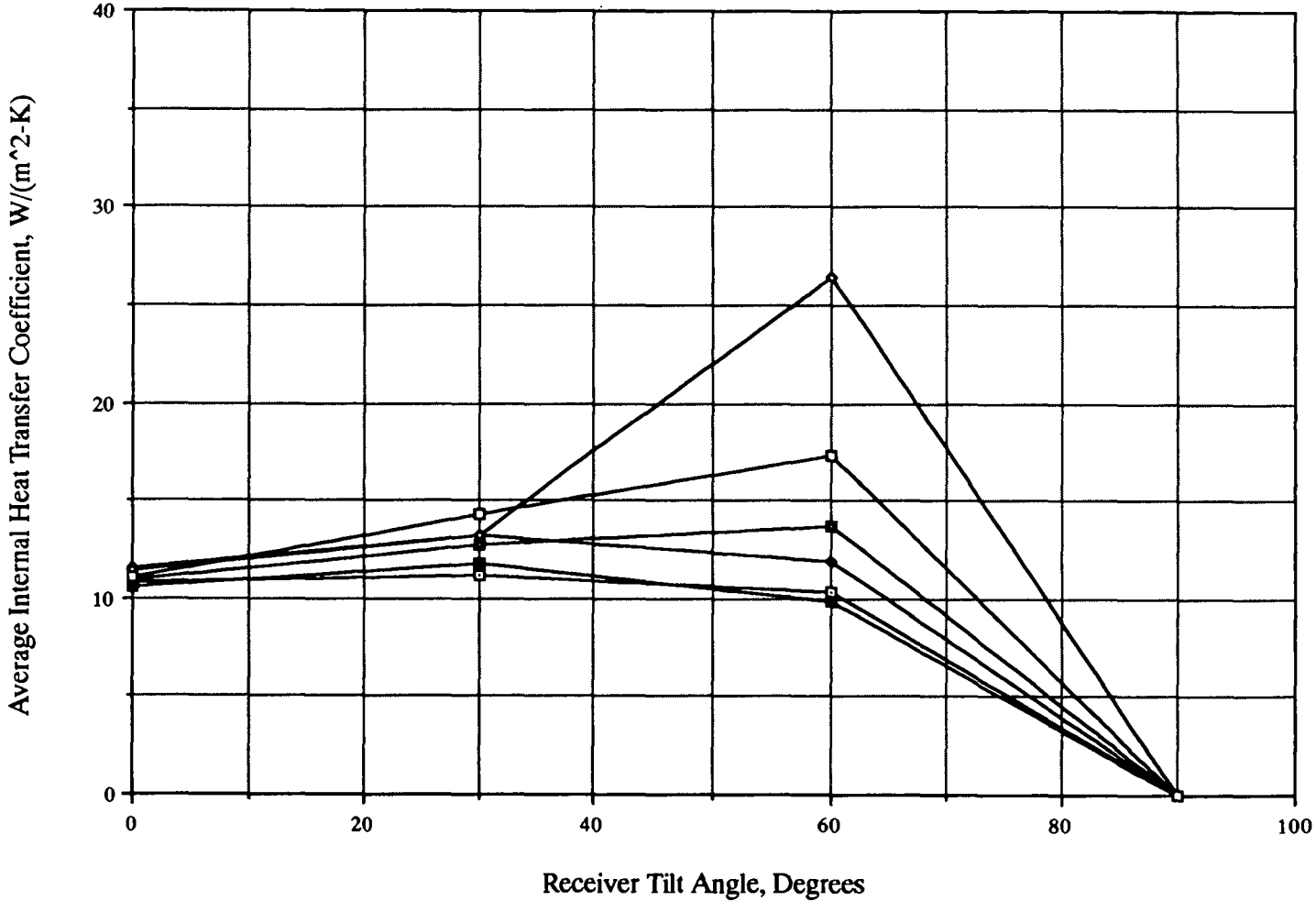

Figure 35. Average air temperatures inside receiver for side-on winds.

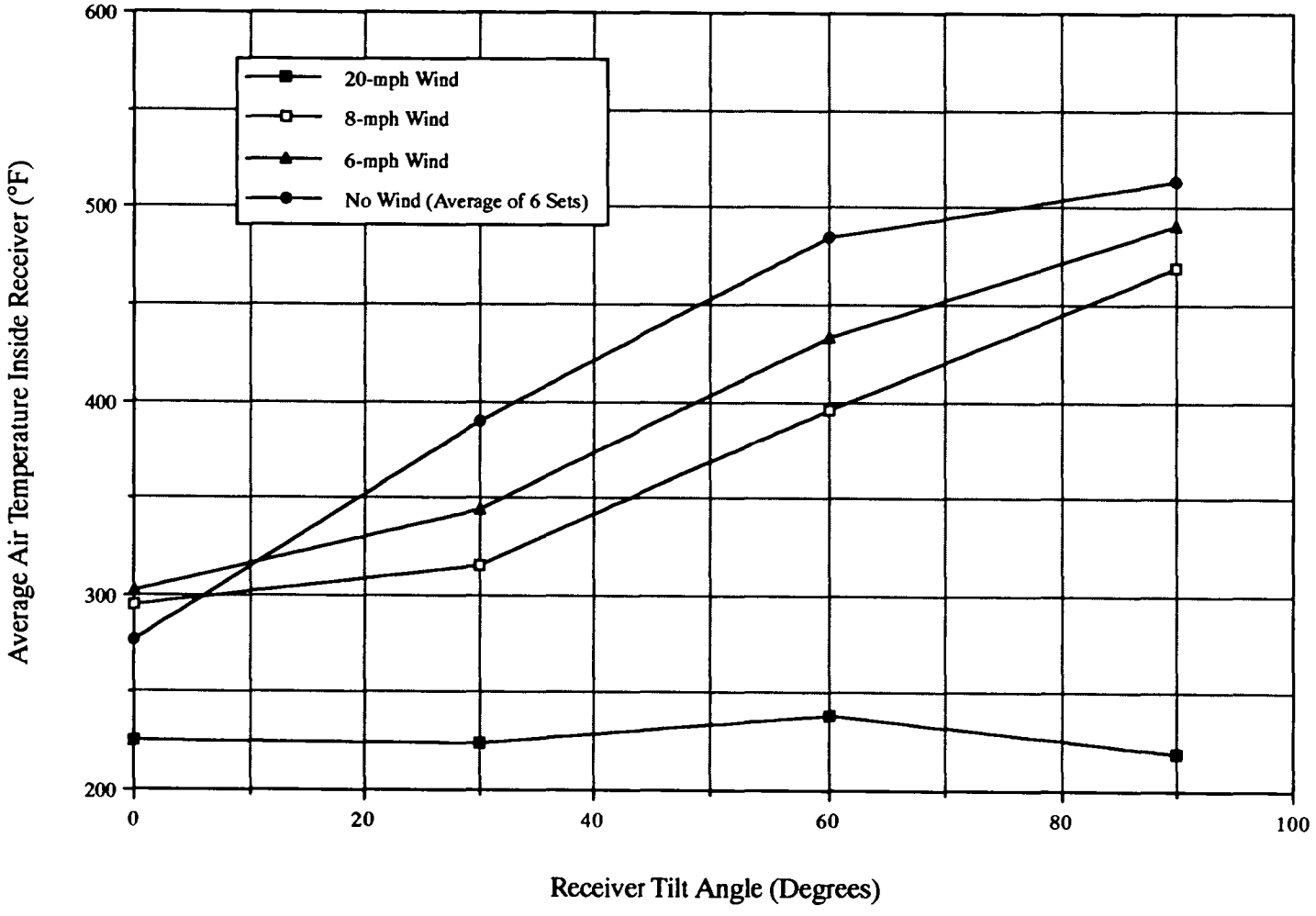

Figure 36. Average internal heat transfer coefficients for side-on winds.

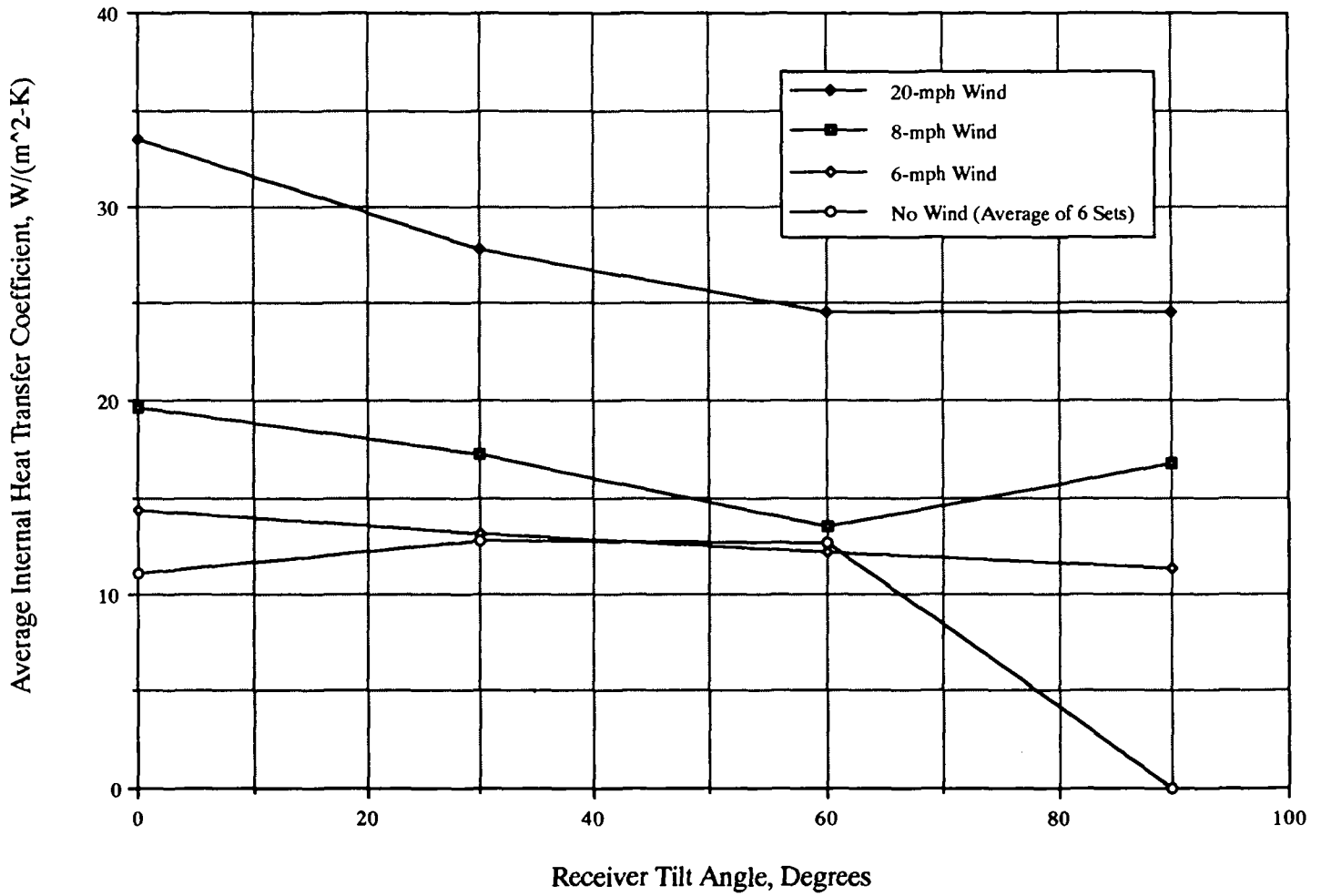

increases is a result of more vigorous air circulation within the receiver as the wind speed increases. The increased heat transfer coefficient as the receiver is tilted upward is somewhat surprising since it was shown previously that the average internal heat transfer coefficient without wind is essentially invariant with tilt angle, and because one would expect forced convection due to side-on wind to also be invariant with tilt angle.

7.2.3 Head-on Wind Tests

Figure 37 shows the average air temperatures for all of the head-on wind tests. Similar to side-on winds, higher wind speeds result in lower average air temperatures. For receiver tilt angles from 0° to 60°, the average air temperature increases for all wind speeds, because of stagnant zone effects. However, going from 60° to 90° tilt angle, the average air temperature inside the receiver decreases. This shows that wind blowing parallel to the aperture plane is relatively effective in replenishing the air inside the receiver.

The average internal heat transfer coefficients for the head-on wind tests are shown in Figure 38. Heat transfer coefficients increase slightly as the receiver is tilted upward from 90° to 30° tilt angle. However, as the receiver approaches 0° tilt angle (wind blowing directly into the receiver), the heat transfer coefficients decrease, especially at 20-mph wind speed. This shows that wind blowing directly into the receiver aperture does not cause strong convective currents within the receiver, which explains why convective heat loss is so low for this receiver-tilt-angle/wind-direction combination.

7.3 Hypothesized Flow Patterns In and Around the Receiver

The air temperature measurements and calculated internal heat transfer coefficients have provided insight into the physical nature of convective flow inside and near the receiver. Based on these results and overall convective heat losses, it is possible to hypothesize flow patterns for several of the different wind conditions and receiver tilt angles.

For the no-wind condition, the flow patterns for the different receiver tilt angles tested are shown in Figure 39. These flow patterns are consistent with past experimental findings for natural convection from cavity receivers. At 0° tilt angle (receiver facing

Figure 37. Average air temperatures inside receiver for head-on winds.

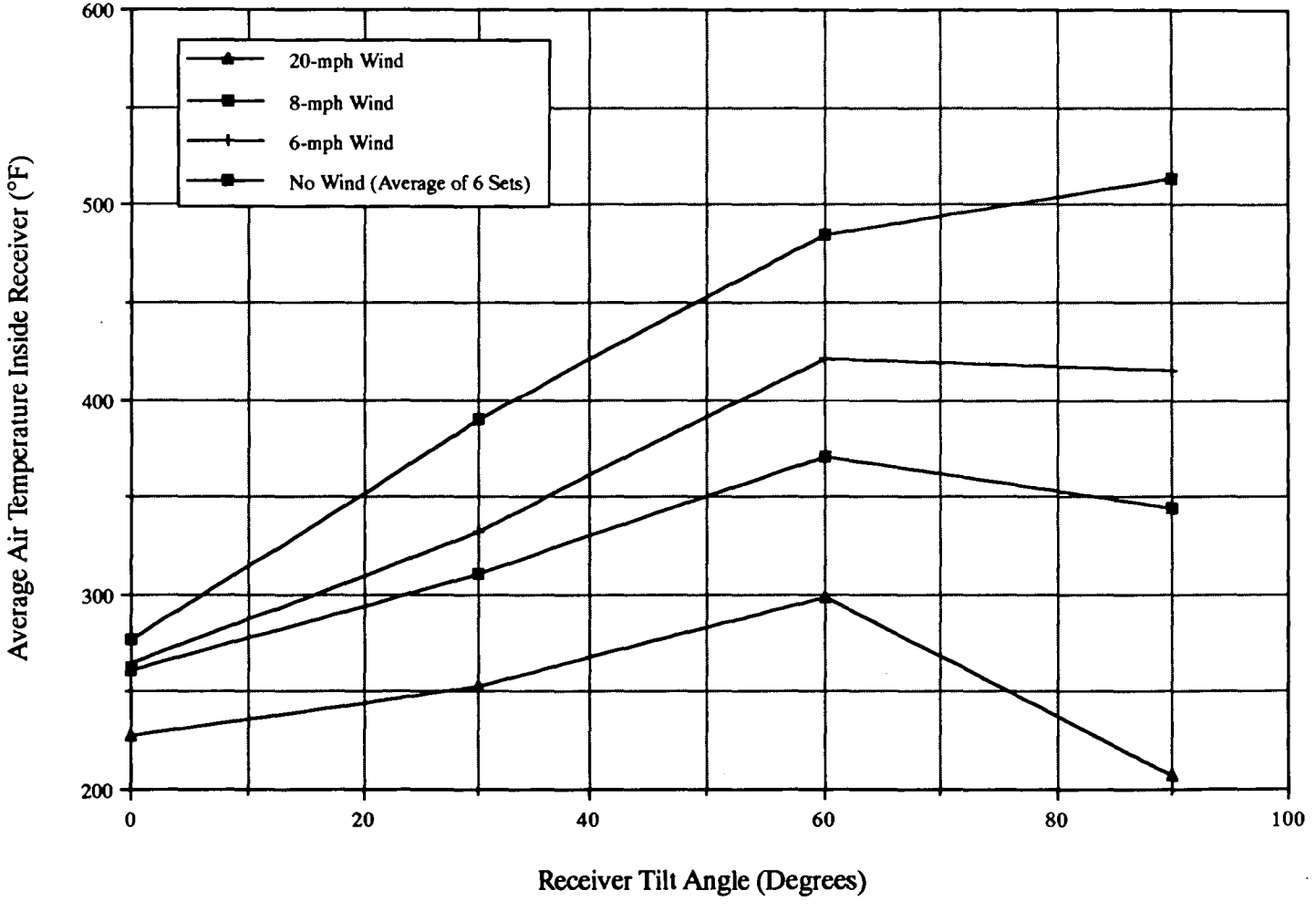

Figure 38. Average internal heat transfer coefficients for head-on winds.

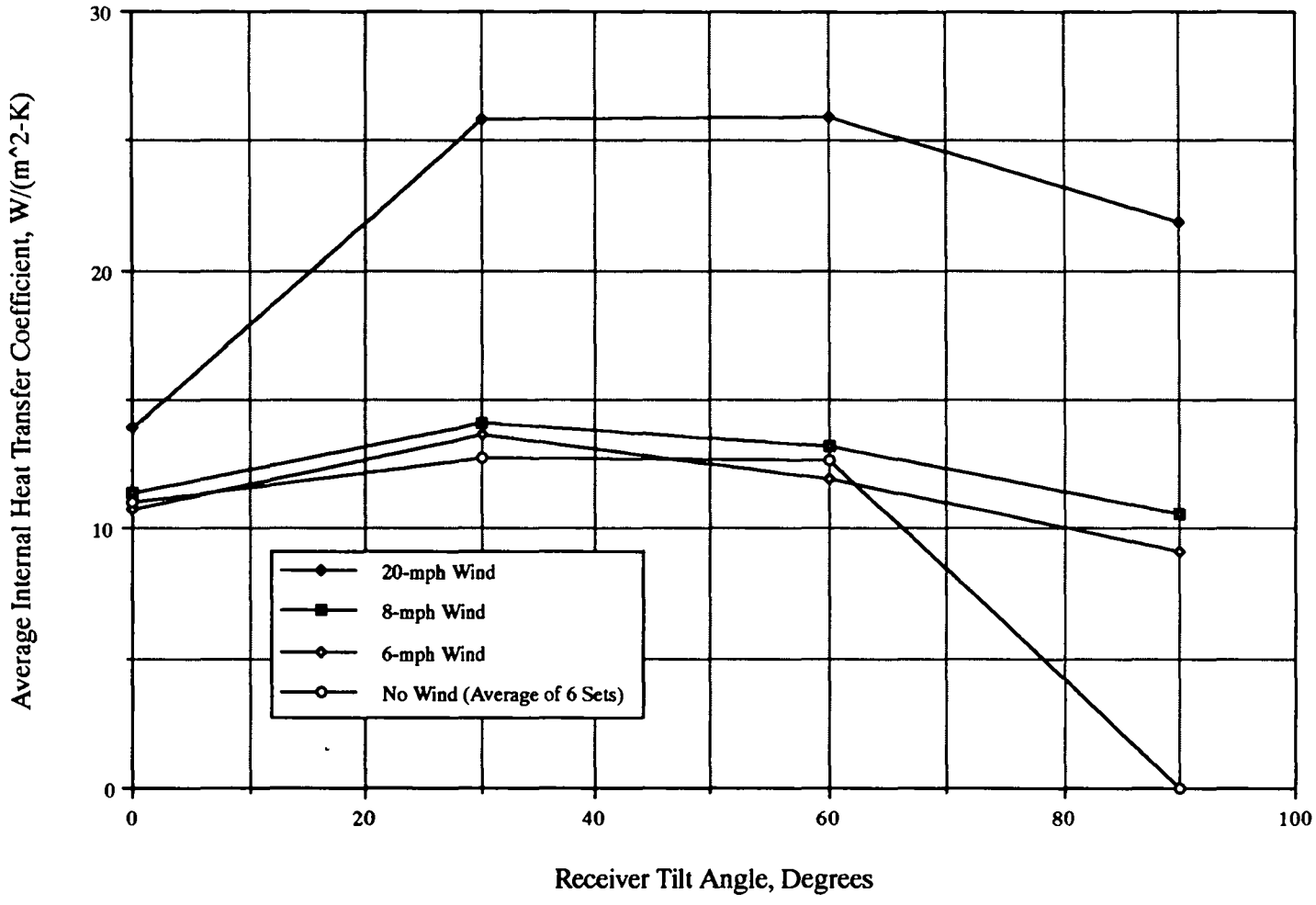

Figure 39. Illustration of natural convection from cavity receiver tested.

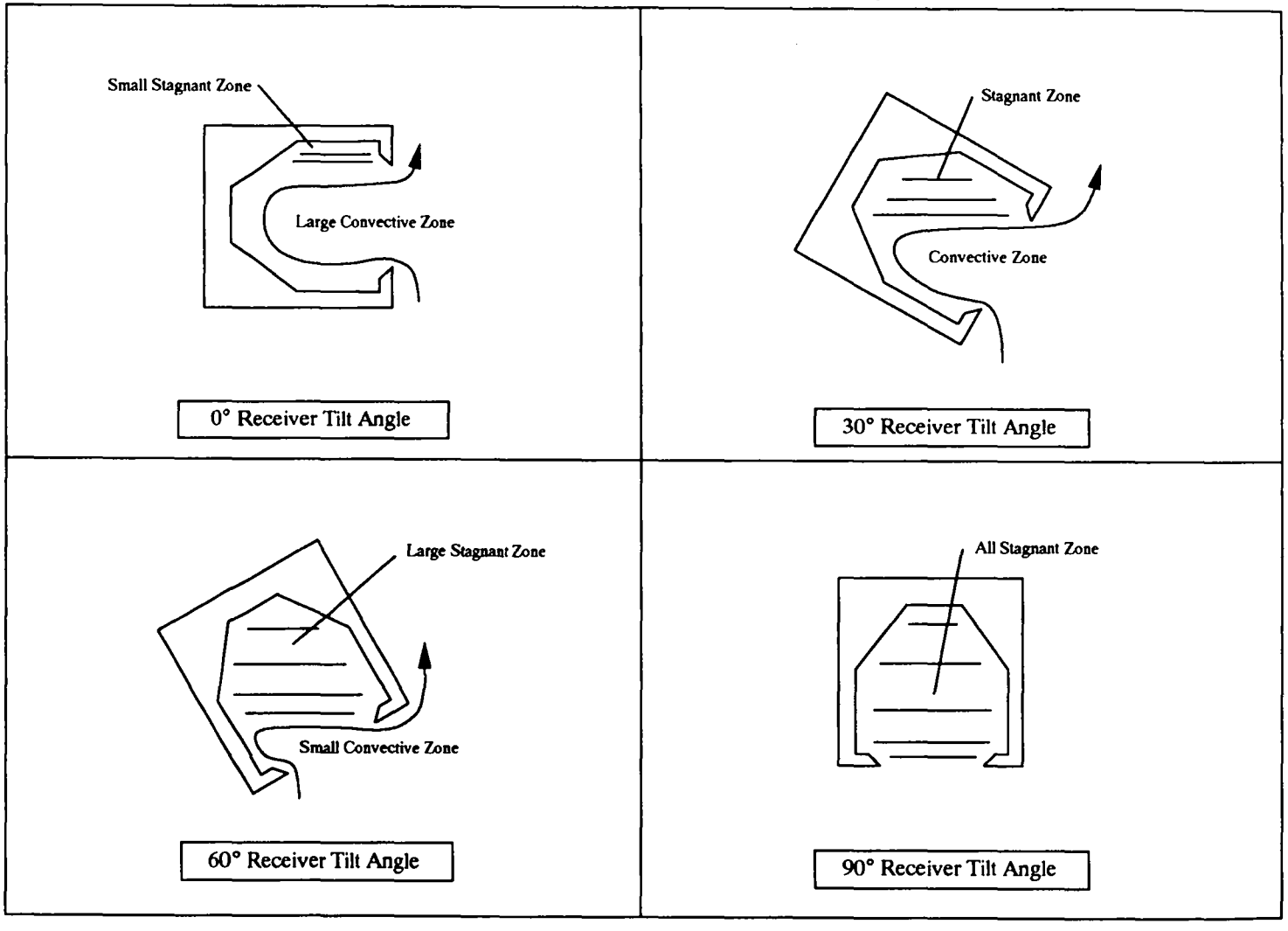

horizontally), natural convective currents occupy most of the receiver, with air temperature being lowest at the bottom and hotter as it rises and picks up heat. The hottest air is in the stagnant zone above the top of the receiver aperture since the air there has nowhere to escape. As the receiver is tilted downward, the stagnant zone becomes larger, which results in an overall increase in receiver average air temperature. With the aperture facing straight down, the entire cavity is a stagnant zone, resulting in the highest receiver average air temperature. It is the increase in the size of the stagnant zone and the resultant increase in average air temperature that causes natural convective heat loss to decrease as the receiver is tilted downward.

Presence of wind significantly alters the flow patterns within the receiver. Although many of the conditions tested result in very complex flow patterns, it is possible to hypothesize flow patterns for several of the less complicated conditions. Figure 40 shows hypothesized flow patterns for several head-on and side-on wind conditions.

At a receiver tilt angle of 0°, a head-on wind does not alter internal air temperatures very much from that resulting from natural convection. It seems that wind blowing directly into the aperture does not induce significant air currents inside the receiver, nor does it augment air flow into and out of the receiver through the aperture. As a result, convective heat loss for this receiver-tilt-angle/wind-direction condition is relatively low.

For a receiver tilted partially downward, but not straight down, the effects of head-on wind appear to be dependent upon wind speed. Low-speed head-on wind appears to result in air circulation mainly in the lower portion of the receiver, while higher-speed wind results in air circulation throughout a larger portion of the receiver. This circulation within the receiver is thought to be a result of a shear forces at the aperture due to the tangential component of wind velocity.

At a receiver tilt angle of 90°, head-on and side-on winds are essentially the same. The wind velocity is parallel to the receiver aperture. At low wind speeds, the effects of wind are only felt in the lower portion of the receiver. Air temperatures in the lower portion of the receiver are much lower than those occurring without wind. However, temperatures in the top portion of the receiver are high, being about the same as those occurring without wind; i.e., momentum transport due to low-speed wind is not strong

Figure 40. Illustration of receiver convection due to head-on and side-on winds.

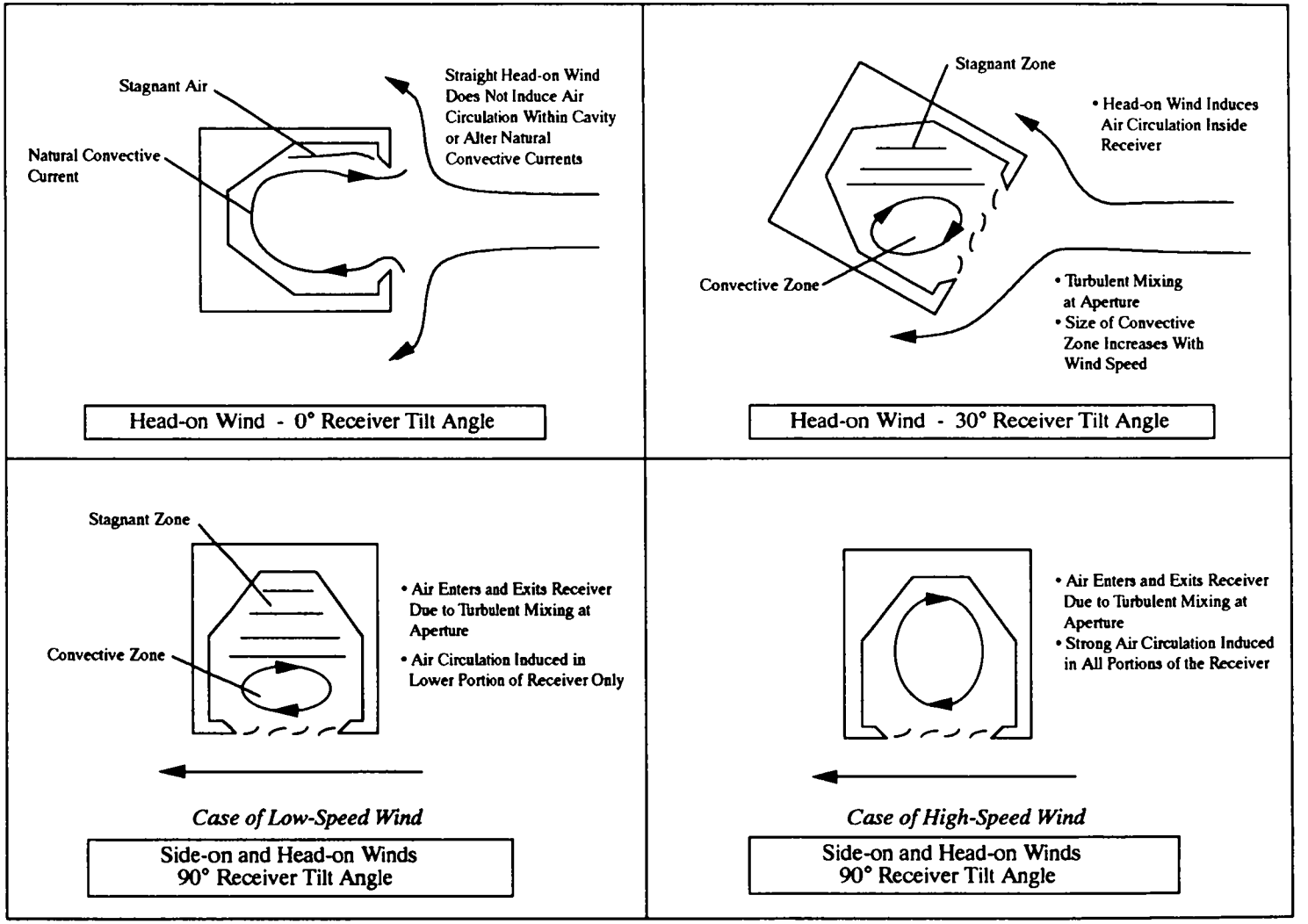

enough to overcome buoyancy forces. However, at high wind speeds, wind effects are felt everywhere in the receiver. The effects of high-speed wind are so strong that vertical temperature gradients due to buoyancy forces are completely eliminated.

For side-on wind at other than 90° tilt angle, receiver flow patterns are similar to those shown for 90° tilt angle. However, the presence of additional natural convective currents, oriented orthogonally to wind-induced currents, decreases the extent of the stagnant zone and results in higher overall convective heat loss.

8.0 Reliability of Test Results

The reliability of the results from these tests is dependent upon the accuracy of the measurements taken during the test and the algorithms used in data reduction. Accurate measurements of temperature difference between the heat-transfer-fluid inlet and outlet, and of the heat-transfer-fluid flow rate, are important because overall receiver heat loss is proportional to these quantities. With respect to the algorithms used in data reduction, each additional step that is required to derive the final convective heat loss value induces more uncertainty. This is because each component used in the data reduction algorithm has associated uncertainties, and these uncertainties are propagated and magnified with each additional mathematical step. The uncertainty in temperature measurements and an overall uncertainty analysis are presented in the next two sections.

8.1 Uncertainty in Temperature Measurements

The accuracy of temperature-difference measurements is important since total receiver heat loss is proportional to it. In the measurement of convection heat loss for these tests, temperature difference was measured two different ways. First, two junctions of a thermocouple were place at the receiver inlet and outlet to obtain a direct temperature-difference measurement. Second, temperature difference was obtained indirectly by measuring absolute temperatures at the receiver inlet and outlet, and then calculating the difference.

Figure 41 shows the comparison of temperature differences measured directly and indirectly, for all of the tests conducted. It can be seen that these two methods for

Figure 41. Comparison of direct and indirect measurements of temperature difference. Delta T is "direct" (obtained from a delta millivolt). Tin-Tout is "indirect" (obtained from the difference between absolute temperature measurements).

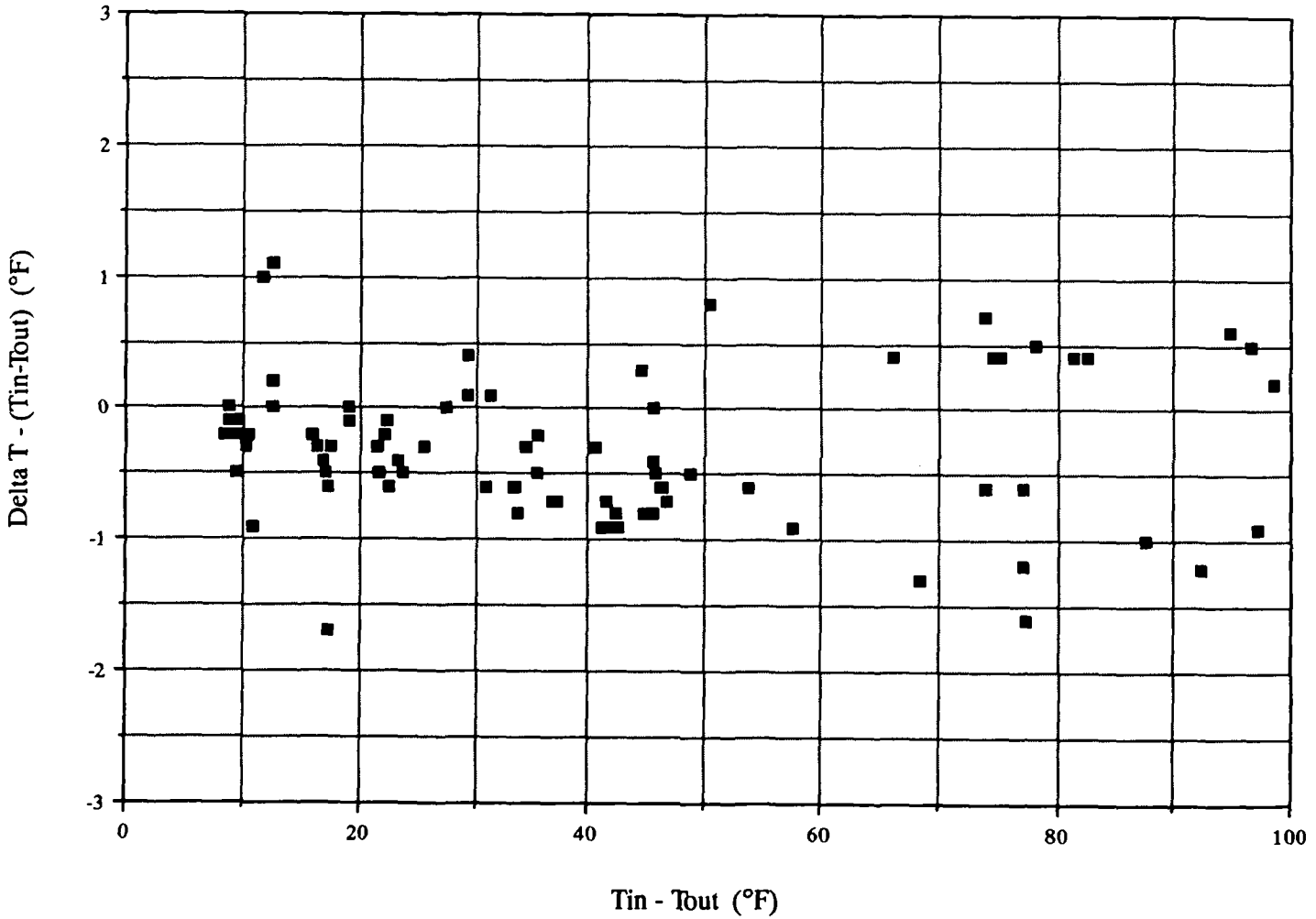

measuring temperature difference agree to within ±1.4°F, except for two data points. This comparison indicates that the two methods agree well with one another; however, it does not say anything about thermocouple accuracy. Nevertheless, in data reduction, a temperature-difference uncertainty of ±1.4°F was used because it was felt that the direct temperature-difference measurements were at least good to within this value. This is thought to be acceptable since each junction of a thermocouple for a direct temperature-difference measurement should have essentially the same characteristics, thereby minimizing temperature-difference uncertainties. The assumed temperature-difference uncertainty of ±1.4°F corresponds to absolute temperature uncertainty in each of the thermocouple junctions of ±1°F.

For situations where absolute temperature measurements were required, an uncertainty of ±2°F was used. However, this level of uncertainty has very little effect on the overall uncertainty of the test results because the only parameters that depend on absolute temperature are heat-transfer-fluid thermal properties and thermocouple characteristics (e.g., Seebeck coefficient), and these parameters are only weak functions of temperature. (The thermal properties of Syltherm® 800 heat transfer fluid are given in Appendix A, and the thermoelectric characteristics of type-K thermocouples are given in Appendix E.)

8.2 Overall Uncertainty Analysis

A complete uncertainty analysis was performed so that the confidence level of these experimental data could be assessed. The analysis takes into account uncertainties in measured temperatures, heat-transfer-fluid flow rate, and material thermal properties. It also accounts for the propagation of uncertainty resulting from data manipulation during the separation of conduction, radiation, and convection heat loss components. The individual parameter uncertainties used to perform the analysis are given below. The details of the uncertainty analysis procedure are given in Appendix F. Tabulated uncertainty analysis results are given in Appendix C, and error bars for receiver convective heat losses are also shown in Figures 8 and 9.

Parameter	Uncertainty
Direct Measurement of Temperature Difference	±1.4°F
Absolute Temperature	±2°F
Heat-Transfer-Fluid Flow Rate	±0.5% of meter reading
Heat-Transfer-Fluid Specific Heat	±1% of value
Heat-Transfer-Fluid Density	±1% of value

Figure 42 illustrates some typical results from the uncertainty analysis. For no wind, heat loss uncertainties are about 0.1 kW for conduction, 0.15 kW for radiation, and 0.21-0.22 kW for convection. The uncertainties are similar for the 20-mph side-on wind condition, except those for convective heat loss are slightly higher at 0.23-0.25 kW. The 0.1 kW uncertainty in conduction heat loss, shown for both conditions, is essentially equal to the uncertainty in overall receiver heat loss with the aperture plugged. The radiation heat loss uncertainties are higher than those for conduction because the calculation of radiation heat loss requires one additional step. Convective heat loss uncertainties are even higher because its calculation requires yet another step.

Although convective heat loss uncertainties do not vary much with receiver tilt angle, the uncertainty percentages vary greatly. At the highest convective heat loss condition, the uncertainty is only about 4 percent of the total convective heat loss. On the other hand, the uncertainty percentage can approach infinity as the heat loss level approaches zero. Fortunately, at low heat loss levels, the accuracy of the experimental results has little effect on overall system efficiency.

At this point, it is worthwhile to discuss the effects of uncertainties in temperature difference and heat-transfer-fluid flow rate, specific heat, and density. Overall receiver heat loss uncertainty is a result of uncertainties in material properties and in measured parameters. It is quantified by Eq. (F4) in Appendix F and repeated here as follows:

Figure 42. Receiver heat loss uncertainties.

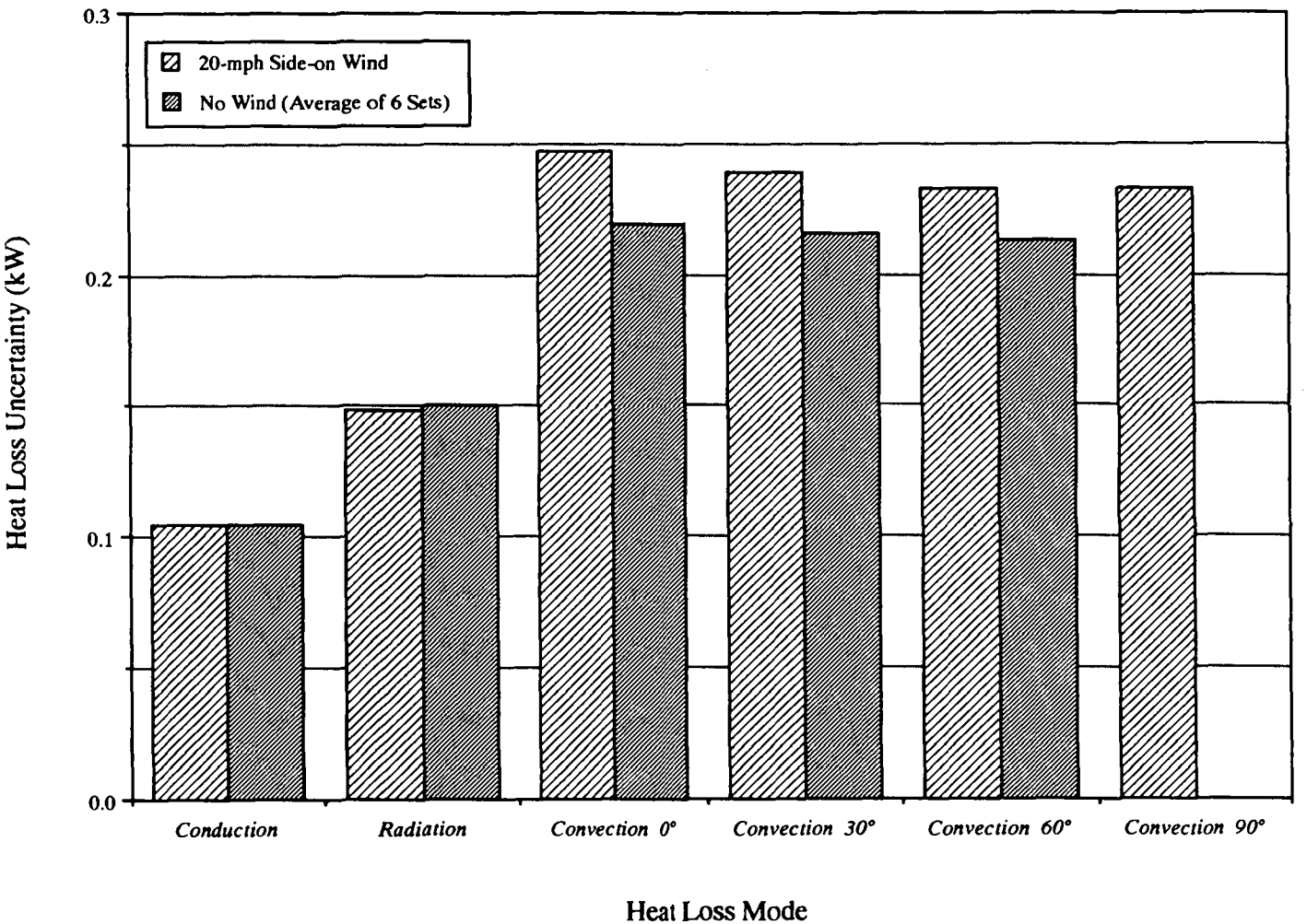

$$w_{q_{meas}} = \left[2.25 \times 10^{-4}\, q_{meas}^2 + 2.0 \frac{q_{meas}^2}{(\Delta T)^2} \right]^{\frac{1}{2}} \qquad (16)$$

where q_{meas} = total receiver heat loss rate derived from measurements

$w_{q_{meas}}$ = uncertainty in total receiver heat loss rate

ΔT = temperature difference between the heat-transfer-fluid inlet and outlet

The first term on the right-hand side of Eq. (16) is the due to uncertainties in heat-transfer-fluid flow rate, specific heat, and density, and increases as receiver heat loss increases. The second term on the right-hand side is due to uncertainty in the measured temperature difference between the receiver inlet and outlet, and is approximately proportional to the heat-transfer-fluid flow rate. In these tests, the heat-transfer-fluid flow rate was held nearly constant, so that the uncertainty due to the second term on the right (temperature uncertainty) is essentially constant. At low heat loss rates, most of the uncertainty in overall receiver heat loss was found to be due to uncertainty in temperature difference. However, at higher heat loss levels, the effects of uncertainty in flow rate and fluid material properties become comparable to that due to temperature difference.

It is interesting to note that given a particular receiver heat loss level and the parameter uncertainties used in this analysis, that the overall heat loss uncertainty can be reduced by reducing the heat-transfer-fluid flow rate. This is because the temperature difference term (the second term on the right) is equal to $2.0\,(Q\rho c_p)^2$. This method appears as though it could be used to reduce heat loss uncertainties without costs. However, at some point, the advantage of reducing heat loss uncertainty would be overshadowed by the disadvantage of a non-isothermal receiver, because low fluid flow rates would result in large temperature differences between the receiver inlet and outlet.

9.0 Comparison of Analytical Predictions to Experimental Results

In order to increase confidence, it is desirable to compare the experimental data and analyses wherever possible. Therefore, an effort was made to predict radiation and conduction heat losses by using a combination of computer modeling and hand

computations. A discussion of these analyses and the comparison of predicted to experimental results are given in the next two sections.

9.1 Radiation Heat Loss

To predict radiation heat loss from the receiver, a computer model was generated using PATRAN (PDA Engineering) which is a model generator for finite-difference and finite-element analysis. This thermal network is shown in Figure 43. The radiation analysis was based on an electrical analogy, which incorporates surface resistances due to gray surfaces, shape resistances associated with the ability of one surface to "see" other surfaces, and radiosity nodes.

A program called VFAC (PDA Engineering) was used to set up the detailed radiation network for the computer model by calculating shape factors and shape and surface resistances, and by defining radiosity nodes. A set of algebraic equations is obtained by setting the summation of heat rate into each radiosity node equal to zero. The general matrix formulation for the set of algebraic equations is as follows:

$$J_i - (1 - \varepsilon_i) \sum_{j=1}^{N} F_{i \rightarrow j} J_j = \varepsilon_i E_{bi} \qquad (17)$$

where J = surface radiosity
F = radiation shape factor
E_b = total blackbody emissive power
ε = surface emissivity

The radiation network was subsequently solved using P-Thermal, which is the PDA thermal analysis computer code.

In the analysis, the receiver internal surfaces were assumed to be gray (emissivity which is constant, i.e., independent of temperature and wavelength). An emissivity of 0.9 was used for the receiver tubing area since it was painted with Pyromark paint. An

Figure 43. Computer thermal model used to help predict radiation and conduction heat loss from the receiver. Conduction model only accounts for heat flow through receiver insulation.

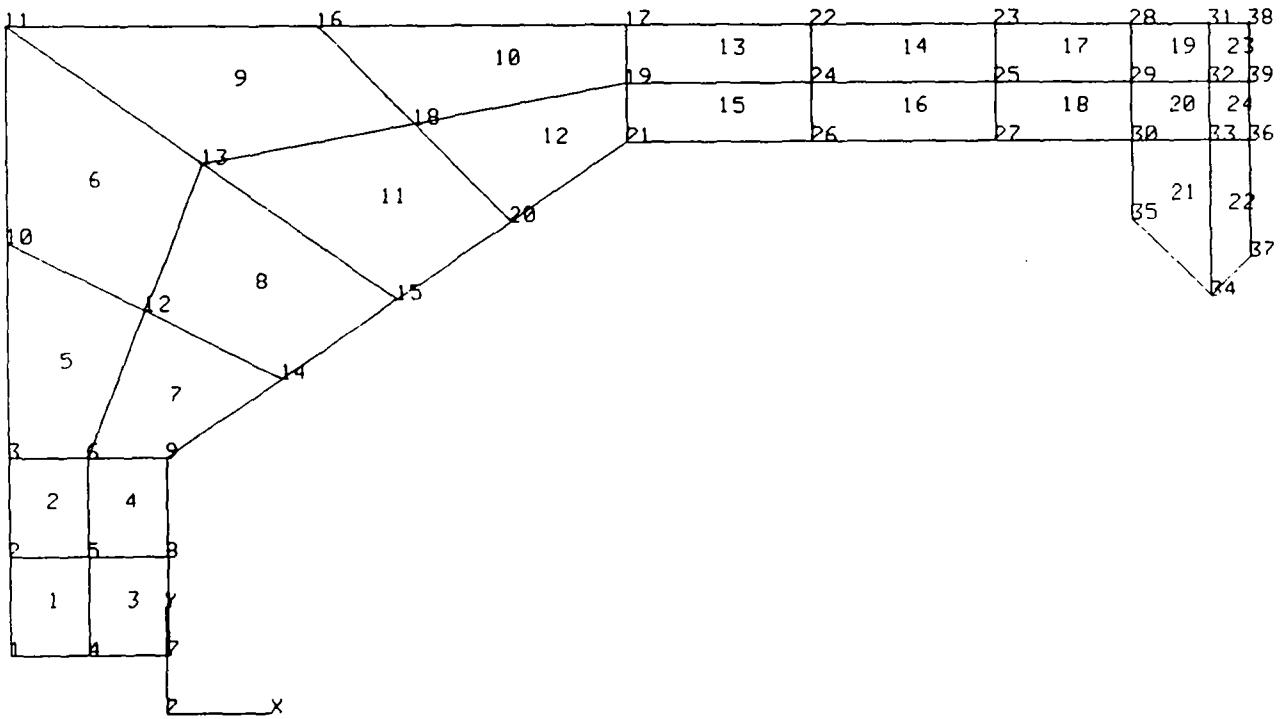

emissivity of 0.3 was used for the chrome-plated-steel surfaces at the forward and aft ends of the receiver tubing area.

For the 530°F nominal receiver temperature in these tests, the predicted radiation heat loss from the receiver is 0.74 kW, which is slightly higher than the 0.62 kW obtained experimentally. Some of this deviation may be due to the chrome-plated-steel portion of the receiver, forward and aft of the heat transfer tubing, being lower in temperature than the average temperature of the heat transfer fluid.

Figure 44 shows measured receiver inner wall temperatures which are typical of the temperatures from tests used to calculate radiation heat loss. A line is drawn in this figure to represent the average heat-transfer-fluid temperature for this case. Recall that the actual average temperature of the heat transfer fluid is slightly different than the nominal receiver temperature of 530°F for which radiation heat loss is given. The data shown in Figure 44 show that the average heat-transfer-fluid temperature is an acceptable representation of the temperatures occurring on the heat-transfer-tubing surfaces (at receiver forward and aft planes). The measured temperatures on the surface of the heat transfer tubing range from 536°F to 546°F, compared to the heat-transfer-fluid average temperature of 541°F. However, the temperature of the chrome-plated-steel area aft of the heat transfer tubing is somewhat lower in temperature at 509°F. Moreover, it is highly likely that the chrome-plated-steel area forward of the heat transfer tubing is also lower in temperature than the average temperature of the heat transfer fluid; however, the actual temperatures in this region are unknown since no temperature measurements were taken there.

In light of the receiver temperatures shown in Figure 44, the radiation heat loss was predicted with the aforementioned computer thermal model using a receiver aft-section temperature of 500°F and an estimated temperature of 300°F in the area forward of the heat transfer tubing. The 500°F temperature in the aft section takes into account the fact that the normalized receiver temperature is 530°F, not 541°F. The resultant predicted radiation heat loss is 0.71 kW, which is closer to, but still about 15 percent above, the experimental value.

Figure 44. Typical temperature distribution on the receiver interior surfaces (90° no-wind test from 6-mph side-on wind test set).

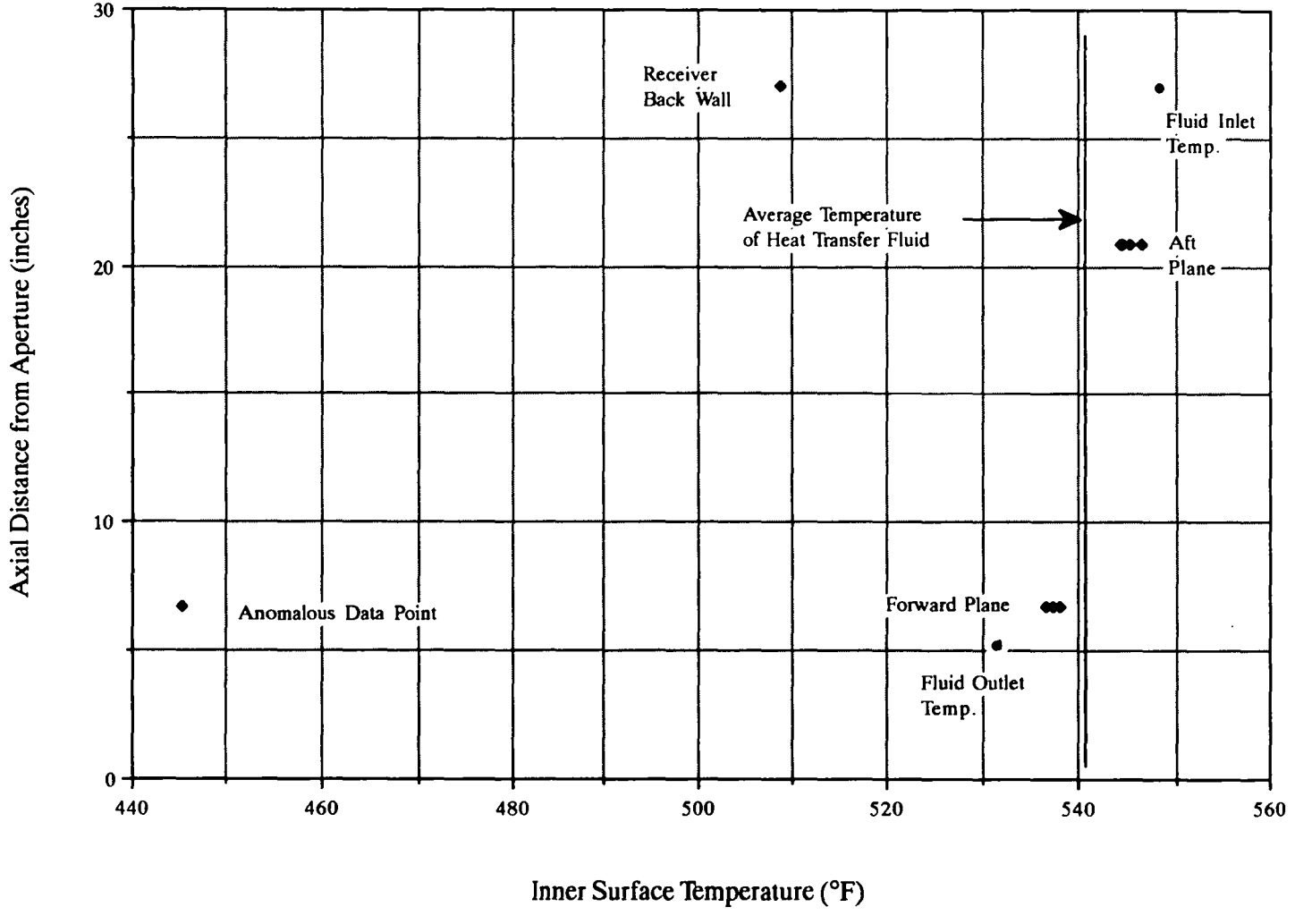

It is interesting to note that a first-order prediction of radiation heat transfer from the receiver can be obtained by using the aperture area and an effective aperture emissivity. The effective emissivity for the cavity receiver tested is 0.94 based on the isothermal radiation model , 0.91 based on the non-isothermal radiation model, and 0.79 based on the experimental results. Thus, it appears that a relatively conservative value of radiation heat loss can be obtained by simply using the emissivity of the receiver tubing of 0.9. To be more conservative, an upper bound for radiation heat loss can be obtained by simply using an effective emissivity of 1.0. Predicted radiation heat loss curves using these effective emissivities are shown in Figure 45.

Another interesting fact to note is that the receiver cavity has radiation characteristics that are similar to that of a hohlraum, which is a large cavity with a very small opening through which radiative heat is transmitted. The unique characteristic of a hohlraum is that the amount of radiation transmitted through the small hole is independent of the emissivity of the interior surfaces. Using the computer radiation model, it was found that a 50 percent reduction in the emissivity of the interior surfaces of the receiver only decreased radiation heat loss by about 10 percent. Thus, an effort to reduce radiation heat loss from the receiver by lowering the emissivity of the cavity surfaces would probably not be productive.

9.2 Conduction Heat Loss

In order to analytically predict conduction heat loss from the receiver, a combination of finite-element heat-transfer modeling and hand computation was performed. The axisymmetric finite-element model was the same basic model as that used for calculating radiation heat loss (Figure 43) and only accounts for conduction heat loss through the receiver-wall insulation. In this model, the receiver inner surface was constrained at 530°F, and the receiver outer surface was constrained at 85°F for the 20-mph wind condition and 115°F for the no-wind condition. These outer surface temperatures were chosen based on actual average outer-surface temperature measurements given in Appendix D.

The hand computation took into account heat conduction through the receiver tubing support structure, which consists of forward and aft supports at three circumferential locations, and a receiver forward-end structure. These structures are depicted in Figure 46.

Figure 45. Predicted radiation heat loss from the receiver as a function of nominal receiver temperature.

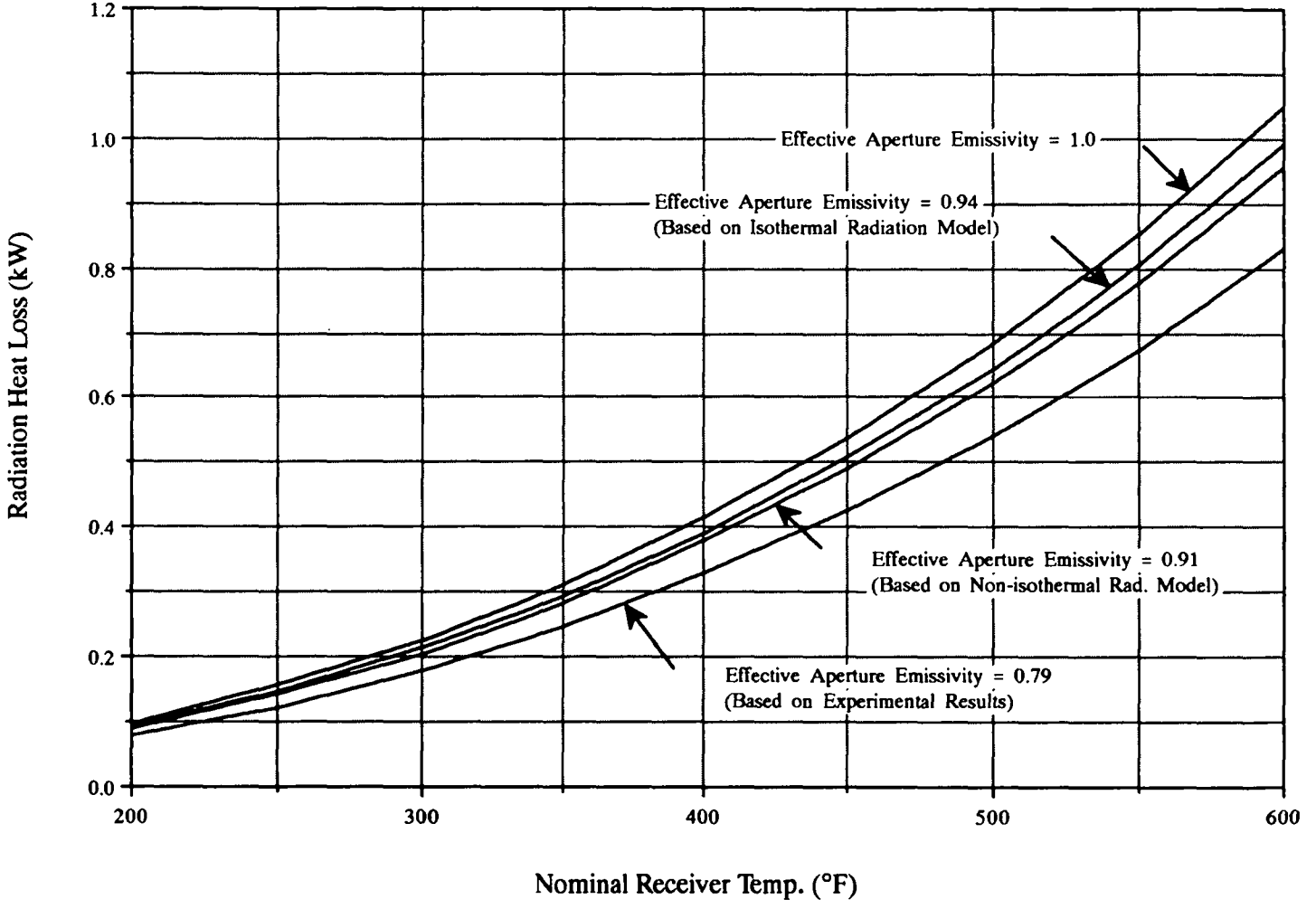

Figure 46. Receiver structure conduction paths.

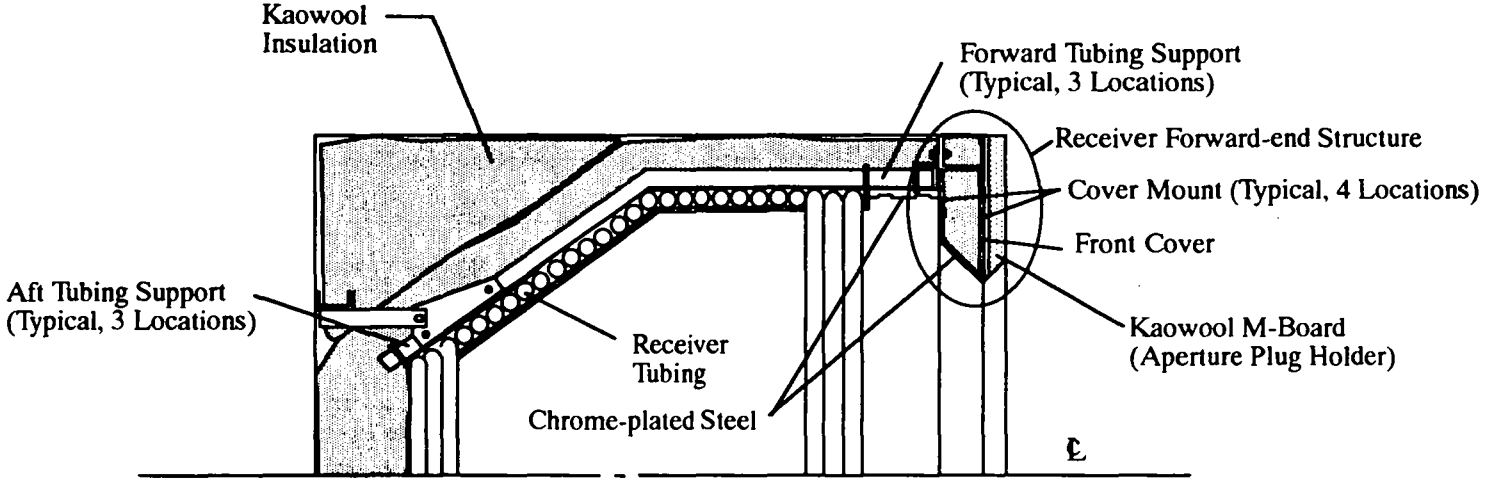

The inner and outer surface temperatures used in these computations are the same as those used in the computer model.

The table below summarizes the amount of conduction heat loss predicted through each conduction path. Values are given for the case of no wind and for a 20-mph wind. The only difference between these two cases is the small difference in receiver outer surface temperature.

Conduction Heat Losses Through Various Receiver Conduction Paths

Conduction Path	Estimated Conduction Heat Loss			
	No Wind		20-mph Wind	
	(kW)	(%)	(kW)	(%)
Receiver Insulation	0.217	30.3	0.232	30.3
Aft Tubing Support (Total of 3 Locations)	0.014	2.0	0.015	2.0
Forward Tubing Support (Total of 3 Locations)	0.010	1.4	0.011	1.4
Receiver Forward-end Structure	0.474	66.3	0.508	66.3
Total	0.715	100	0.766	100

About 66 percent of the conduction heat loss from the receiver is attributed to conduction through the receiver forward-end structure (see Figure 46). Another 30 percent is due to conduction through the receiver insulation. Surprisingly, conduction through the forward and aft tubing supports is very small, being less than 4 percent of the total conduction heat loss.

The conduction heat losses found experimentally are generally lower than the predicted values. Experimental conduction heat loss is 0.60 kW average for the no-wind condition and 0.66 kW for 20-mph side-on wind condition. However, experimental conduction heat loss from the 20-mph head-on wind test is 1.09 kW, which is much higher than the predicted values above. It is believed that the 1.09 kW experimental conduction heat loss is anomalously high, since it is higher than all of the other measured conduction

heat losses from the first test series, which are in the range of 0.5-0.7 kW. In general, analytical conduction heat losses are 15-20 percent higher than experimental values.

A plausible explanation for the difference between the measured and estimated conduction heat loss values (except for the 1.09 kW for the 20-mph head-on wind) is that the actual difference in temperature between the inner and outer surfaces of the receiver at the forward-end structure is probably less than the value used in the conduction analysis. The temperature difference used in the analysis was based on average inner and outer wall temperatures derived from actual measured temperatures. In these measurements, almost all of the thermocouples on the interior surface of the receiver were on the hot heat transfer tubing. In addition, the outer surface thermocouples were located where there is 3 inches of Kaowool insulation in the receiver wall. The high conductive resistance provided by this insulation is a major reason why measured outer surface temperatures are not much higher than the ambient air temperature. For the forward-end structure area, however, the inner surface temperature is probably lower than 530°F, since it is somewhat removed from the heat transfer tubing, and the outer surface temperature is probably slightly higher than that measured on the receiver wall, because of the higher thermal conductivity of steel.

If it is assumed that the inner surface of the forward structure is at 300°F, as was done in the radiation analysis, the estimated levels of conduction through the forward-end structure would then be 0.21 kW and 0.25 kW for the no-wind and 20-mph wind conditions, respectively. The corresponding total conduction heat loss levels would then be 0.45 kW and 0.51 kW, respectively, which are about 25 percent lower the measured conduction heat loss values. The actual inner surface temperature at the receiver forward end, during the tests in which conduction heat loss was measured, was probably less than 530°F, but not as low as 300°F since the aperture was plugged during these tests.

A more representative conduction analysis might be obtained by modeling the convective and radiative boundary conditions on the inner and outer surfaces of the receiver forward-end structure. In this way the inner and outer surface temperatures are obtained analytically. However, the determination of local boundary conditions on the interior of the forward-end structure would involve some uncertainties.

A possible explanation the high conduction heat loss value for the 20-mph head-on wind is that air leakage may have occurred through the receiver joint areas. In fact, during some of the receiver tests in which smoke visualization was used, a small amount of smoke was seen escaping through joints in the receiver walls, indicating that at least some air leakage occurred. However, it is impossible to predict quantitatively the heat loss due to this air leakage. In future testing using this receiver, an effort should be made to seal the receiver as best as possible.

10.0 Conclusions

The convective heat loss characteristics of a cavity receiver for a parabolic-dish concentrating solar collector have been determined experimentally for the no-wind condition, side-on winds of up to 20 mph, and head-on winds of up to 24 mph. Natural convective heat loss from the receiver was found to be the highest with the receiver aperture facing horizontally and negligible with the aperture facing straight down.

For side-on wind, convective heat loss is also the highest with the aperture facing horizontally and decreases as the receiver is tilted downward, but the magnitudes are much higher than those resulting from natural convection. For head-on wind, convective heat loss is generally lower than those for side-on wind. Head-on wind blowing directly into the receiver aperture does not increase convection significantly above natural convection. This is believed to be a result of this type of flow inducing little convective current in the receiver, and generating little convective transport into and out of the receiver. Overall, the effects of wind on convective heat loss from the receiver are the greatest for wind blowing parallel to the aperture and the smallest for wind blowing directly into the aperture. It was found that for wind speeds of 20-24 mph, the total convective heat loss from the receiver can be as much as three times the maximum level of natural convection.

It was found that the total convective heat loss could be expressed as a sum of the natural and forced convection. For side-on wind, a curve-fit is presented in Eq. (11) for determining the forced convection heat transfer coefficient as a function of wind speed only. For head-on wind, a curve-fit is presented in Eq. (14) for determining the forced convection heat transfer coefficient as a function of both wind speed and receiver tilt angle.

The results of the uncertainty analysis indicate that convective heat loss uncertainties are between 0.21-0.26 kW. Although convective heat loss uncertainty only varies slightly from test to test, uncertainty as a percentage of convective heat loss varies greatly. At the highest convective heat loss level, the uncertainty percentage is only about four percent, but for low heat loss rates, uncertainty percentage approaches infinity. Fortunately, at low heat loss rates, the accuracy of the measurements is not critical. The small uncertainty percentages for the higher heat loss rates associated with the different wind conditions indicate good data reliability.

Air temperature measurements made inside the receiver provided useful insight into the receiver convective phenomena. These measurements confirm the presence of the stagnant zone for the no-wind condition and clearly indicate the extent to which head-on and side-on winds affect convective flow within the receiver. Analyses were also performed to predict radiation and conduction heat losses from the receiver for comparison to measured values. Measured and analytical radiation heat loss levels agree to within about 15 percent. Measured and analytical conduction heat loss levels agree to within 15-25 percent.

The correlations presented in this report for predicting forced convective heat loss are only for this particular receiver. It is desirable to have a correlation which takes into account different receiver geometries, temperatures, and aperture sizes. It is therefore recommended that future testing be performed first on this receiver, with different aperture sizes and temperatures, then with different receiver geometries. With a compilation of data from future receiver testing performed at this or any other facility, the curve-fits presented in this thesis can be refined and modified to be more general.

References

Clausing, A. M., 1981, "An Analysis of Convective Losses From Cavity Solar Central Receivers," *Solar Energy*, Vol. 27, No. 4, pp. 295-300.

Faust, K. M., E. J. Plate, and M. Kuczera, 1981, "Experimental Investigation of the Convective Losses from the Cavity Receiver of the Project GAST," In SAND81-8014 (P. Falcone), Sandia National Laboratories, pp. 143-164.

Haddad, G., 1991, "Cavity Receiver Heat Loss Tests in Wind," Master's Project, California State Polytechnic University, Pomona.

Holman, J. P., 1984, *Experimental Methods for Engineers*, 4th ed., McGraw-Hill, New York.

Koenig, A. A., and M. Marvin, 1981, "Convection Heat Loss Sensitivity in Open Cavity Solar Receivers," Final Report, DOE Contract No. EG77-C-04-3985, Department of Energy, Oak Ridge, Tennessee.

Kraabel, J. S., 1983, "An Experimental Investigation of Natural Convection from a Side-Facing Cubical Cavity," *ASME-JSME Thermal Engineering Joint Conference Proceedings*, Vol. 1, pp. 299-306, Honolulu, Hawaii, March 20-24.

Kugath, D. A., G. Drenker, and A. A. Koenig, 1979, "Design and Development of a Paraboloidal Dish Solar Collector for Intermediate Temperature Service," *Proc. ISES Silver Jubilee Congr.*, Vol. 1, pp. 449-453.

LeQuere, P, F. Penot, and M. Mirenayat, 1981, "Experimental Study of Heat Loss Through Natural Convection from an Isothermal Cubic Open Cavity," In SAND81-8014 (P. Falcone), Sandia National Laboratories, pp. 165-174.

McDonald, C. G., 1992, "Cavity Receiver Heat Loss Tests Without Wind," Master's Thesis, California State Polytechnic University, Pomona.

McMordie, R. K., 1984, "Convection Heat Loss From a Cavity Receiver," *ASME Journal of Solar Energy Engineering*, Vol. 106, pp. 98-100.

PDA Engineering, Costa Mesa, CA.

Siebers, D. L., and J. S. Kraabel, 1984, "Estimating Convective Energy Losses From Solar Central Receivers," SAND84-8717, Sandia National Laboratories.

Stine, Wm. B., and C. G. McDonald, 1988, "Cavity Receiver Heat Loss Measurements," *1988 ASME Solar Energy Division Conference*, Denver, Colorado, 10-14 April.

Stine, Wm. B., and C. G. McDonald, 1989, "Cavity Receiver Convective Heat Loss," *Proceedings of International Solar Energy Society Solar World Congress 1989 Kobe*, Kobe, Japan, 4-8 September.

List of Symbols

A	full interior geometric surface area of receiver
A_T	exposed surface area of receiver heat transfer tubing in Eq. (5)
c_p	heat-transfer-fluid specific heat
d	aperture diameter
E_b	total blackbody emissive power
F	radiation shape factor
g	gravitational acceleration
Gr_L	Grashof number = $g\beta\Delta TL^3/\nu^2$
$\bar{h}$	convective heat transfer coefficient
$\bar{h}_{avg\ internal}$	average internal heat transfer coefficient
$\bar{h}_{forced}$	heat transfer coefficient for forced convection
$\bar{h}_{natural}$	heat transfer coefficient for natural convection
$\bar{h}_{overall}$	overall heat transfer coefficient for mixed convection
J	radiosity
k	thermal conductivity
l_c	$R_{aperture}/R_{cavity}$
L	characteristic length
$\dot{m}$	heat-transfer-fluid mass flow rate
$\overline{Nu}_L$	Nusselt number = $\bar{h}L/k$
$P(\theta)$	constant in Eq. (4)
Pr	Prandtl number
q_{cond}	conduction heat loss rate
q_{conv}	convective heat loss rate
$q_{\ conv\ overall}$	overall convective heat loss rate for mixed convection
q_{forced}	convective heat loss rate due to forced convection
q_{meas}	total receiver heat loss rate derived from measurements
$q_{natural}$	convective heat loss rate due to natural convection
$q_{plugged}$	total heat loss rate with the aperture plugged
q_{rad}	radiation heat loss rate
q_{total}	normalized total heat loss rate
Q	heat-transfer-fluid volume flow rate
$R_{aperture}$	radius of aperture

R_{cavity}	radius of receiver cavity
Ra_L	Rayleigh number = $Gr_L Pr$
Re	Reynolds number = VL/ν
$T_{amb,\ meas}$	measured ambient temperature
$T_{amb,\ norm}$	nominal or normal ambient temperature = 70°F
$T_{avg\ i.s.}$	average inner-surface temperature from measurements
$T_{avg\ air}$	average air temperature within cavity from measurements
$T_{rec,\ meas}$	measured receiver temperature (average temperature of heat transfer fluid)
$T_{rec,\ norm}$	nominal or normal receiver temperature = 530°F
T_{cavity}	mean temperature of heat transfer tubing in Eq. (5)
T_{in}	heat-transfer-fluid inlet temperature
T_o	ambient temperature
T_{out}	heat-transfer-fluid outlet temperature
T_{prop}	temperature at which fluid properties are evaluated in Eq. (4)
T_w	average receiver internal wall temperature
V	wind velocity
w	experimental uncertainty
ß	coefficient of thermal expansion of air = 1/T
ΔT	T_w-T_o, T_{cavity}-T_o, or T_{in}-T_{out}
ε	surface emissivity
ν	kinematic viscosity
ρ	heat-transfer-fluid density
θ	receiver tilt angle (0° is horizontal)

Appendix A

Material Properties

Figure A1. Specific heat of Syltherm® 800 heat transfer fluid.

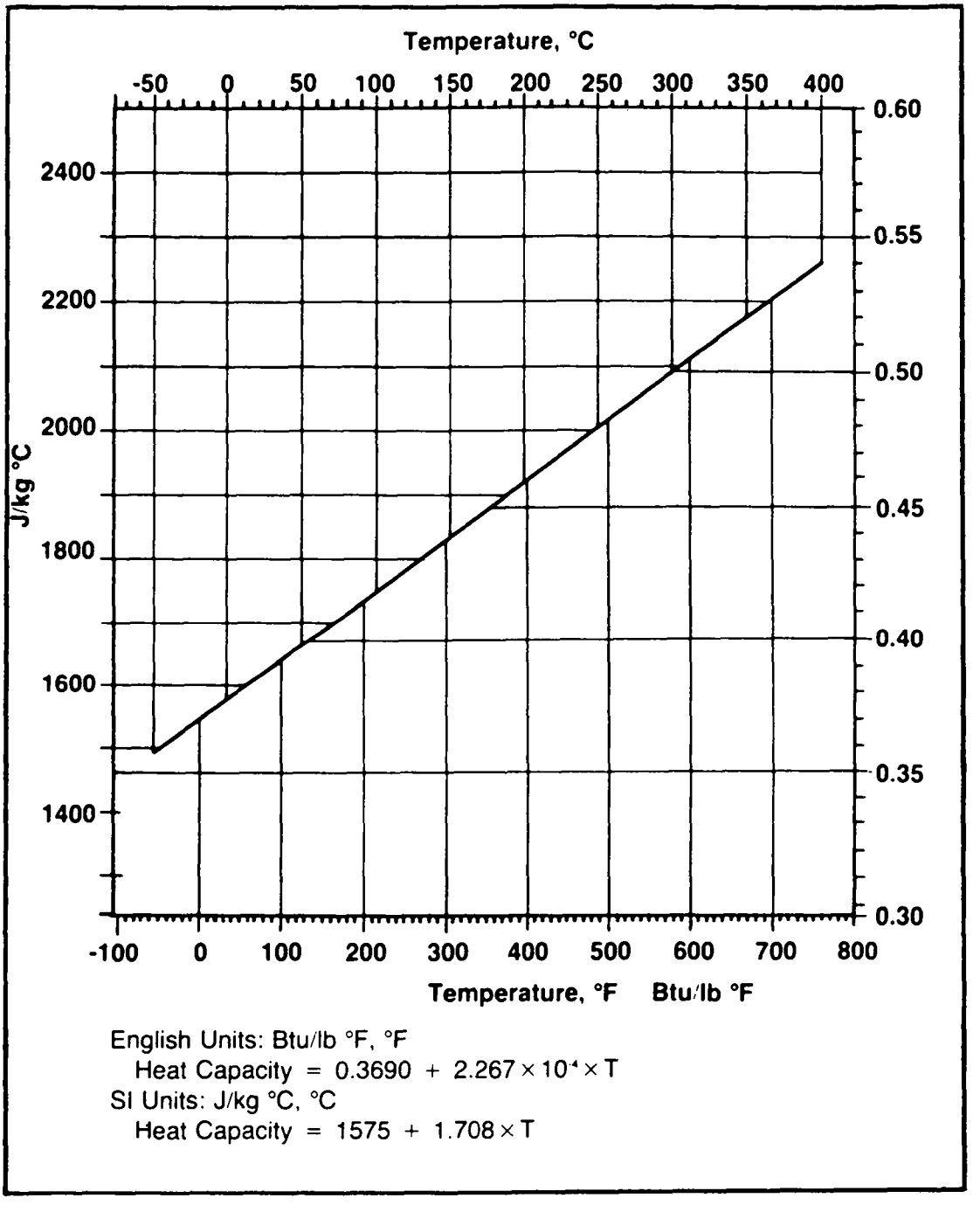

Figure A2. Density of Syltherm® 800 heat transfer fluid.

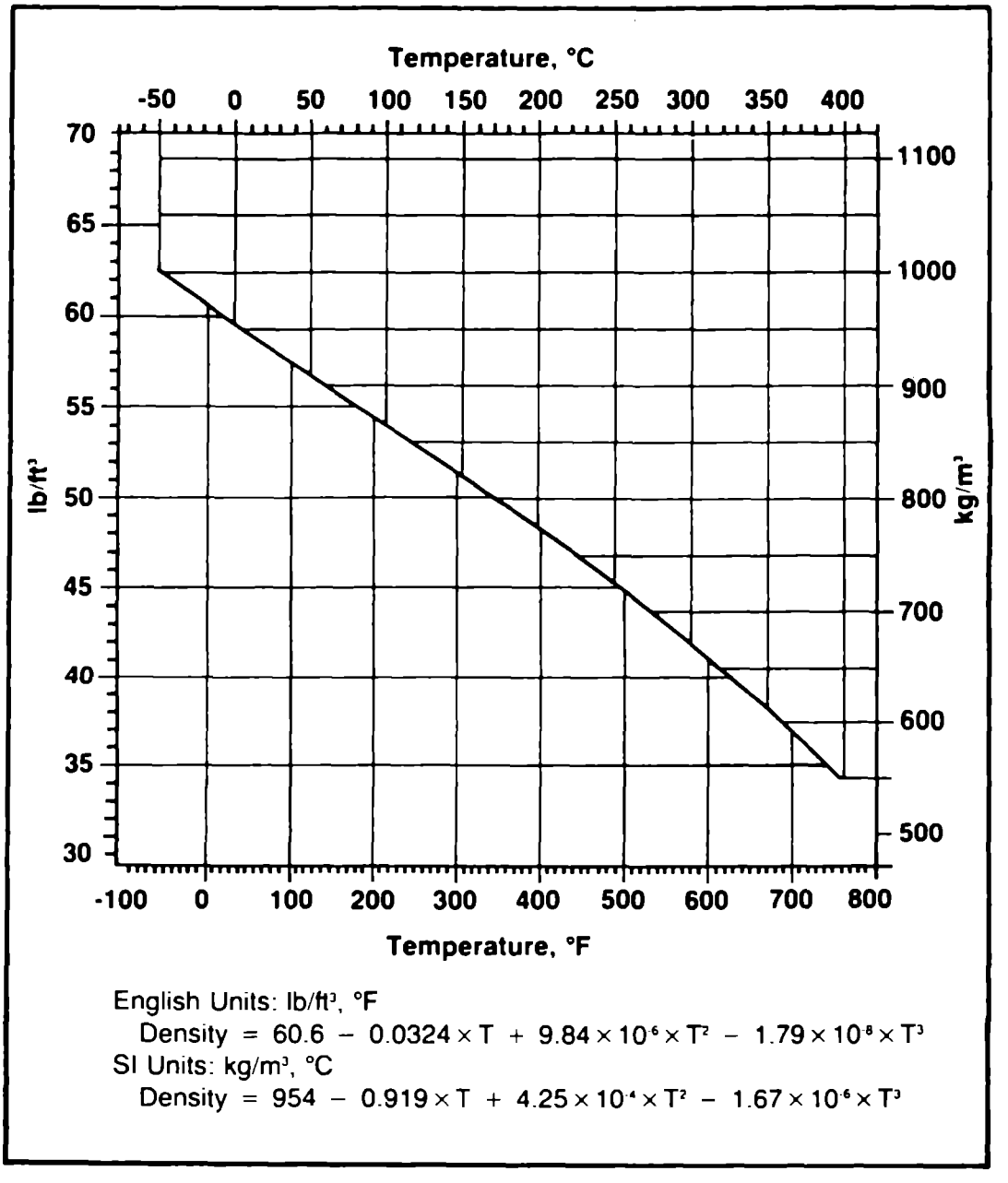

Figure A3. Thermal conductivity of Kaowool insulation.

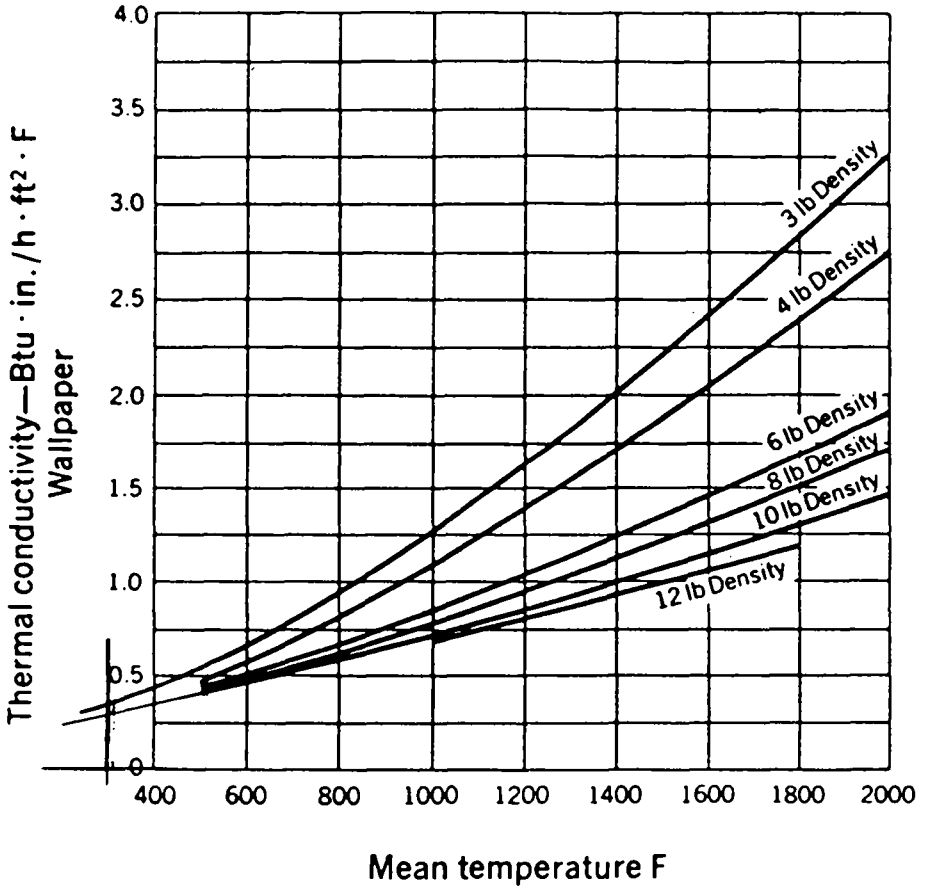

Appendix B

Data Analysis Spreadsheets

TABLE B1. Data Analysis Spreadsheet - 6-mph Side-on Wind

	A	B	C	D	E	F	G	H
1	RECEIVER ANGLE	FLOW 1 (GPM)	T in (°F)	T out (°F)	DE (microV)	T avg (°F)	DT (°F)	Ti-To (°F)
2								
3	90° PLUG/NO FAN	1.535	550.6	541.0	214.80	545.80	9.4	9.6
4	90° PLUG/FAN	1.547	548.9	539.5	204.91	544.20	8.9	9.4
5	90° NO PLUG/NO FAN	1.542	549.0	532.3	373.07	540.65	16.3	16.7
6	90° NO PLUG/FAN	1.511	548.5	526.5	498.84	537.50	21.8	22.0
7	60° NO PLUG/NO FAN	1.517	551.8	529.6	505.91	540.70	22.1	22.2
8	60° NO PLUG/FAN	1.537	551.1	521.9	671.25	536.50	29.3	29.2
9	30° NO PLUG/NO FAN	1.539	551.8	516.6	794.19	534.20	34.7	35.2
10	30° NO PLUG/FAN	1.547	552.4	511.9	919.96	532.15	40.2	40.5
11	0° NO PLUG/NO FAN	1.545	559.3	513.5	1035.84	536.40	45.3	45.8
12	0° NO PLUG/FAN	1.554	560.0	511.2	1105.08	535.60	48.3	48.8
13								
14								
15								

TABLE B1. Data Analysis Spreadsheet - 6-mph Side-on Wind (continued)

	A	I	J	K	L	M	N
1	RECEIVER ANGLE	DENSITY	SPEC HEAT	MASS FLOW	HEAT LOSS	HEAT LOSS	T amb (°F)
2		(lbm/ft^3)	(Btu/lbm-°F)	(lbm/min)	(Btu/min)	(kW)	
3	90° PLUG/NO FAN	42.76	0.4927	8.773	40.49	0.712	70.2
4	90° PLUG/FAN	42.82	0.4924	8.855	38.97	0.685	70.6
5	90° NO PLUG/NO FAN	42.82	0.4916	8.826	70.66	1.242	71.0
6	90° NO PLUG/FAN	42.84	0.4909	8.652	92.54	1.627	71.0
7	60° NO PLUG/NO FAN	42.71	0.4916	8.661	94.03	1.653	72.0
8	60° NO PLUG/FAN	42.74	0.4906	8.781	126.34	2.221	72.0
9	30° NO PLUG/NO FAN	42.71	0.4901	8.787	149.49	2.628	71.3
10	30° NO PLUG/FAN	42.69	0.4896	8.828	173.88	3.057	71.3
11	0° NO PLUG/NO FAN	42.43	0.4906	8.762	194.55	3.420	66.6
12	0° NO PLUG/FAN	42.40	0.4904	8.808	208.58	3.667	66.6
13							
14							
15							

TABLE B1. Data Analysis Spreadsheet - 6-mph Side-on Wind (continued)

	A	O	P	Q	R	S
1	RECEIVER ANGLE	NORM HEAT LOSS	CONV HEAT LOSS	COND HEAT LOSS		HEAT LOSS ERROR
2		(kW)	(kW)	(kW)		(Btu/min)
3	90° PLUG/NO FAN	0.689		no fan		6.144
4	90° PLUG/FAN	0.665		0.619		6.194
5	90° NO PLUG/NO FAN	1.217	0.000	fan		6.226
6	90° NO PLUG/FAN	1.604	0.415	0.591		6.164
7	60° NO PLUG/NO FAN	1.622	0.406			6.184
8	60° NO PLUG/FAN	2.200	1.010	RAD HEAT LOSS		6.381
9	30° NO PLUG/NO FAN	2.612	1.395	(kW)		6.490
10	30° NO PLUG/FAN	3.051	1.862	fan/no fan		6.646
11	0° NO PLUG/NO FAN	3.349	2.132	0.598		6.744
12	0° NO PLUG/FAN	3.597	2.407			6.863
13						
14						
15						

TABLE B1. Data Analysis Spreadsheet - 6-mph Side-on Wind (continued)

	A	T	U	V	W
1	RECEIVER ANGLE	HEAT LOSS ERROR	NORM ERROR	CONV ERROR	COND ERROR
2		(kW)	(kW)	(kW)	(kW)
3	90° PLUG/NO FAN	0.108	0.105		no fan
4	90° PLUG/FAN	0.109	0.106		0.105
5	90° NO PLUG/NO FAN	0.109	0.107	0.212	fan
6	90° NO PLUG/FAN	0.108	0.107	0.213	0.106
7	60° NO PLUG/NO FAN	0.109	0.107	0.212	
8	60° NO PLUG/FAN	0.112	0.112	0.215	RAD ERROR
9	30° NO PLUG/NO FAN	0.114	0.114	0.216	(kW)
10	30° NO PLUG/FAN	0.117	0.118	0.218	fan/no fan
11	0° NO PLUG/NO FAN	0.119	0.117	0.218	0.150
12	0° NO PLUG/FAN	0.121	0.120	0.220	
13					
14					
15					

TABLE B2. Data Analysis Spreadsheet - 8-mph Side-on Wind

	A	B	C	D	E	F	G	H
1	RECEIVER ANGLE	FLOW 1 (GPM)	T in (°F)	T out (°F)	DE (microV)	T avg (°F)	DT (°F)	Ti-To (°F)
2								
3	90° PLUG/NO FAN	1.525	550.6	540.4	227.52	545.50	9.9	10.2
4	90° PLUG/FAN	1.525	550.8	541.2	217.62	546.00	9.5	9.6
5	90° NO PLUG/NO FAN	1.507	551.6	534.3	390.03	542.95	17.0	17.3
6	90° NO PLUG/FAN	1.507	551.7	526.3	575.15	539.00	25.1	25.4
7	60° NO PLUG/NO FAN	1.505	553.1	529.9	522.86	541.50	22.8	23.2
8	60° NO PLUG/FAN	1.491	552.3	518.0	777.23	535.15	34.0	34.3
9	30° NO PLUG/NO FAN	1.498	553.9	517.3	821.04	535.60	35.9	36.6
10	30° NO PLUG/FAN	1.514	554.1	508.5	1033.01	531.30	45.2	45.6
11	0° NO PLUG/NO FAN	1.517	554.4	508.9	1023.12	531.65	44.7	45.5
12	0° NO PLUG/FAN	1.512	554.4	500.6	1215.31	527.50	53.2	53.8
13								
14								
15								

TABLE B2. Data Analysis Spreadsheet - 8-mph Side-on Wind (continued)

	A	I	J	K	L	M	N
1	RECEIVER ANGLE	DENSITY	SPEC HEAT	MASS FLOW	HEAT LOSS	HEAT LOSS	T amb (°F)
2		(lbm/ft^3)	(Btu/lbm-°F)	(lbm/min)	(Btu/min)	(kW)	
3	90° PLUG/NO FAN	42.76	0.4927	8.716	42.61	0.749	71.2
4	90° PLUG/FAN	42.75	0.4928	8.715	40.75	0.716	72.4
5	90° NO PLUG/NO FAN	42.72	0.4921	8.606	72.07	1.267	71.5
6	90° NO PLUG/FAN	42.71	0.4912	8.605	106.16	1.866	71.5
7	60° NO PLUG/NO FAN	42.66	0.4918	8.583	96.32	1.693	71.7
8	60° NO PLUG/FAN	42.69	0.4903	8.509	141.71	2.491	72.7
9	30° NO PLUG/NO FAN	42.63	0.4904	8.537	150.21	2.641	72.1
10	30° NO PLUG/FAN	42.62	0.4894	8.627	190.75	3.353	72.1
11	0° NO PLUG/NO FAN	42.61	0.4895	8.641	189.27	3.327	71.3
12	0° NO PLUG/FAN	42.61	0.4886	8.613	223.84	3.935	71.3
13							
14							
15							

TABLE B2. Data Analysis Spreadsheet - 8-mph Side-on Wind (continued)

	A	O	P	Q	R	S
1	RECEIVER ANGLE	NORM HEAT LOSS	CONV HEAT LOSS	COND HEAT LOSS		HEAT LOSS ERROR
2		(kW)	(kW)	(kW)		(Btu/min)
3	90° PLUG/NO FAN	0.726		no fan		6.106
4	90° PLUG/FAN	0.696		0.656		6.104
5	90° NO PLUG/NO FAN	1.236	0.000	fan		6.086
6	90° NO PLUG/FAN	1.836	0.636	0.621		6.186
7	60° NO PLUG/NO FAN	1.658	0.422			6.141
8	60° NO PLUG/FAN	2.478	1.277	RAD HEAT LOSS		6.272
9	30° NO PLUG/NO FAN	2.621	1.384	(kW)		6.335
10	30° NO PLUG/FAN	3.359	2.159	fan/no fan		6.621
11	0° NO PLUG/NO FAN	3.325	2.089	0.580		6.622
12	0° NO PLUG/FAN	3.968	2.767			6.833
13						
14						
15						

TABLE B2. Data Analysis Spreadsheet - 8-mph Side-on Wind (continued)

	A	T	U	V	W
1	RECEIVER ANGLE	HEAT LOSS ERROR	NORM ERROR	CONV ERROR	COND ERROR
2		(kW)	(kW)	(kW)	(kW)
3	90° PLUG/NO FAN	0.107	0.104		no fan
4	90° PLUG/FAN	0.107	0.104		0.105
5	90° NO PLUG/NO FAN	0.107	0.105	0.209	fan
6	90° NO PLUG/FAN	0.109	0.107	0.211	0.105
7	60° NO PLUG/NO FAN	0.108	0.106	0.210	
8	60° NO PLUG/FAN	0.110	0.110	0.212	RAD ERROR
9	30° NO PLUG/NO FAN	0.111	0.111	0.213	(kW)
10	30° NO PLUG/FAN	0.116	0.118	0.216	fan/no fan
11	0° NO PLUG/NO FAN	0.116	0.118	0.216	0.148
12	0° NO PLUG/FAN	0.120	0.123	0.219	
13					
14					
15					

TABLE B3. Data Analysis Spreadsheet - 20-mph Side-on Wind

	A	B	C	D	E	F	G	H
1	RECEIVER ANGLE	FLOW 1 (GPM)	T in (°F)	T out (°F)	DE (microV)	T avg (°F)	DT (°F)	Ti-To (°F)
2								
3	90° PLUG/NO FAN	1.497	536.6	527.1	211.97	531.85	9.3	9.5
4	90° PLUG/FAN	1.482	535.6	524.7	227.52	530.15	10.0	10.9
5	90° NO PLUG/NO FAN	1.489	539.2	522.2	377.31	530.70	16.5	17.0
6	90° NO PLUG/FAN	1.495	537.4	463.6	1661.86	500.50	73.2	73.8
7	60° NO PLUG/NO FAN	1.493	545.5	521.9	528.52	533.70	23.1	23.6
8	60° NO PLUG/FAN	1.484	539.2	462.1	1738.17	500.65	76.5	77.1
9	30° NO PLUG/NO FAN	1.518	551.5	514.2	836.58	532.85	36.6	37.3
10	30° NO PLUG/FAN	1.513	548.0	460.5	1965.69	504.25	86.5	87.5
11	15° NO PLUG/NO FAN	1.526	549.2	506.7	949.64	527.95	41.6	42.5
12	15° NO PLUG/FAN	1.529	548.1	455.7	2071.67	501.90	91.2	92.4
13	0° NO PLUG/NO FAN	1.521	551.5	505.3	1042.90	528.40	45.6	46.2
14	0° NO PLUG/FAN	1.535	549.2	452.1	2184.73	500.65	96.2	97.1
15								

TABLE B3. Data Analysis Spreadsheet - 20-mph Side-on Wind (continued)

	A	I	J	K	L	M	N
1	RECEIVER ANGLE	DENSITY	SPEC HEAT	MASS FLOW	HEAT LOSS	HEAT LOSS	T amb (°F)
2		(lbm/ft^3)	(Btu/lbm-°F)	(lbm/min)	(Btu/min)	(kW)	
3	90° PLUG/NO FAN	43.28	0.4896	8.662	39.31	0.691	66.2
4	90° PLUG/FAN	43.32	0.4892	8.582	41.78	0.735	67.9
5	90° NO PLUG/NO FAN	43.18	0.4893	8.596	69.41	1.220	69.0
6	90° NO PLUG/FAN	43.25	0.4825	8.644	305.07	5.363	70.5
7	60° NO PLUG/NO FAN	42.95	0.4900	8.572	97.04	1.706	68.6
8	60° NO PLUG/FAN	43.18	0.4825	8.567	316.25	5.560	68.6
9	30° NO PLUG/NO FAN	42.72	0.4898	8.669	155.31	2.730	68.2
10	30° NO PLUG/FAN	42.85	0.4833	8.668	362.18	6.367	68.4
11	15° NO PLUG/NO FAN	42.81	0.4887	8.733	177.36	3.118	68.7
12	15° NO PLUG/FAN	42.85	0.4828	8.758	385.48	6.777	68.4
13	0° NO PLUG/NO FAN	42.72	0.4888	8.686	193.77	3.406	68.0
14	0° NO PLUG/FAN	42.81	0.4825	8.784	407.58	7.165	68.2
15							

TABLE B3. Data Analysis Spreadsheet - 20-mph Side-on Wind (continued)

	A	O	P	Q	R	S
1	RECEIVER ANGLE	NORM HEAT LOSS	CONV HEAT LOSS	COND HEAT LOSS		HEAT LOSS ERROR
2		(kW)	(kW)	(kW)		(Btu/min)
3	90° PLUG/NO FAN	0.683		no fan		6.026
4	90° PLUG/FAN	0.731		0.613		5.970
5	90° NO PLUG/NO FAN	1.216	0.000	fan		6.039
6	90° NO PLUG/FAN	5.737	4.479	0.655		7.465
7	60° NO PLUG/NO FAN	1.687	0.471			6.116
8	60° NO PLUG/FAN	5.919	4.661	RAD HEAT LOSS		7.528
9	30° NO PLUG/NO FAN	2.703	1.487	(kW)		6.441
10	30° NO PLUG/FAN	6.720	5.462	fan/no fan		8.038
11	15° NO PLUG/NO FAN	3.123	1.907	0.603		6.596
12	15° NO PLUG/FAN	7.191	5.933			8.318
13	0° NO PLUG/NO FAN	3.404	2.188			6.671
14	0° NO PLUG/FAN	7.622	6.364			8.562
15						

TABLE B3. Data Analysis Spreadsheet - 20-mph Side-on Wind (continued)

	A	T	U	V	W
1	RECEIVER ANGLE	HEAT LOSS ERROR	NORM ERROR	CONV ERROR	COND ERROR
2		(kW)	(kW)	(kW)	(kW)
3	90° PLUG/NO FAN	0.106	0.105		no fan
4	90° PLUG/FAN	0.105	0.105		0.105
5	90° NO PLUG/NO FAN	0.106	0.106	0.211	fan
6	90° NO PLUG/FAN	0.131	0.144	0.233	0.105
7	60° NO PLUG/NO FAN	0.108	0.107	0.212	
8	60° NO PLUG/FAN	0.132	0.145	0.233	RAD ERROR
9	30° NO PLUG/NO FAN	0.113	0.113	0.215	(kW)
10	30° NO PLUG/FAN	0.141	0.154	0.239	fan/no fan
11	15° NO PLUG/NO FAN	0.116	0.117	0.217	0.149
12	15° NO PLUG/FAN	0.146	0.160	0.243	
13	0° NO PLUG/NO FAN	0.117	0.119	0.218	
14	0° NO PLUG/FAN	0.151	0.166	0.247	
15					

TABLE B4. Data Analysis Spreadsheet - 6-mph Head-on Wind

	A	B	C	D	E	F	G	H
1	RECEIVER ANGLE	FLOW 1 (GPM)	T in (°F)	T out (°F)	DE (microV)	T avg (°F)	DT (°F)	Ti-To (°F)
2								
3	90° PLUG/NO FAN	1.507	544.0	535.1	200.67	539.55	8.8	8.9
4	90° PLUG/FAN	1.500	543.3	533.7	214.80	538.50	9.4	9.6
5	90° NO PLUG/NO FAN	1.502	543.7	527.5	363.18	535.60	15.9	16.2
6	90° NO PLUG/FAN	1.488	542.9	515.5	626.02	529.20	27.4	27.4
7	60° NO PLUG/NO FAN	1.473	543.6	522.2	483.30	532.90	21.1	21.4
8	60° NO PLUG/FAN	1.453	543.2	512.4	691.03	527.80	30.2	30.8
9	30° NO PLUG/NO FAN	1.476	543.8	510.6	744.73	527.20	32.6	33.2
10	30° NO PLUG/FAN	1.469	544.4	502.8	934.09	523.60	40.9	41.6
11	0° NO PLUG/NO FAN	1.494	546.9	504.9	939.74	525.90	41.1	42.0
12	0° NO PLUG/FAN	1.485	547.3	502.6	1003.34	524.95	43.9	44.7
13								
14								
15								

TABLE B4. Data Analysis Spreadsheet - 6-mph Head-on Wind (continued)

	A	I	J	K	L	M	N
1	RECEIVER ANGLE	DENSITY	SPEC HEAT	MASS FLOW	HEAT LOSS	HEAT LOSS	T amb (°F)
2		(lbm/ft^3)	(Btu/lbm-°F)	(lbm/min)	(Btu/min)	(kW)	
3	90° PLUG/NO FAN	43.00	0.4913	8.664	37.30	0.656	78.2
4	90° PLUG/FAN	43.03	0.4911	8.629	39.75	0.699	78.0
5	90° NO PLUG/NO FAN	43.02	0.4904	8.637	67.22	1.182	79.7
6	90° NO PLUG/FAN	43.05	0.4890	8.563	114.68	2.016	79.6
7	60° NO PLUG/NO FAN	43.02	0.4898	8.471	87.67	1.541	80.4
8	60° NO PLUG/FAN	43.03	0.4887	8.359	123.53	2.172	80.4
9	30° NO PLUG/NO FAN	43.01	0.4885	8.487	135.15	2.376	80.3
10	30° NO PLUG/FAN	42.99	0.4877	8.442	168.46	2.962	81.0
11	0° NO PLUG/NO FAN	42.90	0.4882	8.567	172.09	3.025	80.2
12	0° NO PLUG/FAN	42.88	0.4880	8.512	182.52	3.209	79.7
13							
14							
15							

TABLE B4. Data Analysis Spreadsheet - 6-mph Head-on Wind (continued)

	A	O	P	Q	R	S
1	RECEIVER ANGLE	NORM HEAT LOSS	CONV HEAT LOSS	COND HEAT LOSS		HEAT LOSS ERROR
2		(kW)	(kW)	(kW)		(Btu/min)
3	90° PLUG/NO FAN	0.654		no fan		6.046
4	90° PLUG/FAN	0.698		0.584		6.022
5	90° NO PLUG/NO FAN	1.192	0.000	fan		6.075
6	90° NO PLUG/FAN	2.063	0.830	0.624		6.166
7	60° NO PLUG/NO FAN	1.567	0.374			6.013
8	60° NO PLUG/FAN	2.233	1.000	RAD HEAT LOSS		6.066
9	30° NO PLUG/NO FAN	2.446	1.253	(kW)		6.204
10	30° NO PLUG/FAN	3.078	1.845	fan/no fan		6.347
11	0° NO PLUG/NO FAN	3.122	1.930	0.609		6.454
12	0° NO PLUG/FAN	3.315	2.082			6.481
13						
14						
15						

TABLE B4. Data Analysis Spreadsheet - 6-mph Head-on Wind (continued)

	A	T	U	V	W
1	RECEIVER ANGLE	HEAT LOSS ERROR	NORM ERROR	CONV ERROR	COND ERROR
2		(kW)	(kW)	(kW)	(kW)
3	90° PLUG/NO FAN	0.106	0.106		no fan
4	90° PLUG/FAN	0.106	0.106		0.106
5	90° NO PLUG/NO FAN	0.107	0.108	0.214	fan
6	90° NO PLUG/FAN	0.108	0.111	0.216	0.106
7	60° NO PLUG/NO FAN	0.106	0.108	0.214	
8	60° NO PLUG/FAN	0.107	0.110	0.216	RAD ERROR
9	30° NO PLUG/NO FAN	0.109	0.113	0.217	(kW)
10	30° NO PLUG/FAN	0.112	0.117	0.219	fan/no fan
11	0° NO PLUG/NO FAN	0.113	0.118	0.220	0.152
12	0° NO PLUG/FAN	0.114	0.119	0.220	
13					
14					
15					

TABLE B5. Data Analysis Spreadsheet - 8-mph Head-on Wind

	A	B	C	D	E	F	G	H
1	RECEIVER ANGLE	FLOW 1 (GPM)	T in (°F)	T out (°F)	DE (microV)	T avg (°F)	DT (°F)	Ti-To (°F)
2								
3	90° PLUG/NO FAN	1.481	540.7	532.3	187.95	536.50	8.2	8.4
4	90° PLUG/FAN	1.497	539.7	529.2	234.58	534.45	10.3	10.5
5	90° NO PLUG/NO FAN	1.507	540.5	524.7	357.53	532.60	15.6	15.8
6	90° NO PLUG/FAN	1.521	540.2	504.9	801.25	522.55	35.1	35.3
7	60° NO PLUG/NO FAN	1.511	542.5	521.0	480.47	531.75	21.0	21.5
8	60° NO PLUG/FAN	1.524	543.0	506.2	823.87	524.60	36.1	36.8
9	30° NO PLUG/NO FAN	1.527	544.7	511.2	751.79	527.95	32.9	33.5
10	30° NO PLUG/FAN	1.517	544.1	497.7	1045.73	520.90	45.8	46.4
11	0° NO PLUG/NO FAN	1.529	546.0	503.7	946.81	524.85	41.5	42.3
12	0° NO PLUG/FAN	1.526	545.2	498.4	1052.80	521.80	46.1	46.8
13								
14								
15								

TABLE B5. Data Analysis Spreadsheet - 8-mph Head-on Wind (continued)

	A	I	J	K	L	M	N
1	RECEIVER ANGLE	DENSITY	SPEC HEAT	MASS FLOW	HEAT LOSS	HEAT LOSS	T amb (°F)
2		(lbm/ft^3)	(Btu/lbm-°F)	(lbm/min)	(Btu/min)	(kW)	
3	90° PLUG/NO FAN	43.13	0.4906	8.539	34.40	0.605	77.4
4	90° PLUG/FAN	43.17	0.4902	8.638	43.41	0.763	82.0
5	90° NO PLUG/NO FAN	43.14	0.4897	8.690	66.53	1.170	80.6
6	90° NO PLUG/FAN	43.15	0.4875	8.773	150.13	2.639	83.9
7	60° NO PLUG/NO FAN	43.06	0.4895	8.698	89.47	1.573	81.7
8	60° NO PLUG/FAN	43.04	0.4879	8.769	154.38	2.714	81.6
9	30° NO PLUG/NO FAN	42.98	0.4887	8.773	141.06	2.480	80.6
10	30° NO PLUG/FAN	43.00	0.4871	8.720	194.67	3.422	77.4
11	0° NO PLUG/NO FAN	42.93	0.4880	8.775	177.54	3.121	74.3
12	0° NO PLUG/FAN	42.96	0.4873	8.764	197.01	3.463	75.8
13							
14							
15							

TABLE B5. Data Analysis Spreadsheet - 8-mph Head-on Wind (continued)

	A	O	P	Q	R	S
1	RECEIVER ANGLE	NORM HEAT LOSS	CONV HEAT LOSS	COND HEAT LOSS		HEAT LOSS ERROR
2		(kW)	(kW)	(kW)		(Btu/min)
3	90° PLUG/NO FAN	0.606		no fan		5.947
4	90° PLUG/FAN	0.776		0.536		6.023
5	90° NO PLUG/NO FAN	1.190	0.000	fan		6.101
6	90° NO PLUG/FAN	2.768	1.412	0.701		6.454
7	60° NO PLUG/NO FAN	1.608	0.417			6.170
8	60° NO PLUG/FAN	2.818	1.463	RAD HEAT LOSS		6.479
9	30° NO PLUG/NO FAN	2.550	1.360	(kW)		6.422
10	30° NO PLUG/FAN	3.550	2.194	fan/no fan		6.679
11	0° NO PLUG/NO FAN	3.187	1.996	0.654		6.615
12	0° NO PLUG/FAN	3.572	2.217			6.724
13						
14						
15						

TABLE B5. Data Analysis Spreadsheet - 8-mph Head-on Wind (continued)

	A	T	U	V	W
1	RECEIVER ANGLE	HEAT LOSS ERROR	NORM ERROR	CONV ERROR	COND ERROR
2		(kW)	(kW)	(kW)	(kW)
3	90° PLUG/NO FAN	0.105	0.105		no fan
4	90° PLUG/FAN	0.106	0.108		0.105
5	90° NO PLUG/NO FAN	0.107	0.109	0.215	fan
6	90° NO PLUG/FAN	0.113	0.120	0.222	0.108
7	60° NO PLUG/NO FAN	0.108	0.111	0.216	
8	60° NO PLUG/FAN	0.114	0.119	0.221	RAD ERROR
9	30° NO PLUG/NO FAN	0.113	0.117	0.219	(kW)
10	30° NO PLUG/FAN	0.117	0.123	0.224	fan/no fan
11	0° NO PLUG/NO FAN	0.116	0.120	0.220	0.152
12	0° NO PLUG/FAN	0.118	0.123	0.224	
13					
14					
15					

TABLE B6. Data Analysis Spreadsheet - 20-mph Head-on Wind

	A	B	C	D	E	F	G	H
1	RECEIVER ANGLE	FLOW 1 (GPM)	T in (°F)	T out (°F)	DE (microV)	T avg (°F)	DT (°F)	Ti-To (°F)
2								
3	90° PLUG/NO FAN	1.528	546.3	537.4	204.91	541.85	8.9	8.9
4	90° PLUG/FAN	1.528	544.3	527.2	353.29	535.75	15.4	17.1
5	90° NO PLUG/NO FAN	1.536	547.6	530.4	380.14	539.00	16.6	17.2
6	90° NO PLUG/FAN	1.520	536.7	459.6	1722.63	498.15	75.9	77.1
7	60° NO PLUG/NO FAN	1.513	543.5	521.2	496.01	532.35	21.7	22.3
8	60° NO PLUG/FAN	1.504	539.6	471.3	1523.37	505.45	67.0	68.3
9	30° NO PLUG/NO FAN	1.482	539.2	505.6	747.56	522.40	32.8	33.6
10	30° NO PLUG/FAN	1.515	533.3	456.0	1718.39	494.65	75.7	77.3
11	0° NO PLUG/NO FAN	1.513	530.4	489.2	917.13	509.80	40.3	41.2
12	0° NO PLUG/FAN	1.503	528.4	470.7	1290.20	499.55	56.8	57.7
13								
14								
15								

TABLE B6. Data Analysis Spreadsheet - 20-mph Head-on Wind (continued)

	A	I	J	K	L	M	N
1	RECEIVER ANGLE	DENSITY	SPEC HEAT	MASS FLOW	HEAT LOSS	HEAT LOSS	T amb (°F)
2		(lbm/ft^3)	(Btu/lbm-°F)	(lbm/min)	(Btu/min)	(kW)	
3	90° PLUG/NO FAN	42.92	0.4918	8.767	38.56	0.678	73.2
4	90° PLUG/FAN	42.99	0.4905	8.782	66.49	1.169	74.0
5	90° NO PLUG/NO FAN	42.87	0.4912	8.802	71.77	1.262	72.4
6	90° NO PLUG/FAN	43.28	0.4819	8.794	321.52	5.652	71.7
7	60° NO PLUG/NO FAN	43.02	0.4897	8.702	92.42	1.625	76.6
8	60° NO PLUG/FAN	43.17	0.4836	8.679	281.15	4.943	76.7
9	30° NO PLUG/NO FAN	43.18	0.4874	8.555	136.59	2.401	74.0
10	30° NO PLUG/FAN	43.40	0.4811	8.791	320.33	5.631	76.0
11	0° NO PLUG/NO FAN	43.51	0.4846	8.801	171.82	3.021	74.1
12	0° NO PLUG/FAN	43.59	0.4822	8.757	239.90	4.217	70.4
13							
14							
15							

TABLE B6. Data Analysis Spreadsheet - 20-mph Head-on Wind (continued)

	A	O	P	Q	R	S
1	RECEIVER ANGLE	NORM HEAT LOSS	CONV HEAT LOSS	COND HEAT LOSS		HEAT LOSS ERROR
2		(kW)	(kW)	(kW)		(Btu/min)
3	90° PLUG/NO FAN	0.665		no fan		6.125
4	90° PLUG/FAN	1.164		0.595		6.172
5	90° NO PLUG/NO FAN	1.244	0.000	fan		6.209
6	90° NO PLUG/FAN	6.097	4.360	1.088		7.693
7	60° NO PLUG/NO FAN	1.640	0.396			6.184
8	60° NO PLUG/FAN	5.303	3.566	RAD HEAT LOSS		7.281
9	30° NO PLUG/NO FAN	2.463	1.219	(kW)		6.243
10	30° NO PLUG/FAN	6.187	4.450	fan/no fan		7.672
11	0° NO PLUG/NO FAN	3.189	1.945	0.649		6.559
12	0° NO PLUG/FAN	4.521	2.784			6.973
13						
14						
15						

TABLE B6. Data Analysis Spreadsheet - 20-mph Head-on Wind (continued)

	A	T	U	V	W
1	RECEIVER ANGLE	HEAT LOSS ERROR	NORM ERROR	CONV ERROR	COND ERROR
2		(kW)	(kW)	(kW)	(kW)
3	90° PLUG/NO FAN	0.108	0.106		no fan
4	90° PLUG/FAN	0.109	0.108		0.106
5	90° NO PLUG/NO FAN	0.109	0.108	0.214	fan
6	90° NO PLUG/FAN	0.135	0.150	0.239	0.109
7	60° NO PLUG/NO FAN	0.109	0.110	0.215	
8	60° NO PLUG/FAN	0.128	0.141	0.233	RAD ERROR
9	30° NO PLUG/NO FAN	0.110	0.113	0.217	(kW)
10	30° NO PLUG/FAN	0.135	0.153	0.241	fan/no fan
11	0° NO PLUG/NO FAN	0.115	0.123	0.222	0.151
12	0° NO PLUG/FAN	0.123	0.134	0.229	
13					
14					
15					

TABLE B7. Data Analysis Spreadsheet - 15-mph Head-on Wind

	A	B	C	D	E	F	G	H
1	RECEIVER ANGLE	FLOW 1 (GPM)	T in (°F)	T out (°F)	DE (microV)	T avg (°F)	DT (°F)	Ti-To (°F)
2								
3	90° PLUG/NO FAN	1.038	554.0	535.0	436.66	544.50	19.0	19.0
4	90° PLUG/FAN	1.044	548.3	529.3	433.84	538.80	18.9	19.0
5	90° FAN	1.038	524.1	442.8	1849.81	483.45	81.7	81.3
6	60° FAN	1.079	495.7	445.2	1157.37	470.45	51.3	50.5
7	30° FAN	1.058	515.8	442.0	1684.47	478.90	74.5	73.8
8	0° FAN	1.079	508.7	442.5	1505.00	475.60	66.6	66.2
9								
10								
11								
12								
13								
14								
15								

TABLE B7. Data Analysis Spreadsheet - 15-mph Head-on Wind (continued)

	A	I	J	K	L	M	N
1	RECEIVER ANGLE	DENSITY	SPEC HEAT	MASS FLOW	HEAT LOSS	HEAT LOSS	T amb (°F)
2		(lbm/ft^3)	(Btu/lbm-°F)	(lbm/min)	(Btu/min)	(kW)	
3	90° PLUG/NO FAN	42.63	0.4924	5.915	55.48	0.975	80.3
4	90° PLUG/FAN	42.84	0.4911	5.979	55.64	0.978	79.8
5	90° FAN	43.75	0.4786	6.070	237.45	4.174	79.7
6	60° FAN	44.78	0.4757	6.459	157.57	2.770	79.4
7	30° FAN	44.05	0.4776	6.230	221.67	3.897	80.2
8	0° FAN	44.31	0.4768	6.391	203.01	3.569	80.3
9							
10							
11							
12							
13							
14							
15							

TABLE B7. Data Analysis Spreadsheet - 15-mph Head-on Wind (continued)

	A	O	P	Q	R	S
1	RECEIVER ANGLE	NORM HEAT LOSS	CONV HEAT LOSS	COND HEAT LOSS		HEAT LOSS ERROR
2		(kW)	(kW)	(kW)		(Btu/min)
3	90° PLUG/NO FAN	0.966		no fan		4.202
4	90° PLUG/FAN	0.980		0.896		4.236
5	90° FAN	4.756	3.236	fan		5.437
6	60° FAN	3.258	1.738	0.904		4.946
7	30° FAN	4.496	2.976			5.363
8	0° FAN	4.153	2.633	RAD HEAT LOSS		5.277
9				(kW)		
10				fan/no fan		
11				0.616		
12						
13						
14						
15						

TABLE B7. Data Analysis Spreadsheet - 15-mph Head-on Wind (continued)

	A	T	U	V	W
1	RECEIVER ANGLE	HEAT LOSS ERROR	NORM ERROR	CONV ERROR	COND ERROR
2		(kW)	(kW)	(kW)	(kW)
3	90° PLUG/NO FAN	0.074	0.073		no fan
4	90° PLUG/FAN	0.074	0.075		0.074
5	90° FAN	0.096	0.113	0.202	fan
6	60° FAN	0.087	0.104	0.198	0.075
7	30° FAN	0.094	0.112	0.202	
8	0° FAN	0.093	0.111	0.201	RAD ERROR
9					(kW)
10					fan/no fan
11					0.150
12					
13					
14					
15					

TABLE B8. Data Analysis Spreadsheet - 24-mph Head-on Wind, 18-inch Aperture

	A	B	C	D	E	F	G	H
1	RECEIVER ANGLE	FLOW 1 (GPM)	T in (°F)	T out (°F)	DE (microV)	T avg (°F)	DT (°F)	Ti-To (°F)
2								
3	90° PLUG/NO FAN	1.405	528.2	515.7	310.89	521.95	13.6	12.5
4	90° PLUG/FAN	1.407	490.0	477.5	286.87	483.75	12.7	12.5
5	90° FAN	1.374	516.1	417.5	2227.12	466.80	98.8	98.6
6	75° FAN	1.389	515.4	432.9	1872.42	474.15	82.9	82.5
7	60° FAN	1.380	514.4	436.4	1773.50	475.40	78.5	78.0
8	45° FAN	1.384	514.6	419.9	2147.98	467.25	95.3	94.7
9	30° FAN	1.368	510.2	413.7	2184.73	461.95	97.0	96.5
10	15° FAN	1.365	498.5	423.5	1697.19	461.00	75.4	75.0
11	0° FAN	1.370	502.0	427.7	1683.06	464.85	74.7	74.3
12								
13								
14								
15								

TABLE B8. Data Analysis Spreadsheet - 24-mph Head-on Wind, 18-inch Aperture (continued)

	A	I	J	K	L	M	N
1	RECEIVER ANGLE	DENSITY	SPEC HEAT	MASS FLOW	HEAT LOSS	HEAT LOSS	T amb (°F)
2		(lbm/ft^3)	(Btu/lbm-°F)	(lbm/min)	(Btu/min)	(kW)	
3	90° PLUG/NO FAN	43.59	0.4873	8.188	54.36	0.956	74.7
4	90° PLUG/FAN	44.98	0.4787	8.460	51.33	0.902	76.4
5	90° FAN	44.04	0.4748	8.089	379.40	6.670	80.0
6	75° FAN	44.06	0.4765	8.182	323.23	5.682	80.6
7	60° FAN	44.10	0.4768	8.136	304.51	5.353	80.0
8	45° FAN	44.09	0.4749	8.158	369.08	6.488	79.7
9	30° FAN	44.25	0.4737	8.093	371.93	6.538	79.8
10	15° FAN	44.68	0.4735	8.152	290.99	5.115	78.0
11	0° FAN	44.55	0.4744	8.159	289.07	5.082	77.7
12							
13							
14							
15							

TABLE B8. Data Analysis Spreadsheet - 24-mph Head-on Wind, 18-inch Aperture (continued)

	A	O	P	Q	R	S
1	RECEIVER ANGLE	NORM HEAT LOSS	CONV HEAT LOSS	COND HEAT LOSS		HEAT LOSS ERROR
2		(kW)	(kW)	(kW)		(Btu/min)
3	90° PLUG/NO FAN	0.983		no fan		5.701
4	90° PLUG/FAN	1.019		0.913		5.779
5	90° FAN	7.932	6.373	fan		7.867
6	75° FAN	6.642	5.083	0.943		7.342
7	60° FAN	6.228	4.669			7.138
8	45° FAN	7.701	6.142	RAD HEAT LOSS		7.789
9	30° FAN	7.870	6.312	(kW)		7.779
10	15° FAN	6.144	4.585	fan/no fan		6.989
11	0° FAN	6.038	4.479	0.616		6.983
12						
13						
14						
15						

TABLE B8. Data Analysis Spreadsheet - 24-mph Head-on Wind, 18-inch Aperture (continued)

	A	T	U	V	W
1	RECEIVER ANGLE	HEAT LOSS ERROR	NORM ERROR	CONV ERROR	COND ERROR
2		(kW)	(kW)	(kW)	(kW)
3	90° PLUG/NO FAN	0.100	0.103		no fan
4	90° PLUG/FAN	0.102	0.115		0.104
5	90° FAN	0.138	0.172	0.256	fan
6	75° FAN	0.129	0.156	0.245	0.115
7	60° FAN	0.125	0.151	0.242	
8	45° FAN	0.137	0.170	0.254	RAD ERROR
9	30° FAN	0.137	0.172	0.256	(kW)
10	15° FAN	0.123	0.153	0.243	fan/no fan
11	0° FAN	0.123	0.151	0.242	0.150
12					
13					
14					
15					

TABLE B9. Data Analysis Spreadsheet - 24-mph Head-on Wind, 6-inch Aperture

	A	B	C	D	E	F	G	H
1	RECEIVER ANGLE	FLOW 1 (GPM)	T in (°F)	T out (°F)	DE (microV)	T avg (°F)	DT (°F)	Ti-To (°F)
2								
3	90° PLUG/NO FAN	1.049	536.0	524.3	291.11	530.15	12.7	11.7
4	90° PLUG/FAN	1.055	531.8	519.2	288.28	525.50	12.6	12.6
5	90° FAN	1.038	534.9	503.7	715.05	519.30	31.3	31.2
6	60° FAN	0.986	534.0	504.8	675.48	519.40	29.6	29.2
7	30° FAN	1.001	534.3	489.8	1020.29	512.05	44.8	44.5
8	0° FAN	0.999	537.0	491.4	1040.08	514.20	45.6	45.6
9								
10								
11								
12								
13								
14								
15								

TABLE B9. Data Analysis Spreadsheet - 24-mph Head-on Wind, 6-inch Aperture (continued)

	A	I	J	K	L	M	N
1	RECEIVER ANGLE	DENSITY	SPEC HEAT	MASS FLOW	HEAT LOSS	HEAT LOSS	T amb (°F)
2		(lbm/ft^3)	(Btu/lbm-°F)	(lbm/min)	(Btu/min)	(kW)	
3	90° PLUG/NO FAN	43.30	0.4892	6.073	37.83	0.665	84.6
4	90° PLUG/FAN	43.46	0.4881	6.129	37.77	0.664	85.8
5	90° FAN	43.35	0.4867	6.015	91.77	1.613	84.7
6	60° FAN	43.38	0.4867	5.718	82.42	1.449	82.9
7	30° FAN	43.37	0.4851	5.803	126.11	2.217	84.1
8	0° FAN	43.27	0.4856	5.778	128.07	2.252	82.9
9							
10							
11							
12							
13							
14							
15							

TABLE B9. Data Analysis Spreadsheet - 24-mph Head-on Wind, 6-inch Aperture (continued)

	A	O	P	Q	R	S
1	RECEIVER ANGLE	NORM HEAT LOSS	CONV HEAT LOSS	COND HEAT LOSS		HEAT LOSS ERROR
2		(kW)	(kW)	(kW)		(Btu/min)
3	90° PLUG/NO FAN	0.687		no fan		4.239
4	90° PLUG/FAN	0.695		0.679		4.269
5	90° FAN	1.708	0.953	fan		4.363
6	60° FAN	1.527	0.772	0.687		4.125
7	30° FAN	2.383	1.629			4.408
8	0° FAN	2.401	1.647	RAD HEAT LOSS		4.408
9				(kW)		
10				fan/no fan		
11				0.068		
12						
13						
14						
15						

TABLE B9. Data Analysis Spreadsheet - 24-mph Head-on Wind, 6-inch Aperture (continued)

	A	T	U	V	W
1	RECEIVER ANGLE	HEAT LOSS ERROR	NORM ERROR	CONV ERROR	COND ERROR
2		(kW)	(kW)	(kW)	(kW)
3	90° PLUG/NO FAN	0.075	0.077		no fan
4	90° PLUG/FAN	0.075	0.079		0.077
5	90° FAN	0.077	0.082	0.115	fan
6	60° FAN	0.073	0.077	0.111	0.079
7	30° FAN	0.077	0.084	0.117	
8	0° FAN	0.077	0.084	0.116	RAD ERROR
9					(kW)
10					fan/no fan
11					0.017
12					
13					
14					
15					

Appendix C

Tabulated Summary of Receiver Heat Loss Results

TABLE C1. Summary of Conduction, Radiation, and Convection Heat Losses from the Receiver at 530°F for the No-Wind Tests (6 Sets Corresponding to 6 Wind-Condition Sets) from the First Test Series

Test Set/ Heat Loss Mode	Heat Loss (kW)	Uncertainty (kW)	Uncertainty Percentage
6-mph Side-on Set			
- Conduction	0.619	0.105	17.0
- Radiation	0.598	0.150	25.1
- Convection: 0° tilt angle	2.132	0.218	10.2
30°	1.395	0.216	15.5
60°	0.406	0.212	52.2
90°	0.000	-	-
8-mph Side-on Set			
- Conduction	0.656	0.105	16.0
- Radiation	0.580	0.148	25.5
- Convection: 0° tilt angle	2.089	0.216	10.3
30°	1.384	0.213	15.4
60°	0.422	0.210	49.8
90°	0.000	-	-
20-mph Side-on Set			
- Conduction	0.613	0.105	17.1
- Radiation	0.603	0.149	24.7
- Convection: 0° tilt angle	2.188	0.218	10.0
30°	1.487	0.215	14.5
60°	0.471	0.212	45.0
90°	0.000	-	-

TABLE C1. Summary of Conduction, Radiation, and Convection Heat Losses from the Receiver at 530°F for the No-Wind Tests (6 Sets Corresponding to 6 Wind-Condition Sets) from the First Test Series (continued)

Test Condition/ Heat Loss Mode	Heat Loss (kW)	Uncertainty (kW)	Uncertainty Percentage
6-mph Head-on Set			
- Conduction	0.584	0.106	18.2
- Radiation	0.609	0.152	25.0
- Convection: 0° tilt angle	1.930	0.220	11.4
30°	1.253	0.217	17.3
60°	0.374	0.214	57.2
90°	0.000	-	-
8-mph Head-on Set			
- Conduction	0.536	0.105	19.6
- Radiation	0.654	0.152	23.2
- Convection: 0° tilt angle	1.996	0.220	11.0
30°	1.360	0.219	16.1
60°	0.417	0.216	51.8
90°	0.000	-	-
20-mph Head-on Set			
- Conduction	0.595	0.106	17.8
- Radiation	0.649	0.151	23.3
- Convection: 0° tilt angle	1.945	0.222	11.4
30°	1.219	0.217	17.8
60°	0.396	0.215	54.3
90°	0.000	-	-

TABLE C2. Summary of Conduction, Radiation, and Convection Heat Losses from the Receiver at 530°F for Side-On Wind Tests from the First Test Series

Test Condition/ Heat Loss Mode		Heat Loss (kW)	Uncertainty (kW)	Uncertainty Percentage
6-mph Side-On Wind				
- Conduction		0.591	0.106	17.9
- Radiation		0.598	0.150	25.1
- Convection:	0° tilt angle	2.407	0.220	9.1
	30°	1.862	0.218	11.7
	60°	1.010	0.215	21.3
	90°	0.415	0.213	51.3
8-mph Side-On Wind				
- Conduction		0.621	0.105	16.9
- Radiation		0.580	0.148	25.5
- Convection:	0° tilt angle	2.767	0.219	7.9
	30°	2.159	0.216	10.0
	60°	1.277	0.212	16.6
	90°	0.636	0.211	33.2
20-mph Side-On Wind				
- Conduction		0.655	0.105	16.0
- Radiation		0.603	0.149	24.7
- Convection:	0° tilt angle	6.364	0.247	3.9
	30°	5.462	0.239	4.4
	60°	4.661	0.233	5.0
	90°	4.479	0.233	5.2

TABLE C3. Summary of Conduction, Radiation, and Convection Heat Losses from the Receiver at 530°F for Head-On Wind Tests from the First Test Series

Test Condition/ Heat Loss Mode	Heat Loss (kW)	Uncertainty (kW)	Uncertainty Percentage
6-mph Head-On Wind			
- Conduction	0.624	0.106	17.0
- Radiation	0.609	0.152	25.0
- Convection: 0° tilt angle	2.082	0.220	10.6
30°	1.845	0.219	11.9
60°	1.000	0.216	21.6
90°	0.830	0.216	26.0
8-mph Head-On Wind			
- Conduction	0.701	0.108	15.4
- Radiation	0.654	0.152	23.2
- Convection: 0° tilt angle	2.217	0.224	10.1
30°	2.194	0.224	10.2
60°	1.463	0.221	15.1
90°	1.412	0.222	15.7
20-mph Head-On Wind			
- Conduction	1.088	0.109	10.0
- Radiation	0.649	0.151	23.3
- Convection: 0° tilt angle	2.784	0.229	8.2
30°	4.450	0.241	5.4
60°	3.566	0.233	6.5
90°	4.360	0.239	5.5

TABLE C4. Summary of Conduction and Convection Heat Losses from the Receiver at 530°F for Head-on Wind Tests from the Second Test Series

Test Condition/ Heat Loss Mode	Heat Loss (kW)	Uncertainty (kW)	Uncertainty Percentage
15-mph Head-On Wind (18-inch dia. aperture)			
- Conduction (no wind)	0.896	0.074	8.3
- Conduction (with wind)	0.904	0.075	8.3
- Convection (with wind)			
0° tilt angle	2.633	0.201	7.6
30°	2.976	0.202	6.8
60°	1.738	0.198	11.4
90°	3.236	0.202	6.2
24-mph Head-On Wind (18-inch dia. aperture)			
- Conduction (no wind)	0.913	0.104	11.4
- Conduction (with wind)	0.943	0.115	12.2
- Convection (with wind)			
0° tilt angle	4.479	0.242	5.4
15°	4.585	0.243	5.3
30°	6.312	0.256	4.1
45°	6.142	0.254	4.1
60°	4.669	0.242	5.2
75°	5.083	0.245	4.8
90°	6.373	0.256	4.0
24-mph Head-On Wind (6-inch dia. aperture)			
- Conduction (no wind)	0.679	0.077	11.3
- Conduction (with wind)	0.687	0.079	11.5
- Convection (with wind)			
0° tilt angle	1.647	0.116	7.0
30°	1.629	0.117	7.2
60°	0.772	0.111	14.4
90°	0.953	0.115	12.1

Appendix D

Tabulated Measured Receiver Temperatures

TABLE D1. Measured Receiver Temperatures (°F) - 6-mph Side-on Wind

	A	B	C	D	E	F	G	H	I	J	K
1	TC No.	0° No Fan	30° No Fan	60° No Fan	90° No Fan	0° Fan	30° Fan	60° Fan	90° Fan	90° Plug, No Fan	90° Plug, Fan
2	1	232.9	278.1	503.3	516.1	273.4	263.7	329.8	445.5	536.9	535.8
3	2	517.5	435.7	447.2	445.3	518.3	520.3	529.1	533.5	545.0	445.0
4	3	114.0	207.7	211.7	209.9	77.9	82.0	82.1	175.3	117.6	185.7
5	4	168.1	181.8	298.6	506.4	331.0	216.4	250.2	483.0	528.0	527.0
6	5	517.6	437.4	533.0	537.2	520.9	517.8	528.2	534.5	545.2	543.2
7	6	122.2	127.4	128.5	131.5	86.8	90.5	106.3	95.9	123.8	99.9
8	7	277.7	327.7	507.3	515.7	193.8	234.6	323.1	457.4	537.4	536.1
9	8	519.1	523.3	537.6	537.9	512.7	516.3	529.0	534.7	450.8	446.0
10	9	122.2	126.6	133.3	130.6	93.2	97.0	106.5	98.8	126.2	104.1
11	10	425.1	498.6	508.2	508.6	473.8	487.7	485.0	453.8	534.8	534.0
12	11	521.0	526.3	451.6	536.4	521.5	522.1	531.5	533.9	450.3	543.5
13	12	110.1	112.9	138.0	115.3	84.7	87.2	90.5	89.2	111.6	92.2
14	13	293.7	397.5	523.4	525.8	310.7	358.4	514.0	522.3	542.3	541.3
15	14	542.9	542.1	545.8	544.2	537.0	539.2	546.1	545.2	548.6	547.7
16	15	91.5	103.2	107.2	101.3	73.0	75.2	80.1	78.8	95.3	80.5
17	16										
18	17	543.1	541.6	546.6	545.2	541.0	538.8	546.4	545.5	548.9	547.8
19	18	92.0	111.8	115.8	102.2	74.6	83.0	87.3	81.7	91.5	81.2
20	19	225.9	417.7	527.3	529.0	203.6	260.4	519.7	525.8	544.2	543.5
21	20	544.4	544.0	548.0	546.4	538.0	539.5	547.9	546.3	550.4	549.5
22	21	97.3	106.9	112.2	107.7	83.7	87.2	90.1	88.5	102.0	89.0
23	22	285.4	521.9	528.6	528.6	331.1	517.1	526.0	524.9	543.4	542.1
24	23	544.0	544.1	546.5	544.6	539.2	543.6	546.1	544.1	549.0	547.4
25	24	94.6	97.6	105.4	94.5	77.3	79.5	81.7	80.0	86.8	80.5
26	25	316.1	503.6	519.0	517.9	297.4	414.7	514.8	513.2	538.9	537.6
27	26	371.9	493.5	507.1	508.9	342.0	426.1	502.3	503.4	532.5	531.9
28	Ambient Temp.	66.6	71.3	72.0	71.0	66.6	71.3	72.0	71.0	70.2	70.6
29	Avg. Air Temp.	278.1	390.9	489.5	518.5	301.9	344.1	432.8	490.7	538.2	537.2
30	Avg. In. Surf. Temp.	513.5	509.8	518.2	527.3	507.8	518.2	534.1	535.7	524.5	522.4
31	Avg. Out. Surf. Temp.	105.5	124.3	131.5	124.1	81.4	85.2	90.6	98.5	106.8	101.6
32	I.S. - Air Temp.	235.4	118.9	28.7	8.8	206.0	174.1	101.2	44.9	-13.7	-14.7
33	I.S. - O.S. Temp.	408.0	385.5	386.6	403.2	428.4	433.0	443.5	437.2	417.7	420.8
34	O.S. - Amb. Temp.	38.9	53.0	59.5	53.1	14.8	13.9	18.6	27.5	36.6	31.0

TABLE D2. Measured Receiver Temperatures (°F) - 8-mph Side-on Wind

	A	B	C	D	E	F	G	H	I	J	K
1	TC No.	0° No Fan	30° No Fan	60° No Fan	90° No Fan	0° Fan	30° Fan	60° Fan	90° Fan	90° Plug, No Fan	90° Plug, Fan
2	1	227.2	277.4	502.8	517.3	260.1	253.0	280.2	368.5	534.7	536.8
3	2	515.1	434.6	447.7	448.1	419.0	426.5	432.0	533.1	543.7	444.2
4	3	118.8	111.4	120.2	124.7	80.3	173.3	172.2	82.8	210.4	181.8
5	4	169.5	186.0	292.6	508.2	357.3	234.4	257.8	443.6	525.3	527.3
6	5	513.5	521.7	446.1	442.4	511.8	516.0	527.2	535.4	544.1	545.0
7	6	125.4	120.7	126.7	130.0	85.0	90.4	99.4	92.0	119.7	90.7
8	7	284.2	332.3	506.5	516.5	184.5	201.2	285.1	422.7	535.5	537.3
9	8	515.6	523.8	538.2	539.6	501.9	423.1	527.2	535.3	544.7	546.0
10	9	125.5	124.6	126.9	131.5	93.6	96.4	100.2	94.4	126.5	95.1
11	10	420.9	498.4	508.5	509.6	457.2	461.7	416.8	432.2	532.6	535.1
12	11	431.2	526.9	536.9	447.5	424.8	519.5	527.3	442.6	448.5	544.9
13	12	110.7	110.2	120.5	117.6	84.3	85.6	85.8	85.8	112.7	85.5
14	13	292.6	394.6	524.1	526.9	282.6	320.6	468.6	522.3	540.2	542.3
15	14	539.0	543.3	547.1	545.8	528.2	537.2	545.5	546.3	546.7	548.7
16	15	92.2	94.0	101.3	103.5	77.1	75.6	78.9	77.3	93.3	75.3
17	16										
18	17	538.7	543.1	454.8	453.2	438.6	442.6	448.7	451.3	547.5	447.3
19	18	93.6	106.0	107.7	103.8	76.6	81.5	80.9	82.2	88.8	75.6
20	19	229.0	416.1	527.8	530.3	206.1	239.7	429.2	526.0	542.4	544.4
21	20	540.1	544.9	549.1	547.9	528.3	440.3	546.6	548.3	549.3	447.4
22	21	98.0	103.8	107.5	108.5	85.5	85.0	85.3	85.3	101.1	81.8
23	22	283.0	522.0	528.8	530.2	333.3	469.5	518.7	526.0	542.0	543.3
24	23	540.4	545.2	547.6	546.7	531.1	542.2	546.1	546.6	450.5	549.2
25	24	94.6	96.2	99.7	96.9	77.9	77.9	78.8	78.6	88.9	76.5
26	25	314.0	503.1	519.5	519.6	281.2	347.0	510.6	514.8	537.3	538.9
27	26	368.7	493.2	507.8	510.3	325.4	379.4	498.8	505.0	530.6	533.1
28	Ambient Temp.	71.3	72.1	71.7	71.5	71.3	72.1	72.7	71.5	71.2	72.4
29	Avg. Air Temp.	277.6	391.2	488.8	519.8	295.3	315.9	395.9	469.5	536.3	538.2
30	Avg. In. Surf. Temp.	500.3	519.6	508.4	497.9	467.7	469.6	511.0	516.0	522.8	511.8
31	Avg. Out. Surf. Temp.	107.4	108.4	113.8	114.6	82.5	95.7	97.7	84.8	117.7	95.3
32	I.S. - Air Temp.	222.7	128.4	19.5	-21.9	172.4	153.8	115.2	46.5	-13.4	-26.4
33	I.S. - O.S. Temp.	392.9	411.3	394.6	383.4	385.1	373.9	413.4	431.2	405.2	416.5
34	O.S. - Amb. Temp.	36.1	36.3	42.1	43.1	11.2	23.6	25.0	13.3	46.5	22.9

TABLE D3. Measured Receiver Temperatures (°F) - 20-mph Side-on Wind

	A	B	C	D	E	F	G	H	I	J	K
1	TC No.	0° No Fan	30° No Fan	60° No Fan	90° No Fan	0° Fan	30° Fan	60° Fan	90° Fan	90° Plug, No Fan	90° Plug, Fan
2	1	222.0	283.8	492.8	504.4	200.0	200.4	204.8	200.0	522.1	522.1
3	2	511.9	519.7	526.8	436.2	459.2	467.4	471.5	391.2	530.4	530.6
4	3	111.8	113.4	113.4	203.0	75.0	76.2	74.8	157.9	114.7	162.7
5	4	170.8	183.3	288.8	494.3	304.2	334.2	231.6	231.5	513.3	512.5
6	5	509.8	518.8	523.5	526.0	473.2	480.0	476.4	477.3	530.5	530.4
7	6	116.2	116.5	119.0	123.9	75.8	79.0	81.0	81.3	121.1	79.5
8	7	273.4	326.8	497.0	503.8	137.0	141.0	190.0	161.1	522.6	520.1
9	8	511.7	520.6	528.0	436.8	449.2	458.5	466.4	463.8	531.5	431.8
10	9	114.4	117.7	120.4	123.8	82.2	82.6	84.0	83.7	122.8	81.6
11	10	415.5	495.4	498.7	497.4	352.6	327.4	203.8	202.0	520.0	517.9
12	11	515.5	524.0	527.2	436.0	472.1	476.5	468.9	393.4	530.1	433.3
13	12	102.7	105.5	122.0	109.3	76.0	76.4	76.4	77.2	110.6	75.4
14	13	289.1	395.4	513.8	514.6	201.2	217.5	267.2	257.3	527.0	526.8
15	14	536.2	540.1	536.8	533.4	500.2	508.0	507.7	508.7	533.1	535.1
16	15	85.3	91.5	98.0	96.7	74.0	73.7	74.3	75.1	95.8	72.0
17	16										
18	17	536.1	540.1	538.0	533.9	507.9	513.0	512.6	423.2	533.7	436.6
19	18	91.3	90.5	92.6	94.6	73.2	74.8	76.0	74.3	91.2	71.5
20	19	222.2	404.6	517.5	517.9	160.4	161.6	334.1	260.6	529.1	527.2
21	20	537.3	542.6	538.7	535.6	497.2	503.6	513.1	506.1	535.5	534.6
22	21	89.2	96.3	102.4	103.5	78.0	76.9	78.0	79.0	104.4	76.0
23	22	286.6	520.0	519.4	518.0	252.6	205.2	211.1	194.1	528.5	527.1
24	23	536.8	543.2	537.7	534.5	507.2	508.4	502.1	502.4	534.7	534.6
25	24	87.3	91.4	96.2	89.9	73.7	74.8	75.2	74.5	90.6	72.2
26	25	309.2	500.9	509.9	507.6	191.2	205.8	267.2	246.6	524.7	522.3
27	26	363.0	488.8	498.5	498.1	246.5	265.7	312.5	312.5	519.3	516.8
28	Ambient Temp.	68.0	68.2	68.6	69.0	68.2	68.4	68.6	70.5	66.2	67.9
29	Avg. Air Temp.	273.6	388.8	479.7	507.3	224.9	224.1	238.7	219.2	523.4	522.0
30	Avg. In. Surf. Temp.	506.5	526.4	528.1	496.7	457.0	464.6	470.1	442.1	531.0	498.2
31	Avg. Out. Surf. Temp.	99.8	102.9	108.0	118.1	76.0	76.8	77.5	87.9	106.4	86.4
32	I.S. - Air Temp.	232.9	137.7	48.4	-10.5	232.1	240.4	231.4	222.9	7.6	-23.8
33	I.S. - O.S. Temp.	406.7	423.6	420.1	378.6	381.0	387.8	392.7	354.2	424.6	411.8
34	O.S. - Amb. Temp.	31.8	34.6	39.4	49.1	7.8	8.4	8.9	17.4	40.2	18.5

TABLE D4. Measured Receiver Temperatures (°F) - 6-mph Head-on Wind

	A	B	C	D	E	F	G	H	I	J	K
1	TC No.	0° No Fan	30° No Fan	60° No Fan	90° No Fan	0° Fan	30° Fan	60° Fan	90° Fan	90° Plug, No Fan	90° Plug, Fan
2	1	239.0	283.0	496.7	511.2	186.4	330.7	377.7	269.0	530.7	529.4
3	2	511.1	516.4	529.3	531.4	505.4	508.5	519.7	520.1	538.8	538.0
4	3	133.1	128.5	128.9	128.0	110.3	98.6	105.1	105.3	129.3	104.2
5	4	173.5	191.0	298.6	501.4	167.7	164.0	186.6	359.5	521.4	520.0
6	5	510.1	515.8	525.8	531.9	507.1	506.0	515.8	523.9	539.0	538.0
7	6	138.6	133.7	138.3	139.7	113.7	122.2	111.8	110.7	137.4	108.6
8	7	287.0	332.2	500.6	510.6	283.5	336.7	377.0	340.1	531.4	529.9
9	8	511.1	517.4	530.4	532.5	509.5	512.0	520.0	525.1	537.7	538.7
10	9	138.6	134.6	134.8	137.4	115.7	103.5	105.6	101.9	138.7	100.9
11	10	417.7	492.9	501.2	503.5	412.0	449.2	446.8	313.0	528.3	527.1
12	11	512.8	519.8	528.8	530.6	510.7	427.1	520.5	521.9	538.2	442.5
13	12	121.4	122.0	129.5	123.8	111.2	99.2	96.2	96.3	122.8	95.1
14	13	297.5	399.1	516.1	519.8	265.6	345.7	476.3	503.6	535.0	533.5
15	14	532.5	534.6	538.0	538.2	528.6	530.7	535.8	537.2	540.9	540.6
16	15	107.5	109.3	110.4	109.6	97.8	94.2	92.5	90.4	106.3	87.6
17	16										
18	17	532.5	534.6	538.5	538.7	530.0	528.1	534.0	538.0	541.6	541.2
19	18	106.1	120.4	116.5	111.0	92.2	100.4	93.6	95.2	105.9	91.3
20	19	235.5	423.0	520.0	523.1	219.5	253.1	485.6	515.3	537.2	536.0
21	20	533.6	536.8	540.0	540.5	533.1	532.9	538.8	539.4	543.3	542.8
22	21	113.8	116.0	116.5	117.6	107.3	97.0	93.4	92.8	114.4	89.8
23	22	290.5	515.8	521.0	523.2	283.3	425.5	516.1	515.2	536.7	535.2
24	23	533.8	537.3	539.0	539.3	531.1	533.6	537.9	538.0	542.6	541.7
25	24	106.9	107.0	108.0	104.9	101.7	93.4	90.8	87.3	100.4	84.7
26	25	316.8	498.6	512.0	512.9	304.0	348.1	506.6	504.9	532.7	530.9
27	26	369.5	488.8	500.4	504.1	364.2	395.2	494.8	496.0	527.2	525.6
28	Ambient Temp.	80.2	80.3	80.4	79.7	79.7	81.0	80.4	79.6	78.2	78.0
29	Avg. Air Temp.	282.2	392.0	483.3	513.2	265.3	331.6	421.6	415.1	531.7	530.3
30	Avg. In. Surf. Temp.	505.2	522.4	530.0	531.9	502.2	497.1	524.1	526.6	538.8	527.7
31	Avg. Out. Surf. Temp.	120.8	121.4	122.9	121.5	106.2	101.1	98.6	97.5	119.4	95.3
32	I.S. - Air Temp.	223.0	130.4	46.7	18.7	236.9	165.5	102.6	111.5	7.1	-2.6
33	I.S. - O.S. Temp.	384.5	401.0	407.2	410.4	396.0	396.1	425.5	429.1	419.4	432.4
34	O.S. - Amb. Temp.	40.5	41.1	42.5	41.8	26.5	20.1	18.2	17.9	41.2	17.3

TABLE D5. Measured Receiver Temperatures (°F) - 8-mph Head-on Wind

	A	B	C	D	E	F	G	H	I	J	K
1	TC No.	0° No Fan	30° No Fan	60° No Fan	90° No Fan	0° Fan	30° Fan	60° Fan	90° Fan	90° Plug, No Fan	90° Plug, Fan
2	1	239.2	283.8	495.9	508.5	177.8	330.7	351.6	253.3	530.1	523.7
3	2	509.1	517.3	442.7	528.3	501.8	505.0	427.1	427.7	537.0	533.8
4	3	210.5	130.1	133.1	131.1	103.8	96.3	102.5	102.6	141.0	103.4
5	4	177.6	191.7	296.3	499.0	164.7	166.5	183.8	288.8	521.0	514.4
6	5	508.4	515.4	524.3	528.5	503.3	503.0	509.5	513.8	537.0	533.5
7	6	135.5	133.8	140.5	146.0	105.1	117.9	111.1	109.1	153.0	110.2
8	7	287.9	335.5	499.2	507.7	271.6	348.5	366.3	288.5	529.9	523.0
9	8	509.3	517.2	528.6	529.4	506.8	507.9	515.0	513.7	537.7	533.8
10	9	131.6	134.1	139.0	138.5	107.4	99.3	103.0	100.4	145.7	101.2
11	10	412.9	492.9	500.1	500.9	421.2	386.1	420.5	282.5	527.3	520.0
12	11	510.6	520.0	527.2	527.7	508.4	507.2	515.0	509.9	535.6	532.7
13	12	120.1	123.3	136.8	125.2	106.1	97.7	96.5	97.5	130.0	97.5
14	13	297.5	397.9	514.8	517.0	264.5	355.2	425.7	403.7	533.3	528.0
15	14	531.4	535.0	536.7	534.8	526.6	529.7	532.3	532.0	538.5	536.5
16	15	105.0	111.4	116.6	113.8	95.0	92.2	92.7	92.7	119.0	92.0
17	16										
18	17	532.2	535.0	537.2	446.7	526.7	526.0	528.2	533.5	538.9	537.2
19	18	105.5	120.5	127.5	117.0	88.8	97.9	95.6	96.9	120.0	96.2
20	19	231.3	417.4	518.4	520.1	212.1	229.7	277.5	410.8	535.0	530.4
21	20	532.1	537.1	538.4	537.0	529.7	530.3	533.4	531.7	540.3	538.7
22	21	111.1	116.2	120.8	120.2	103.7	94.1	94.2	94.4	123.8	94.0
23	22	288.8	516.0	519.6	520.0	279.3	345.3	501.8	360.0	534.2	529.4
24	23	532.2	537.6	537.7	536.0	528.8	528.5	535.5	532.8	539.3	537.7
25	24	105.2	107.9	112.6	108.1	97.0	92.2	93.0	90.5	111.1	89.4
26	25	316.4	498.6	510.7	510.1	296.5	323.4	433.5	464.4	531.3	524.4
27	26	367.4	488.7	498.6	501.4	356.3	372.0	452.8	472.2	527.0	519.4
28	Ambient	74.3	80.6	81.7	80.6	75.8	77.4	81.6	83.9	77.4	82.0
29	Avg. Air Temp.	281.5	391.7	481.9	510.4	261.0	310.7	370.1	344.0	530.3	524.2
30	Avg. In. Surf. Temp.	503.6	522.6	519.0	518.9	498.7	501.1	505.4	507.5	536.8	533.7
31	Avg. Out. Surf. Temp.	128.1	122.2	128.4	125.0	100.9	98.5	98.6	98.0	130.5	98.0
32	I.S. - Air Temp.	222.2	130.9	37.2	8.5	237.7	190.4	135.3	163.5	6.5	9.5
33	I.S. - O.S. Temp.	375.6	400.4	390.7	393.9	397.8	402.6	406.8	409.5	406.4	435.7
34	O.S. - Amb. Temp.	53.8	41.6	46.7	44.4	25.1	21.1	17.0	14.1	53.0	16.0

TABLE D6. Measured Receiver Temperatures (°F) - 20-mph Head-on Wind

	A	B	C	D	E	F	G	H	I	J	K
1	TC No.	0° No Fan	30° No Fan	60° No Fan	90° No Fan	0° Fan	30° Fan	60° Fan	90° Fan	90° Plug, No Fan	90° Plug, Fan
2	1	228.2	267.2	496.7	512.6	174.9	313.5	378.0	192.4	532.7	518.6
3	2	496.2	512.3	528.4	536.0	477.7	471.6	486.7	452.7	540.8	537.2
4	3	122.7	124.4	125.6	118.7	95.8	89.1	88.8	83.0	130.0	85.5
5	4	168.2	184.1	295.2	504.3	170.3	148.0	177.6	210.2	524.1	510.1
6	5	494.4	511.6	524.7	534.0	479.3	464.4	476.2	458.8	540.5	538.0
7	6	125.8	127.2	127.7	129.2	95.1	99.5	99.0	92.1	139.5	100.2
8	7	273.2	324.9	499.8	511.4	223.8	327.6	403.2	211.9	533.1	515.5
9	8	497.0	513.0	529.3	535.5	478.6	473.5	489.4	457.6	543.3	536.7
10	9	125.2	129.0	132.1	127.5	90.1	87.7	87.3	84.1	140.2	85.2
11	10	400.7	488.9	500.7	504.9	275.5	243.0	260.4	208.3	529.8	510.5
12	11	499.0	514.3	527.7	535.2	477.7	465.8	477.3	452.7	541.3	538.1
13	12	118.9	119.1	130.8	116.4	100.2	91.9	88.0	83.7	124.3	86.0
14	13	286.2	394.0	515.2	522.5	260.2	319.0	418.9	231.2	536.9	530.0
15	14	518.7	530.6	537.2	542.2	505.5	509.5	520.2	491.3	542.4	544.0
16	15	105.6	104.7	105.3	103.9	87.0	84.5	83.0	80.4	109.3	80.5
17	16										
18	17	517.0	530.0	538.1	542.7	505.4	496.7	419.5	493.6	543.2	543.3
19	18	111.5	114.3	114.6	113.2	85.5	86.6	87.3	86.2	117.1	90.8
20	19	223.1	413.0	518.8	526.0	204.1	199.4	233.3	194.9	537.3	530.5
21	20	518.8	532.0	539.0	542.8	503.8	508.0	517.0	487.1	546.8	543.5
22	21	110.5	112.3	112.0	110.2	91.9	85.8	84.5	81.0	117.4	81.4
23	22	279.6	511.1	520.3	525.7	252.5	227.7	246.3	198.0	537.2	530.7
24	23	518.4	532.0	538.5	541.9	505.7	497.0	502.7	489.2	543.4	543.3
25	24	106.5	103.9	104.0	100.0	94.6	87.4	84.4	80.5	104.0	80.0
26	25	303.9	493.5	510.6	513.0	257.7	240.4	266.0	211.6	532.7	526.0
27	26	355.8	483.5	498.1	505.0	307.3	282.9	307.8	273.3	531.3	522.7
28	Ambient Temp.	74.1	74.0	76.6	72.4	70.4	76.0	76.7	71.7	73.2	74.0
29	Avg. Air Temp.	270.4	384.6	482.2	515.1	227.4	252.3	298.0	207.3	533.0	521.5
30	Avg. In. Surf. Temp.	490.6	517.7	529.0	535.0	471.2	463.3	466.3	450.7	541.4	538.5
31	Avg. Out. Surf. Temp.	115.8	116.9	119.0	114.9	92.5	89.1	87.8	83.9	122.7	86.2
32	I.S. - Air Temp.	220.2	133.1	46.8	20.0	243.8	210.9	168.3	243.4	8.5	17.0
33	I.S. - O.S. Temp.	374.8	400.8	410.0	420.1	378.7	374.2	378.5	366.8	418.7	452.3
34	O.S. - Amb. Temp.	41.7	42.9	42.4	42.5	22.1	13.1	11.1	12.2	49.5	12.2

Appendix E

Thermoelectric Characteristics of Type-K Thermocouples

Figure E1. Thermoelectric voltage of a type-K thermocouple for the temperature range of interest.

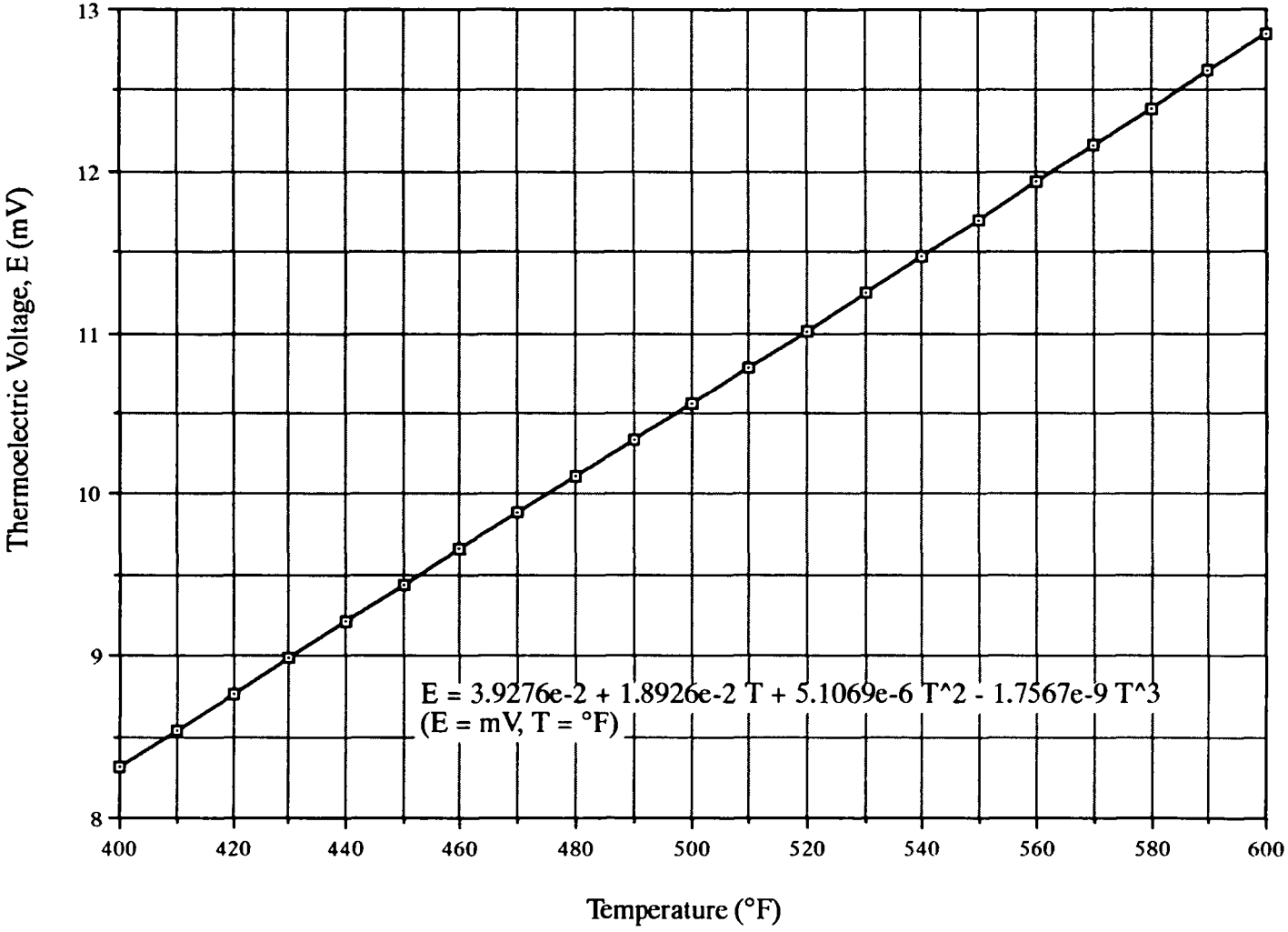

Figure E2. Thermoelectric sensitivity of a type-K thermocouple for the temperature range of interest.

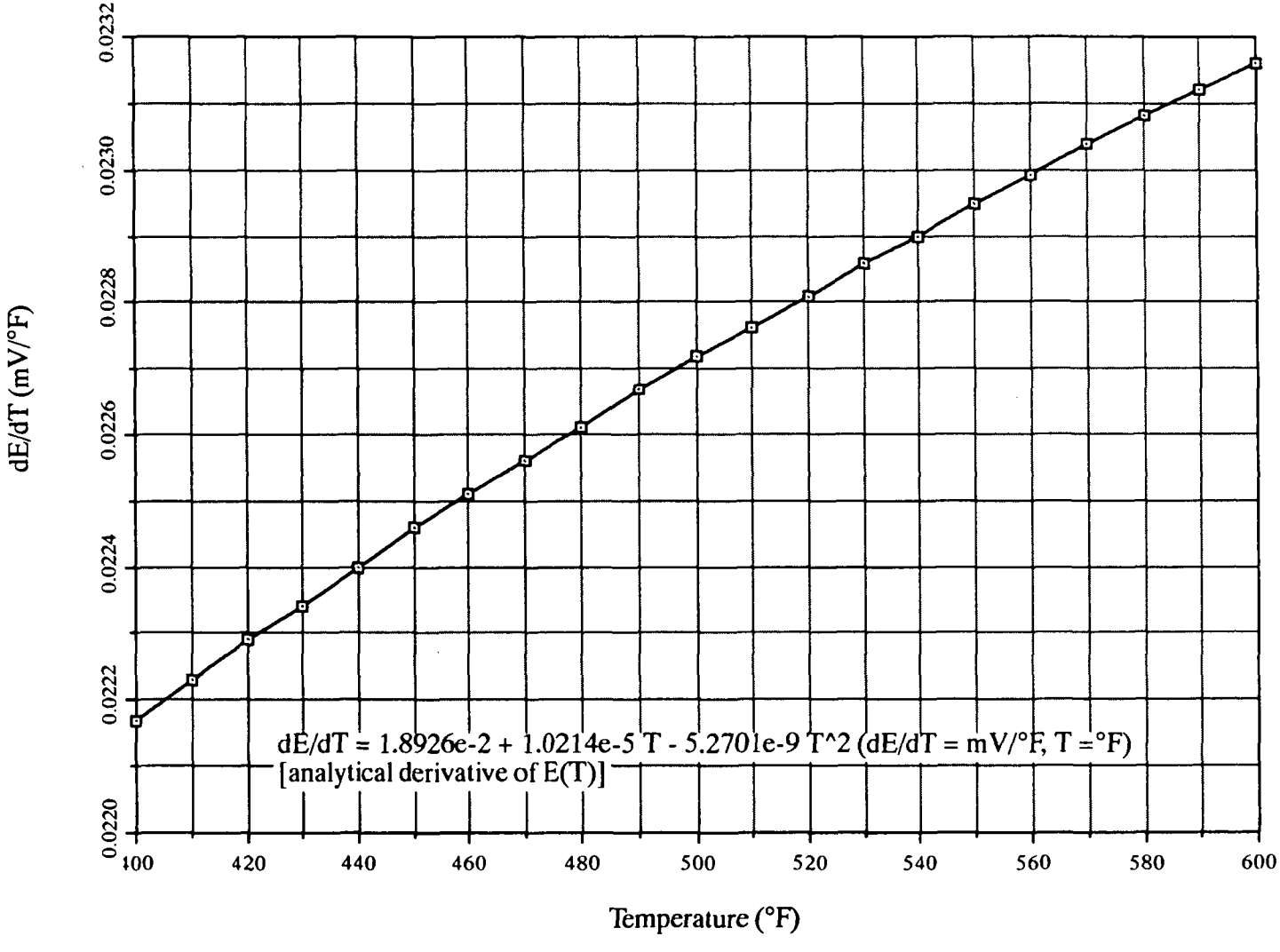

Appendix F

Uncertainty Analysis Procedure

Appendix F
Uncertainty Analysis Procedure

This appendix summarizes the uncertainty analysis procedure used to produce the error bars shown in Figures 8 and 9 and the tabulated values in Tables C1-C4 in Appendix C.

I. Uncertainty in Deriving Total Heat Loss Rate from Experimental Measurements

Total receiver heat loss rate is derived from measurements using

$$q_{meas} = Q\rho c_p \Delta T \tag{F1}$$

where q_{meas} = total receiver heat loss rate calculated from measurements, Btu/min
Q = heat-transfer-fluid volume flow rate, ft^3/min
ρ = heat-transfer-fluid density, lb_m/ft^3
c_p= heat-transfer-fluid specific heat, $Btu/(lb_m \cdot °F)$
ΔT = heat transfer fluid temperature drop from receiver inlet to outlet, °F

The uncertainty in the total heat loss rate is calculated using the following formula from Holman (1984):

$$w_{q_{meas}} = \left[\left(\frac{\partial q_{meas}}{\partial Q} w_Q \right)^2 + \left(\frac{\partial q_{meas}}{\partial \rho} w_\rho \right)^2 + \left(\frac{\partial q_{meas}}{\partial c_p} w_{c_p} \right)^2 + \left(\frac{\partial q_{meas}}{\partial \Delta T} w_{\Delta T} \right)^2 \right]^{\frac{1}{2}} \tag{F2}$$

where the partial derivatives, derived from Eq. (F1), are

$$\frac{\partial q_{meas}}{\partial Q} = \rho c_p \Delta T \qquad \frac{\partial q_{meas}}{\partial \rho} = Q c_p \Delta T \qquad \frac{\partial q_{meas}}{\partial c_p} = Q \rho \Delta T \qquad \frac{\partial q_{meas}}{\partial \Delta T} = Q \rho c_p$$

and the uncertainties of the individual parameters are

$w_Q = 0.005\ Q$
$w_{cp} = 0.01\ c_p$

$w_\rho = 0.01\ \rho$

$w_{\Delta T} = 1.414°F$ (based on individual thermocouple uncertainty of 1°F)

Substituting the partial derivatives and individual parameter uncertainties into Eq. (F2) gives

$$w_{q_{meas}} = \left[(0.005\ Q\rho c_p \Delta T)^2 + (0.01\ Q\rho c_p \Delta T)^2 + (0.01\ Q\rho c_p \Delta T)^2 + (1.414\ Q\rho c_p)^2\right]^{\frac{1}{2}} \quad \text{(F3)}$$

Then, by substituting Eq. (F1) into Eq. (F3), the uncertainty in the measured total heat loss rate is

$$w_{q_{meas}} = \left[2.25 \times 10^{-4}\ q_{meas}^2 + 2.0\ \frac{q_{meas}^2}{(\Delta T)^2}\right]^{\frac{1}{2}} \quad \text{(F4)}$$

or in terms of uncertainty percentage

$$\frac{w_{q_{meas}}}{q_{meas}} = \left[2.25 \times 10^{-4} + \frac{2.0}{(\Delta T)^2}\right]^{\frac{1}{2}} \quad \text{(F5)}$$

II. Error Introduced in Normalizing Total Heat Loss Rate

Since the receiver and air temperatures varied from test to test, it is desirable to normalize the total heat loss to nominal receiver and air temperatures so that data manipulation can be performed and representative comparisons can be drawn. The overall heat loss rate is normalized using

$$q_{total} = \frac{q_{meas}\,(T_{rec,\ norm} - T_{amb,\ norm})}{T_{rec,\ meas} - T_{amb,\ meas}} \quad \text{(F6)}$$

where q_{total} = normalized total heat loss rate

q_{meas} = total heat loss rate calculated from measurements using Eq. (F1)

$T_{rec,\ meas}$ = measured receiver temperature
(average temperature of the heat transfer fluid)
$T_{amb,\ meas}$ = measured ambient temperature
$T_{rec,\ norm}$ = nominal or normal receiver temperature
$T_{amb,\ norm}$ = nominal or normal ambient temperature

For these experiments, the nominal receiver temperature is 530°F and the nominal ambient temperature is 70°F, so that Eq. (F6) becomes

$$q_{total} = \frac{460\ q_{meas}}{T_{rec,\ meas} - T_{amb,\ meas}} \tag{F7}$$

Now, the uncertainty in the normalized total heat loss rate is calculated using

$$w_{q_{total}} = \left[\left(\frac{\partial q_{total}}{\partial q_{meas}} w_{q_{meas}}\right)^2 + \left(\frac{\partial q_{total}}{\partial T_{rec,\ meas}} w_{T_{rec,\ meas}}\right)^2 + \left(\frac{\partial q_{total}}{\partial T_{amb,\ meas}} w_{T_{amb,\ meas}}\right)^2\right]^{\frac{1}{2}} \tag{F8}$$

where the partial derivatives, derived from Eq. (F7), are

$$\frac{\partial q_{total}}{\partial q_{meas}} = \frac{460}{T_{rec,\ meas} - T_{amb,\ meas}}$$

$$\frac{\partial q_{total}}{\partial T_{rec,\ meas}} = \frac{-460\ q_{meas}}{(T_{rec,\ meas} - T_{amb,\ meas})^2}$$

$$\frac{\partial q_{total}}{\partial T_{amb,\ meas}} = \frac{460\ q_{meas}}{(T_{rec,\ meas} - T_{amb,\ meas})^2}$$

and the individual uncertainties are

$w_{q_{meas}}$ defined by Eq. (F4)
$w_{T_{rec,\ meas}}$ = 1.414°F (based on individual thermocouple uncertainty of ±2°F)
$w_{T_{amb,\ meas}}$ = ±2°F

Substituting the partial derivatives and individual uncertainties into Eq. (F8) results in

$$w_{q_{total}} = \left[2.116 \times 10^5 \left(\frac{w_{q_{meas}}}{T_{rec,\ meas} - T_{amb,\ meas}} \right)^2 + 1.269 \times 10^6 \frac{q_{meas}^2}{(T_{rec,\ meas} - T_{amb,\ meas})^4} \right]^{\frac{1}{2}} \quad \text{(F9)}$$

III. Uncertainty in Heat Loss Components

A. Uncertainty in Conduction Heat Loss Rate

The conduction heat loss rate is calculated as the total heat loss rate with the aperture plugged minus the calculated amount of heat conducted through the aperture:

$$q_{cond} = q_{plugged} - q_{aperture} \quad \text{(F10)}$$

where q_{cond} = conduction heat loss rate

$q_{plugged}$ = total heat loss rate with the aperture plugged

$q_{aperture}$ = calculated amount of heat conducted through the aperture

The uncertainty in the conduction heat loss rate is then calculated using

$$w_{q_{cond}} = \left[\left(\frac{\partial q_{cond}}{\partial q_{plugged}} W_{q_{plugged}} \right)^2 + \left(\frac{\partial q_{cond}}{\partial q_{aperture}} W_{q_{aperture}} \right)^2 \right]^{\frac{1}{2}} \quad \text{(F11)}$$

where the partial derivatives of Eq. (F10) are

$$\frac{\partial q_{cond}}{\partial q_{plugged}} = 1 \qquad \frac{\partial q_{cond}}{\partial q_{aperture}} = -1$$

The uncertainty in the conduction heat loss rate is then

$$w_{q_{cond}} = \left[w_{q_{plugged}}^2 + w_{q_{aperture}}^2 \right]^{\frac{1}{2}} \quad \text{(F12)}$$

where the individual uncertainties are those for the aperture-plugged case and the amount of heat conducted through the aperture, respectively.

B. Uncertainty in Radiation Heat Loss Rate

The radiation heat loss rate is calculated as the total heat loss rate for a 90° receiver tilt angle, without wind and with the aperture open, minus the conduction heat loss rate without wind:

$$q_{rad} = q_{open} - q_{cond,\ no\text{-}wind} \tag{F13}$$

where q_{rad} = radiation heat loss rate

q_{open} = total heat loss rate at 90° tilt angle, without wind and with the aperture open

$q_{cond,\ no\text{-}wind}$ = conduction heat loss rate without

Following the same procedure as that used for determining uncertainty in the conduction heat loss rate, the equation for the uncertainty in the radiation heat loss rate is

$$w_{q_{rad}} = \left[w_{q_{open}}^2 + w_{q_{cond}}^2 \right]^{\frac{1}{2}} \tag{F14}$$

C. Uncertainty in Convective Heat Loss Rate

The convective heat loss rate is calculated by subtracting conduction and radiation heat loss rates from the total heat loss rate:

$$q_{conv} = q_{total} - q_{rad} - q_{cond} \tag{F15}$$

Following the same procedure as that used for determining uncertainty in the conduction heat loss rate, the equation for the uncertainty in the convective heat loss rate is as follows:

$$w_{q_{conv}} = \left[w_{q_{total}}^2 + w_{q_{rad}}^2 + w_{q_{cond}}^2 \right]^{\frac{1}{2}} \tag{F16}$$

UNLIMITED RELEASE
INITIAL DISTRIBUTION

U.S. Department of Energy (5)
Forrestal Building
Code EE-132
1000 Independence Avenue, SW
Washington, DC 20585
Attn: G. Burch
S. Gronich

U.S. Department of Energy (2)
Forrestal Building
Code EE-13
1000 Independence Avenue, SW
Washington, DC 20585
Attn: R. Annan

U.S. Department of Energy (2)
Albuquerque Operations Office
P.O. Box 5400
Albuquerque, NM 87115
Attn: G. Tennyson
N. Lackey

U.S. Department of Energy
San Francisco Operations Office
1333 Broadway
Oakland, CA 94612
Attn: R. Hughey

Arizona Dept. of Commerce
3800 N. Central, Suite 1200
Phoenix, AZ 85012
Attn: F. Mancini

Battelle Pacific Northwest Laboratory
P.O. Box 999
Richland, WA 99352
Attn: D. Brown

California Polytechnic University
Dept. of Mechanical Engineering
3801 West Temple Avenue
Pomona, CA 91768
Attn: Dr. Wm. B. Stine (10)

Central and Southwest Services
Mail Stop 7RES
1616 Woodall Rogers Freeway
Dallas, TX 75202
Attn: Edward L. Gastineau

Clever Fellows
Innovation Consortium, Inc.
R.D. 1, Box 410, River Road
Melrose, NY 12121
Attn: J. A. Corey, P.E.

Cummins Power Generation (2)
MC 60125
P. O. Box 3005
Columbus, IN 47202-3005
Attn: R. Kubo

Cummins Power Generation South
150 Tannehill Drive
Abilene, TX 79602
Attn: M. McGlaun

Dynatherm Corporation
1 Beaver Court
P.O. Box 398
Cockeysville, MD 21030
Attn: David Wolf

Electric Power Research Institute
P.O. Box 10412
Palo Alto, CA 94303
Attn: J. Schaeffer

Energy Technology Engr. Center (2)
Rockwell International Corp.
P. O. Box 1449
Canoga Park, CA 91304
Attn: W. Bigelow
R. LeChevalier

Karl Thomas Feldman, Jr. Ph.D., P.E.
Mechanical Engineering Consultant
1704 Stanford Dr. NE
Albuquerque, NM 87106

Florida Solar Energy Center
300 State Road, Suite 401
Cape Canaveral, FL 32920
Attn: Library

Georgia Power
7 Solar Circle
Shenandoah, GA 30265
Attn: W. King

Institute of Gas Technology
34245 State Street
Chicago, IL 60616
Attn: Library

Jet Propulsion Laboratory
4800 Oak Grove Drive
Pasadena, CA 91109
Attn: M. Alper

Lawrence Berkeley Laboratory
MS 90-2024
One Cyclotron Road
Berkeley, CA 94720
Attn: A. Hunt

Los Alamos National Laboratory
MS-E13
Los Alamos, NM 87545
Attn: M. Merrigan

McDonnell-Douglas Astronautics Company
5301 Bolsa Avenue
Huntington Beach, CA 92647
Attn: R. L. Gervais,
J. Rogan,
D. Steinmeyer

Mechanical Technology, Inc. (2)
968 Albany Shaker Road
Latham, NY 12110
Attn: G. Dochat
J. Wagner

NASA Lewis Research Center (4)
21000 Brook Park Road
Cleveland, OH 44135
Attn: R. Shaltens
J. Schrieber

National Renewable Energy Laboratory (6)
1617 Cole Boulevard
Golden, CO 80401
Attn: T. Williams
L. M. Murphy
G. Jorgensen
T. Wendelin
A. Lewandowski
M. Bohn

Northern Research and Engineering Corp.
39 Olympia Avenue
Woburn, MA 01801-2073
Attn: J. Kesseli

Power Kinetics, Inc.
415 River Street
Troy, NY 12180-2822
Attn: W. E. Rogers

Research International
18706 142nd Avenue NE
Woodinville, WA 98072
Attn: E. Saaski

Science Applications International Corporation
15000 W. 6th Avenue, Suite 202
Golden, CO 80401
Attn: Kelly Beninga

Science Applications International Corporation
Mail Stop 32
10260 Campus Point Court
San Diego, CA 92121
Attn: B. Butler

Solar Energy Industries Assoc. (2)
777 North Capitol St. NE
Suite 805
Washington, D.C. 20002
Attn: S. Sklar
K. Sheinkopf

Solar Kinetics, Inc. (2)
P.O. Box 540636
Dallas, TX 75354-0636
Attn: J. A. Hutchison
P. Schertz

Stirling Technology Company (3)
2952 George Washington Way
Richland, WA 99352
Attn: Maurice A. White

Stirling Thermal Motors (2)
275 Metty Drive
Ann Arbor, MI 48103
Attn: Lennart Johansson

Stirling Machine World
1823 Hummingbird Court
West Richland, WA 99352-9542
Attn: Brad Ross

Sunpower, Inc.
6 Byard Street
Athens, OH 45701
Attn: W. Beale

Tech Reps, Inc. (2)
5000 Marble NE, Suite 222
Albuquerque, NM 87110
Attn: J. Stikar

Thermacore, Inc. (2)
780 Eden Road
Lancaster, PA 17601
Attn: Donald Ernst

University of Houston
Solar Energy Laboratory
4800 Calhoun
Houston, TX 77704
Attn: J. Richardson

University of Minnesota
Dept. of Mechanical Engineering
111 Church St., SE
Minneapolis, MN 55455
Attn: E. A. Fletcher

Australian National University
Department of Engineering
Physics
P. O. Box 4
Canberra ACT 2600 AUSTRALIA
Attn: S. Kaneff

DLR
Pfaffenwaldring 38-40
7000 Stuttgart 80 GERMANY
Attn: R. Buck

Energy Research Centre
R. S. Phy. Sc.
Australian National University
Canberra ACT 2601 AUSTRALIA
Attn: K. Inall

Dr. David Hagen
134 Kitchener St.
Garran, ACT 2605
AUSTRALIA

Pacific Power
Park and Elizabeth Streets
GPO Box 5257, Sydney
New South Wales 2001, Australia
Attn: Peter Lynch

Schlaich, Bergermann & Partner
Hohenzollernstr. 1
D - 7000 Stuttgart 1 GERMANY
Attn: W. Schiel

1513	D. R. Adkins
1513	R. E. Hogan
1513	V. J. Romero
1513	R. D. Skocypec
1561	E. L. Hoffman
1561	C. M. Stone
1833	J. A VanDenAvyle
2756	G. S Phipps
4313	J. F.Muir
6000	D. L.Hartley
6115	W. C. Ginn
6200	D. E. Arvizu
6201	P. C. Klimas
6213	A. R. Mahoney
6215	C. P.Cameron
6215	K. S .Rawlinson
6215	Library (5)
6216	C. E.Tyner
6216	C. E.Andraka
6216	R. B.Diver
6216	T. R.Mancini
6216	D. F. Menicucci
6216	J. B. Moreno
6216	T. A. Moss
6216	Library (5)
7141	Technical Library (5)
7151	G. C. Claycomb
7613-2	Document Processing for DOE/OSTI (10)
8523-2	Central Technical Files

*U.S. GOVERNMENT PRINTING OFFICE 1993-0-573-026/80008

THIS PAGE INTENTIONALLY LEFT BLANK